Volume 7, No. 4
March, 1961

THE SOVIET JOURNAL OF

ATOMIC ENERGY

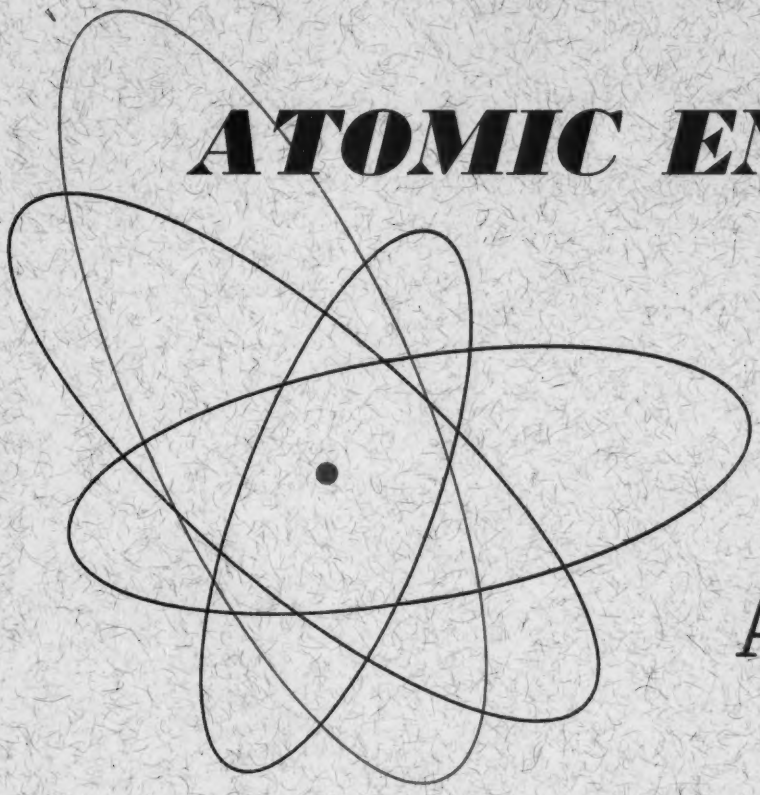

Атомная энергия

TRANSLATED FROM RUSSIAN

CONSULTANTS BUREAU

THE SOVIET JOURNAL OF

ATOMIC ENERGY

A translation of ATOMNAYA ENERGIYA, a publication of the Academy of Sciences of the USSR

(Russian original dated October, 1959)

Vol. 7, No. 4 March, 1961

CONTENTS

Annual subscription $75.00
Single issue 20.00
Single article 12.50

CONTENTS (continued)

NOTE

The Table of Contents lists all material that appears in Atomnaya Énergiya. Those items that originated in the English language are not included in the translation and are shown enclosed in brackets. Whenever possible, the English-language source containing the omitted reports will be given.

Consultants Bureau Enterprises, Inc.

PASSAGE OF FAST NEUTRONS THROUGH LEAD AND IRON

D. L. Broder, A. A. Kutuzov, V. V. Levin,
V. V. Orlov, and A. V. Turusova

Translated from Atomnaya Énergiya, Vol. 7, No. 4, pp. 313-320
October, 1959
Original article submitted January 21, 1959

The present article describes the results obtained in measuring the spatial distribution of fast neutrons, which are emitted from sources of monoenergetic neutrons, with E_0 = 4 Mev and E_0 = 14.9 Mev, as well as neutrons from atomic reactors, in lead and iron.

In order to calculate the space-energy distribution of fast neutrons at large distances from the source, we have developed a method of solving the kinetic equation for media where the neutrons are moderated due to inelastic scattering on nuclei.* The anisotropy of elastic scattering is taken into account. The energy losses of neutrons in elastic scattering are neglected.

Introduction

One of the main problems in designing nuclear reactors is the calculation of biological shielding. Materials which contain a mixture of light and heavy nuclei have the best protective properties. Substances with medium and large atomic numbers, for instance, iron, serve as structural materials for screens, reactor vessels, and first shielding layers. Therefore, the study of the spatial and energetic distribution of neutrons in these substances is of considerable interest. Iron is a good moderator for neutrons with $E > 1$ Mev because of the inelastic scattering on nuclei. In this, the elastic scattering of neutrons with such energies does not play an important role in moderation, however, it materially affects their spatial distribution. Until the present time, little information has been published on neutron distribution in iron and lead. We have performed experiments in measuring the attenuation of fast neutron fluxes in these substances.

Experimental Devices

Neutron Sources and Media Under Investigation. As neutron sources, we used the reactor of the First Atomic Power Station [2], the VVR experimental nuclear reactor with ordinary water and enriched uranium [3], and a neutron generator yielding neutrons with an average energy (E_0) of 4 Mev [reaction $D(d, n)He^3$] and of 14.9 Mev [reaction $T(d, n)He^4$]. Investigations of the shielding properties of lead were conducted on the top shield of the reactor in the First Atomic Power Station. A converter made of uranium 90% enriched with U^{235}, which was 65 mm in diameter and 20 mm thick, was installed at the upper part of a vertical channel reaching the reactor core. The channel was filled with cylindrical graphite rods up to a height of 60 cm from the core level in order to reduce the shooting of fast neutrons from the reactor through the channel. A block composed of lead plates with dimensions of 710 × 710 × 700 mm was placed above the converter. The detectors were placed in horizontal channels which were provided in the block. The spatial distribution of neutrons in iron was measured in the VVR reactor.† Specimens of the materials under investigation were placed on a special truck in an experimental recess with dimensions 1720 × 1720 mm. The measurements were performed for semiinfinite geometry (the source was placed outside the medium under investigation at a certain distance from its boundary, and the detector was placed inside the medium).

The minimum distance from the core center to the measurement point was 645 mm. The specimens consisted of Steel-3 slabs with dimensions of 1500 × 1500 mm. Vertical channels 50 mm in diameter, where detectors were placed, were provided in the slabs. The unoccupied channels were stopped with Steel-3 plugs.

The spatial distribution of neutrons in iron and lead was measured also by means of a neutron generator. Targets of heavy ice (E_0 = 4 Mev) and tritium, which was adsorbed by zirconium (E_0 = 14.9 Mev), were in the shape of disks 10 mm in diameter. Iron and lead specimens were in the shape of prisms with

* S. A. Kurkin collaborated in developing the calculation method [1].

† M. B. Egiazarov, V. S. Dikarev, V. G. Madeev, E. N. Korolev, and N. S. Il'inskii collaborated in these measurements.

dimensions of 710 × 710 × 830 mm. The neutron source was placed inside the prisms at a distance of 150 mm from their front faces. The detectors were placed in vertical channels in the prisms, and the unoccupied channels were stopped with steel or lead plugs. In all experiments, the density of lead was 11.3 g/cm^3, and the density of steel was 7.83 g/cm^3.

Neutron Detectors. A Th^{232} fission chamber and the threshold indicators $Al^{27}(n, p)Mg^{27}$, $P^{31}(n, p)Si^{31}$, and $S^{32}(n, p)P^{32}$ were used as detectors of fast neutrons. The distribution of thermal and epithermal neutrons was measured by means of a fission chamber with U^{235}

The fission chambers consisted of pulse-counting ion chambers; in these chambers, two nickel strips served as electrodes, on both sides of which the fissionable substance was deposited. The strips were wound into helices 25 mm in diameter and 37 mm long. The layer thickness of the fissionable substance was 2.5 mg/cm^2, and the over-all amount of the fissionable substance in the chamber was ~ 1 g. The fission reaction threshold for thorium was 1.1 Mev. A check showed that the correction for the influence of γ rays and slow neutrons did not exceed 10% of the magnitude of the effect in all measurements in the thorium chamber.

Two types of the threshold indicators $P^{31}(n, p)Si^{31}$ (reaction threshold: 1.5 Mev), $Al^{27}(n, p)Mg^{27}$ (reaction threshold: 2.1 Mev), and $S^{32}(n, p)P^{32}$ (reaction threshold: 1.5 Mev) were used: disk-shaped indicators with a diameter of 15 mm and a thickness of 3 mm (for small distances from the source) and indicators in the shape of hollow cylinders with an outside diameter of 35 mm, a length of 46 mm, and a wall thickness of 3 mm (for large distances from the source).

During measurements, all indicators were enclosed in cadmium cases, which had a thickness of 0.6 mm.

The activity of the indicators was determined by means of devices with β counters. In order to reduce the background, the β counter for cylindrical indicators was connected to an anticoincidence circuit with γ counters, which were surrounding the β counter. The effect was separated by analyzing the decay curves for the activity of the indicators.

Experimental

Figures 1 and 2 show the results of measurements for iron, which were obtained with neutron sources with average energies of 4 and 14.9 Mev and with the VVR reactor. The magnitudes of neutron fluxes,

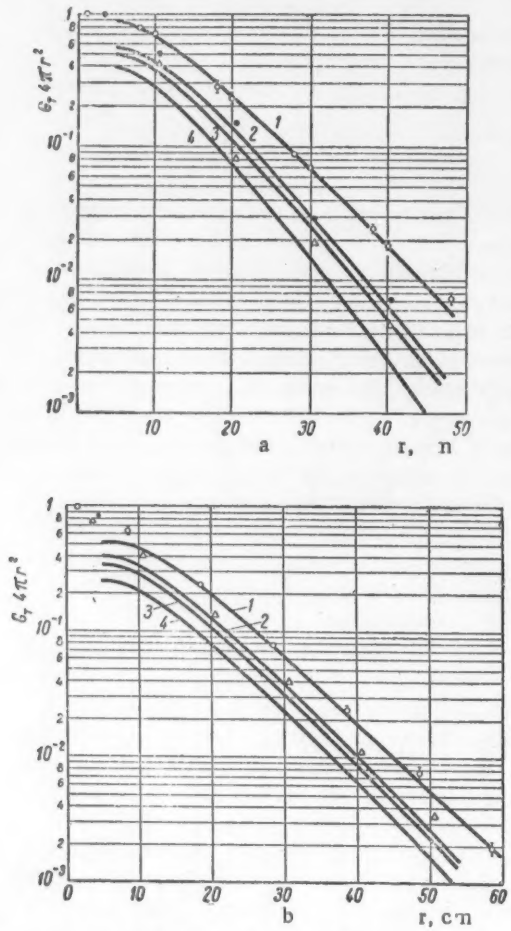

Fig. 1. Spatial distribution of fast neutrons in iron: a) E_0 = 4 Mev; b) E_0 = 14.9 Mev. Infinite geometry; ○) measurement by means of a fission chamber with Th^{232}; ●) measurement by means of the $P^{31}(n, p)Si^{31}$ indicator; △) measurement by means of the $S^{32}(n, p)P^{32}$ indicator; 1), 2), 3) and 4) theoretical curves for Th, P, S, and Al, respectively.

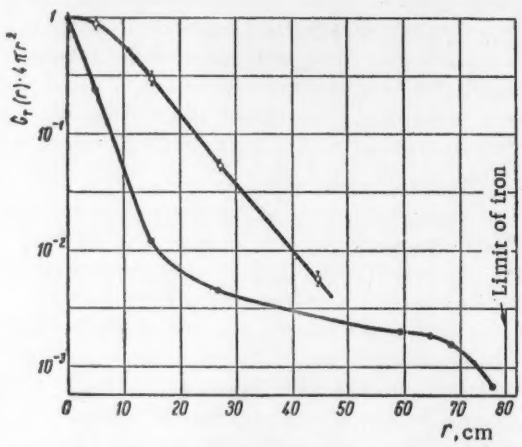

Fig. 2. Spatial distribution of neutrons from the VVR reactor in iron, measured by means of fission chambers with Th^{232} and U^{235}. Semiinfinite geometry: ●) thermal neutrons; ○) fast neutrons.

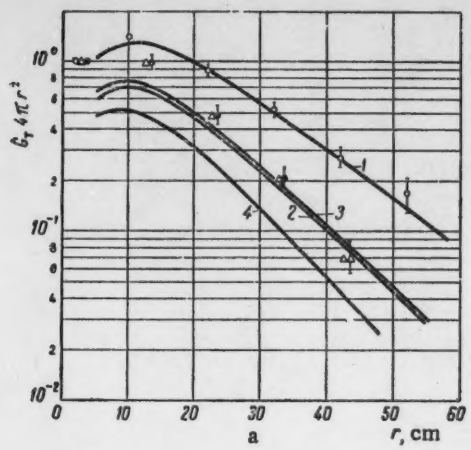

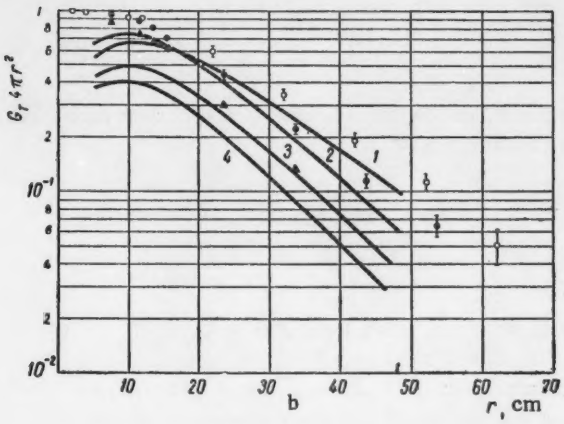

Fig. 3. Spatial distribution of fast neutrons in lead: a) E_0 = 4 Mev; b) E_0 = 14.9 Mev. Infinite geometry; ○) measurement by means of a fission chamber with Th^{232}; ●) by means of the P^{31} (n, p) Si^{31} indicator; Δ) by means of the S^{32} (n, p) P^{32} indicator; ▲) by means of the Al^{27} (n, p) Mg^{27} indicator; 1), 2), 3) and 4) theoretical curves for Th, P, S, and Al, respectively.

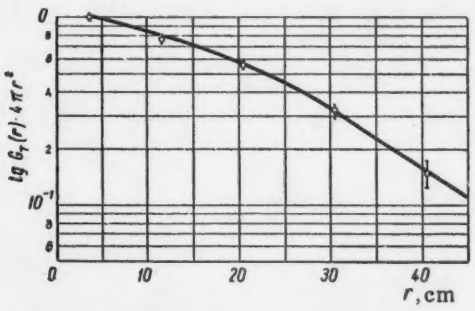

Fig. 4. Spatial distribution of neutrons of the fission spectrum in lead, measured by means of the S^{32} (n, p) P^{32} indicator. Infinite geometry.

multiplied by the square of the distance from the detector to the source in the case where the fluxes were measured by means of threshold detectors and by the square of the distance from the detector to the core center in the case where the measurements were performed in the reactor, are plotted on the axis of ordinates.

The measurement results for lead are shown in Figs. 3 and 4. The curves in these diagrams were plotted with respect to the results obtained in calculations for an isotropic point source. The calculation method is explained below.

The experimental data obtained in measurements with a converter in the reactor of the First Atomic Power Station were converted for an isotropic point source

Theory

Consider an infinite homogenous medium containing an infinite flat isotropic source of monoenergetic neutrons with an energy E_0.

If we neglect the slowing down of neutrons in elastic scattering and if we consider the inelastic scattering as isotropic, we can write the kinetic equation $\psi(z, E)$ for the density of neutron collisions in the following form:

$$\mu\lambda\frac{\partial\Psi}{\partial z}+\Psi=\frac{\sigma_s}{\sigma}\int d\vec{\Omega}\Psi(z, E, \mu')\varphi(E, \mu_0)+$$
$$+\frac{1}{4\pi}\int_E^{E_0}\psi_0(z, E')\frac{\sigma_{in}}{\sigma}F_{in}(E', E)\,dE'+$$
$$+q\frac{\delta(z)\,\delta(E-E_0)}{4\pi}, \qquad (1)$$

where μ is the cosine of the angle between the direction of the neutron velocity $\vec{\Omega}$ and the z axis, $\mu_0 = \vec{\Omega}\vec{\Omega}_0$, σ_s is the elastic scattering cross section, σ_{in} is the inelastic scattering cross section, $\sigma(E) = \sigma_s(E) + \sigma_{in}(E) + \sigma_c(E)$ (σ_c is the absorption cross section), $\lambda = 1/\rho\sigma$, $\varphi(E, \vec{\Omega}\,\vec{\Omega}')$ is the angular distribution of elastically scattered neutrons, $F_{in}(E', E)$ is the energy distribution of neutrons in inelastic scattering, q is the source strength, and ρ is the number of nuclei per cm^3 of substance;

$$\Psi_0(z, E)=\int\Psi(z, \mu, E)\,d\vec{\Omega}.$$

We shall further consider that q is always equal to 1.

We shall apply the Fourier transformation to (1):

$$\left.\begin{aligned}\Psi(z, \mu, E)&=\frac{1}{2\pi i}\int_{-i\infty}^{i\infty}\Phi(k, \mu, E)\,e^{-kz}\,dk;\\ \Phi(k, \mu, E)&=\int_{-i\infty}^{i\infty}\Psi(z, \mu, E)\,e^{kz}\,dz.\end{aligned}\right\} \qquad (2)$$

For $\Phi(k, \mu, E)$, we then obtain the equation

$$[1-k\lambda(E)\mu]\Phi(k,\mu,E)=$$
$$=\frac{\sigma_s(E)}{\sigma(E)}\int d\vec{\Omega}'\varphi(E,\mu_0)\Phi(k,\mu',E)+$$
$$+\int d\vec{\Omega}'\frac{\sigma_{in}(E')}{\sigma(E')}\frac{F_{in}(E',E)}{4\pi}\Phi(k,\mu',E')dE'+$$
$$+q\frac{\delta(E-E_0)}{4\pi}. \qquad (3)$$

In order to solve (3) we shall use the method of spherical harmonics. Let us apply the Legendre polynomial expansion to $\Phi(k, \mu, E)$ and $\varphi(\mu_0, E)$:

$$\left.\begin{aligned}\Phi(k,\mu,E)&=\sum_{l=0}^{\infty}\frac{2l+1}{4\pi}\Phi_l(k,E)P_l(\mu);\\ \varphi(\mu_0,E)&=\sum_{l=0}^{\infty}\frac{2l+1}{4\pi}\varphi_l(E)P_l(\mu_0),\end{aligned}\right\} \qquad (4)$$

where

$$\Phi_l(k,E)=\int\Phi(k,\mu,E)P_l(\mu)d\vec{\Omega};$$
$$\varphi_l(E)=\int\varphi(\mu_0,E)P_l(\mu_0)d\vec{\Omega}_0.$$

By substituting (4) in (3), we obtain a system of equations for $\Phi_n(k, E)$:

$$\left[1-\frac{\sigma_s(E)}{\sigma(E)}\varphi_n(E)\right]\Phi_n(k,E)-$$
$$-k\lambda(E)\frac{n+1}{2n+1}\Phi_{n+1}(k,E)-$$
$$-k\lambda(E)\frac{n}{2n+1}\Phi_{n-1}(k,E)=$$
$$=\left[\int_E^{E_0}\frac{\sigma_{in}(E')}{\sigma(E')}\Phi_0(k,E')F_{in}(E',E)dE'+\right.$$
$$\left.+q\delta(E-E_0)\right]\delta_{n0} \qquad (5)$$

If we denote $\Phi_n(k, E)/\Phi_0(k, E)$ by $R_n(k, E)$, we obtain a system of equations for $R_n(k, E)$:

$$\left[1-\frac{\sigma_s(E)}{\sigma(E)}\varphi_n(E)\right]R_n(k,E)-$$
$$-k\lambda(E)\frac{n+1}{2n+1}R_{n+1}(k,E)-$$
$$-k\lambda(E)\frac{n}{2n+1}R_{n-1}(k,E)=0; \qquad (6)$$
$$R_0(k,E)=1;\ n>0.$$

By solving this system of equations, we find

$$k\lambda(E)R_1(k,E)=\cfrac{\beta_1(k,E)}{\gamma_1(E)-\cfrac{\beta_2(k,E)}{\gamma_2(E)-\cfrac{\beta_3(k,E)}{\gamma_3(E)-\ldots}}}$$
$$\ldots-\frac{\beta_{n-1}(k,E)}{\gamma_{n-1}(E)-\chi_n(k,E)}, \qquad (7)$$

where

$$\beta_m(k,E)=k^2\lambda^2(E)\frac{m^2}{4m^2-1};$$
$$\gamma_m(E)=1-\frac{\sigma_s(E)}{\sigma(E)}\varphi_m(E);$$
$$\chi_m(k,E)=\frac{m}{2m-1}k\lambda(E)\frac{R_m(k,E)}{R_{m+1}(k,E)}.$$

By using the properties of infinite fractions (see [4]), for the function

$$R(k,E)=\frac{1}{\gamma_0-R_1(k,E)k\lambda(E)} \qquad (8)$$

we obtain the function

$$R(k,E)=\frac{V_{n+1}(k,E)-\chi_n(k,E)V_n(k,E)}{U_{n+1}(k,E)-\chi_n(k,E)U_n(k,E)}, \qquad (9)$$

where V_n and U_n are polynomials in k^2, which satisfy the recurrent relation

$$w_{m+1}(k,E)=\gamma_m(E)w_m(E)-$$
$$-\beta_m(k,E)w_{m-1}(k,E) \qquad (10)$$

with the initial values $U_0(k, E) = 1$, $U_1(k, E) = \gamma_0(E)$, $V_0(k, E) = 0$; and $V_1(k, E) = 1$. If, in expanding the scattering indicatrix into Legendre polynomials, we can neglect the nth and the successive terms, i.e., if we assume that $\gamma_n = \gamma_{n+1} = \ldots = 1$, then

$$\chi_n(k,E)=\frac{Q_n\left(\frac{1}{k\lambda(E)}\right)}{Q_{n+1}\left(\frac{1}{k\lambda(E)}\right)}\frac{n}{(2n-1)}k\lambda(E),$$

where Q_n is the nth Legendre function of the second kind. For $n \gg 1$, $\chi_n(k, E) \simeq \frac{1}{2}[1-\sqrt{1-k^2\lambda^2(E)}]$.

By substituting the solution of (8) in (5) for $n = 0$ and $\Phi(k, E) = R_1(k, E)\Phi_0(k, E)$, we obtain the integral equation for

$$\Phi_0(k,E):$$
$$\frac{\Phi_0(k,E)}{R(k,E)}=\int_E^{E_0}\frac{\sigma_{in}(E')}{\sigma(E')}\Phi_0(k,E')F_{in}(E',E)dE'+$$
$$+q\delta(E-E_0). \qquad (11)$$

In the process of inelastic scattering, the neutrons lose energy by discrete amounts corresponding to the system of nuclear excitation levels. Under these assumptions, (11) assumes the form

$$\frac{\Phi_0(k, E)}{R(k, E)} = \sum_i \Phi_0(k, E+\Delta E_i) \times$$

$$\times \frac{\sigma_{in}(E+\Delta E_i)}{\sigma(E+\Delta E_i)} F_i(E+\Delta E_i) + \delta(E-E_0), \quad (12)$$

where ΔE_i is the excitation energy of the ith level, and $F_i(E)$ is the probability that the ith level of a nucleus will become excited in inelastic scattering of neutrons with the energy E. The solution of (12) breaks down into a number of monoenergetic lines:

$$\Phi_0(k, E) = R(k, E_0)\,\delta(E-E_0);$$

$$\Phi_0(k, E_1) = \frac{\sigma_{in}(E_0)}{\sigma(E_0)} F_1(E_0) R(k, E_1) \times$$

$$\times R(k, E_0)\,\delta(E-E_0+\Delta E_1) \text{ etc.}$$

The asymptotic solution for each neutron group can be obtained by taking the residues at the poles of each of these expressions:

$$\psi_0(z, E_0) = \frac{\delta(E-E_0)^{-k_0 z}}{\left|\frac{\partial}{\partial k}\frac{1}{R(k, E_0)}\right|_{k=k_0}};$$

$$\psi_0(z, E_1) = \frac{\sigma_{in}(E_0)}{\sigma(E_0)} F_1(E_0)\,\delta(E-E_0+$$

$$+\Delta E_1)\left[\frac{e^{-k(E_1)z}}{\left|\frac{\partial}{\partial k}\frac{1}{R(k, E)}\right|_{k=k(E_1)}} R(k(E_1), E_0) + \right.$$

$$\left. + \frac{e^{-k_0 z}}{\left|\frac{\partial}{\partial k}\frac{1}{R(k, E_0)}\right|_{k=k_0}} R(k_0, E_1)\right];$$

$$E_1 = E_0 - \Delta E_1 \text{ etc.}$$

Discussion of Results

By means of the described method, we calculated the neutron fluxes $\psi_0(z, E)$ in an infinite medium for an isotropic flat source. The flux of neutrons with the energy E in a medium with a point source of unit strength can be expressed in terms of ψ by the equation

$$\Phi_\tau(r, E_i) = -\lambda(E_i)\left[\frac{1}{2\pi z}\frac{\partial \psi_0(z, E_i)}{\partial z}\right]_{z=r}$$

Then, the total flux of fast neutrons will be

$$\Phi_\tau(r) = \sum_{E_i} \Phi_\tau(r, E_i),$$

and the flux of neutrons counted by the fission chamber with Th^{232} or by a threshold indicator and normalized to unity for r = 0 will be

$$G_\tau(r) = \sum_{E_i} \frac{\sigma_a(E_i)}{\sigma_a(E_0)} \Phi_\tau(r, E_i),$$

where $\sigma_a(E_i)$ and $\sigma_a(E_0)$ are the activation cross sections of indicator nuclei or the cross sections of Th^{232} fission by fast neutrons with energies E_i and E_0.

The quantities φ_n, which characterize the angular distribution of neutrons in elastic scattering on iron and lead nuclei, were determined on the basis of experimental data from [5-10].

Figure 5 shows the magnitudes of φ_n in the 1-15 Mev interval for iron and lead, which were obtained by interpolation of experimental data.

Iron. It was assumed that, in inelastic scattering the neutrons of the E_0 = 4 Mev source are distributed among the following energy groups: 4; 3.15; 2.3; 1.9; 1.45; 1.34 Mev in correspondence with the system of lower levels of iron nuclei. Lower-energy neutrons are not detected by the thorium chamber and by threshold detectors, and we did not take them into consideration. The differential cross sections of inelastic neutron scattering for these levels were taken from a survey by V. S. Stavinskii and L. N. Usachev and from [11 and 12].

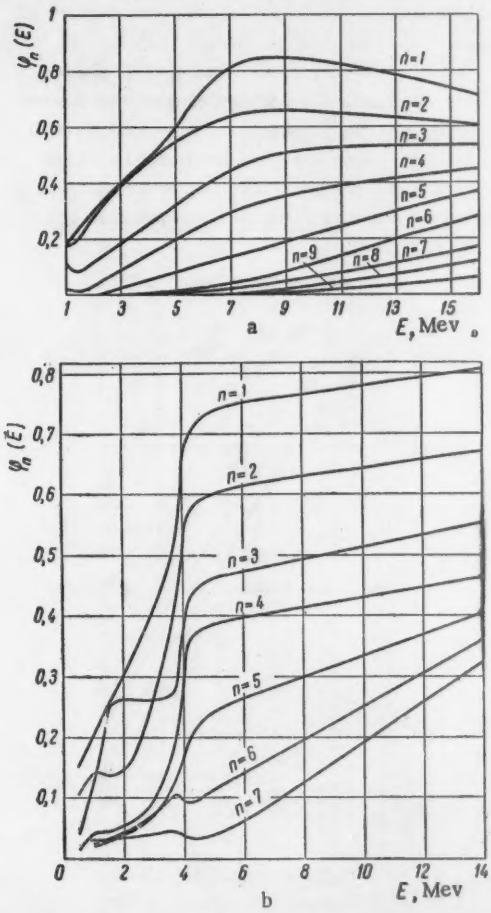

Fig. 5. Energy dependence of coefficients in the Legendre polynomial expansion of the indicatrix of neutron elastic scattering in iron a) and in lead b).

Figure 6 shows the spatial distribution of the total flux and of fluxes of neutrons with the indicated energies in iron for a neutron source with E_0 = 4 Mev.

In calculating the distribution of neutrons from the source with E_0 = 14.9 Mev, it was assumed that discrete energy groups of moderated neutrons were also present, where the probability of source neutrons falling into each group by a single inelastic scattering was found from the Maxwellian distribution. The energy corresponding to the iron nucleus temperature was assumed to be equal to 0.76 Mev. The assumption of the Maxwellian distribution of neutrons inelastically scattered on iron nuclei was confirmed by data from [13 and 14]. It was shown that the overall number of neutrons for all calculated iron thicknesses is determined by neutrons which are slowed down to E<4 Mev. The number of neutrons with E > 4 Mev was small in comparison with the number of neutrons with E < 4 Mev.

As can be seen from Fig. 1, the calculation results are in good agreement with experimental data. Figure 7 shows the calculated spatial distributions of neutrons of all groups for the source with E_0 = 14.9 Mev.

A study of the calculated flux magnitudes for moderated neutrons of all groups for the source with E_0 = 4 Mev (see Fig. 9) indicates that neutrons with energies from 1.2 to 1.5 Mev constitute the main contribution to the total flux of fast neutrons for large thicknesses. The same conclusion pertains to the neutron source with E_0 = 14.9 Mev.

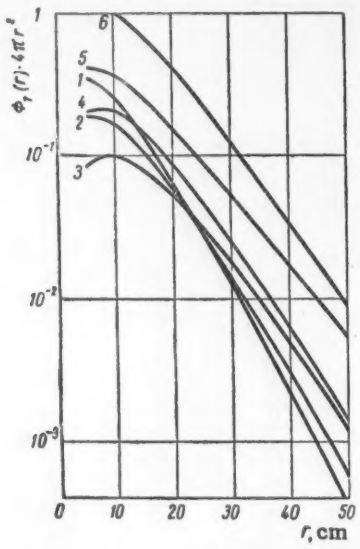

Fig. 6. Theoretical spatial distribution of moderated neutrons of different energies in iron. The energy of source neutrons is E_0 = 4 Mev. The neutron energies (Mev): 1) 4; 2) 3.155; 3) 2.31; 4) 1.9; 5) 1.34; 6) total neutron flux.

The approximately equal attentuation of the flux of neutrons from the VVR reactor and from a neutron source with E_0 = 4 Mev, which was measured by means of a fission chamber with Th^{232}, is determined by a predominant contribution of groups which have been slowed down to a great extent.

Lead. On the basis of the well-known level diagram for lead nuclei, it was assumed that, for a source with E_0 = 4 Mev, the neutrons are distributed in the following energy groups in inelastic scattering: 4; 3.43; 3.16; 2.32; 1.8; 1.48; 1.22; 0.96 Mev.

In order to simplify calculations, the groups of moderated neutrons which were close to each other with respect to energies were combined. However, the accuracy of calculations was not reduced to a great

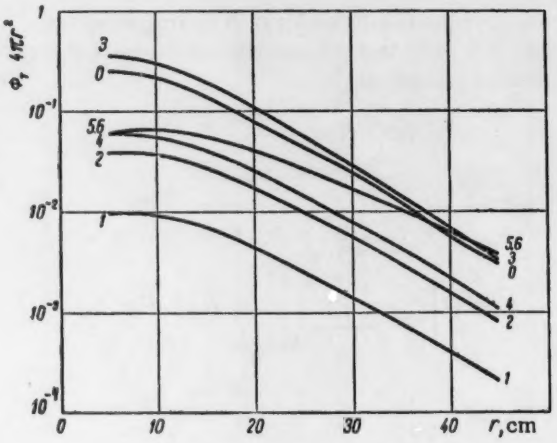

Fig. 7. Theoretical spatial distribution of moderated neutrons of different energies in iron. The energy of source neutrons is E_0 = 14.9 Mev. The neutron energies (Mev): 0) 14.9; 1) 4; 2) 3.15; 3) 2.31; 4) 1.9; 5) 1.34; 6) 1.45.

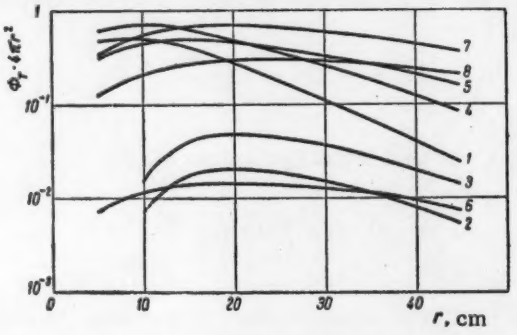

Fig. 8. Theoretical spatial distribution of moderated neutrons of different energies in lead. The energy of source neutrons is E_0 = 4 Mev. Neutron energies (Mev): 1) 4; 2) 3.43; 3) 3.16; 4) 2.32; 5) 1.8; 6) 1.48; 7) 1.22; 8) 0.96.

extent due to a weak dependence of the interaction of neutrons with lead nuclei on neutron energy.

The diagram of energy groups for the neutron source with E_0 = 14.9 Mev is similar.

It should be noted that in inelastic scattering of neutrons with E_0 = 14.9 Mev on lead nuclei, the inelastic scattering spectrum of neutrons with E > 4 Mev differs from the Maxwellian spectrum to a great extent. In this case, the probability of the source neutrons passing into each group was found on the basis of the measured spectra, obtained as a result of inelastic scattering of neutrons with E_0 = 14 Mev on lead nuclei [14].

The spatial distributions of neutrons of all groups, obtained as a result of calculations for neutrons with average energies of 4 and 14.9 Mev, are given in Figs. 8 and 9.

As can be seen from Figs. 4 and 5, the experimental and the theoretical values for a neutron source with E_0 = 4 Mev are in good agreement, and for a neutron source with E_0 = 14.9 Mev the maximum deviation is 30%. This discrepancy can be explained by the inaccuracy of data on inelastic neutron scattering spectra in the 14 > E > 8 Mev region of differential inelastic scattering cross sections and by a certain anisotropy of inelastic scattering at high neutron energies.

SUMMARY

The proposed calculation method makes it possible to find with sufficient accuracy the spatial energy distribution of neutrons in thick layers of substances with comparatively large atomic numbers (for instance, larger than 56) if sufficient data are available on differential cross sections of inelastic and elastic neutron scattering. Calculations show that, at large distances from the source, the neutron spectrum is enriched with neutrons which are decelerated to a great extent. If the energy distribution is known, multigroup calculations for the shielding can be performed.

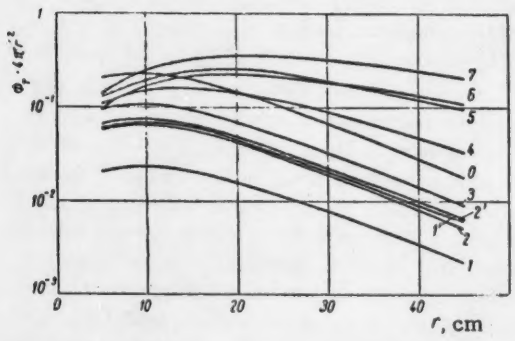

Fig. 9. Theoretical spatial distribution of moderated neutrons of different energies in lead. The energy of source neutrons is E_0 = 14.9 Mev. Neutron energies (Mev): 0) 14.9; 1') 8; 2') 6; 1) 4; 2) 3.43; 3) 3.16; 4) 2.32; 5) 1.8; 6) 1.48; 7) 1.22.

In conclusion, the authors express their gratitude to Prof. A. K. Krasin, Cand. Tech. Sci. A. N. Serbinov, and scientific collaborator V. A. Romanov for their continued interest in the work and help in organizing the experiments. The authors extend their thanks also to V. G. Liforov, Z. S. Blistanova, and V. S. Tarasenko for their help in conducting the experiments.

LITERATURE CITED

1. D. L. Broder, S. A. Kurkin, A. A. Kutuzov, V. V. Levin, and V. V. Orlov, Report No. 2147, submitted to the Second International Conference on the Peaceful Use of Atomic Energy (Geneva, 1958).
2. D. I. Blokhintsev and N. A. Nikolaev, "Reactor construction and reactor theory," Reports of the Soviet Delegation to the International Conference on the Peaceful Use of Atomic Energy (Geneva, 1955) [in Russian] (Izd. AN SSSR, Moscow, 1955) p. 3.
3. D. I. Blokhintsev and N. A. Nikolaev, "Reactor construction and reactor theory," Reports of the Soviet Delegation to the International Conference on the Peaceful Use of Atomic Energy (Geneva, 1955) [in Russian] (Izd. AN SSSR, Moscow, 1955) p. 91.
4. A. Wick, Phys. Rev. 75, 738 (1949).
5. L. Cranberg and J. Levin, Phys. Rev. 103, 343 (1956).
6. C. Muelhause, S. Bloom, H. Wegner, and A. Glasoe, Phys. Rev. 103, 720 (1956).
7. M. Walt and H. Barschall, Phys. Rev. 93, 1062 (1954).
8. A. Culler, S. Fernbach, and N. Sherman, Phys. Rev. 101, 1047 (1956).
9. J. Beyster, M. Walt and E. Salmi, Phys. Rev. 104, 1319 (1956).
10. M. Walt and J. Beyster, Phys. Rev. 98, 677 (1955).
11. B. Feld, Phys. Rev. 75, 1115 (1949).
12. D. Hughes and J. Harvey, "Neutron cross sections," US AEC report BNL-375 (1955).
13. Jagadish Garg and Bechir Torki, Compt. rend. 246, 750 (1958).
14. Yu. S. Zamyatin, E. K. Gutnikova, N. I. Ivanova, and I. N. Safina, Atomnaya Énergiya 3, 540 (1957).‡

‡ Original Russian pagination See C. B. translation.

ON M1-TRANSITIONS FROM HIGHLY EXCITED STATES

L. V. Groshev and A. M. Demidov

Translated from Atomnaya Énergiya, Vol. 7, No. 4, pp. 321-328
October, 1959,
Original article submitted May 15, 1959

This article is concerned with the probabilities of M1-transitions from states created by the capture of thermal neutrons for even-odd and odd-odd emitting nuclei with A from 20 to 60. In the single-particle model, such transitions are forbidden with respect to l. A comparison with the probabilities of E1-transistions shows that in even-odd nuclei, the probabilities of forbidden M1-transitions which we observed, did not differ much from the probabilities of l-allowed M1-transitions for lighter nuclei. In the case of odd-odd nuclei, certain M1-transitions are characterized by a large number of quanta per single neutron capture and a large value of $\frac{|M|^2_{M1}}{(|M|^2_{E1})\max}$

In a number of papers [1-4], attempts have recently been made to use the single-particle model in analyzing processes of thermal neutrons capture by nuclei and of the subsequent transition of nuclei into lower states. Such a model explains certain irregularities in γ-ray spectra from the (n, γ) reaction. In particular, within the framework of this model, it is easy to explain the correlation of intensities of E1-transitions from the initial state created by the capture of thermal neutrons with the reduced neutron widths of levels to which these transitions are directed, which is observed in nuclei with A from 20 to 60 [4]. Therefore, it is also of interest to use the single-particle model in considering the probabilities of M1-transitions from the initial state in nuclei from the same atomic weight region.

Prohibition of the Considered M1-Transitions in the Single-Particle Model.

We shall first restrict our analysis to M1-transitions of even-odd nuclei formed in the (n, γ) reaction. In nuclei with A from 20 to 60, the M1-transitions were separated in the following even-odd nuclei: Mg^{25}, Si^{29}, S^{33}, and Ca^{41}.

Since in the given case the thermal neutrons are captured by even-even nuclei, the M1-transitions from the initial state are directed to levels with $1/2^+$ or $3/2^+$ characteristics. For the majority of such levels, the value $l_n = 0$ or $l_n = 2$ was found from the angular distribution of protons in the (d, p) reaction. The possibility of detecting M1-transitions in nuclei with A from 20 to 40 is connected with the fact that in these nuclei the $2s_{1/2}$ - and $1d_{3/2}$ - states of neutrons are not highly excited. From the point of view of captured neutron transitions, the M1-transitions in question must pertain to the $(ns_{1/2} \to 2s_{1/2})$ or $(ns_{1/2} \to 1d_{3/2})$ types, where $n > 2$. For both neutron transition types, the matrix element in the single-particle model is exactly equal to zero.

The Degree of Forbiddenness of M1-Transitions

In order to determine the degree of forbiddenness of the M1-transitions in question, it is necessary to compare their probabilities with the probabilities of allowed transitions, which are defined by equations of the single-particle model, i.e., to find the quantity

$$|M|^2 = \frac{\Gamma_{exp}}{\Gamma_B D/D_0}, \qquad (1)$$

where D is the density of neutron s-resonances with a given angular moment, and D_0 is the density of single-particle levels (with a given angular moment and parity) for small excitations.

In our case, the quantity Γ_{exp} can be found from the total radiation width Γ_γ and the number I_γ of γ quanta per single neutron capture for the given transition according to the equation $\Gamma_{exp} = \Gamma_\gamma I_\gamma$. In this, it is assumred that the total radiation width is the same for the neutron resonance, for which the value of Γ_γ was found and for the state created by the capture of a thermal neutron. The quantity Γ_B which enters (1) will determine the neutron transition probability found from equations for the single-particle model [5]. Taking into account the motion of the nucleus carcass, we shall accept the following values for neutron transitions:

$$\Gamma_B(E1) = 0{,}021\, A^{2/3} E_\gamma^3 \text{ ev}, \qquad (2)$$

$$\Gamma_B(M1) = 0{,}015\, E_\gamma^3 \text{ ev}, \qquad (3)$$

TABLE 1. Radiation Widths and Densities of Neutron s-Resonances of Nuclei with A From 20 to 40.

Nucleus	Na^{21}	Al^{28}	Si^{29}	S^{33}	Cl^{36}
E_{res}, kev	2,9	—	190	111	—0,14
Γ_γ, ev	0,4 [6]	0,24?	9 [6]	25 [6]	0,48 [7]
D, kev	400 [6]	50 [8]	500 [6]	200 [6]	40 [9]

where Eγ is expressed in megaelectron volts. It should be emphasized that the quantity D_0 has a high degree of indeterminancy.

Data on Γ_γ and D for nuclei with A from 20 to 40 are given in Table 1. These data are very inaccurate, and, in certain cases, it may possibly be wrong. By using data on Γ_γ and D for Si^{29} and S^{33} and by assuming that D_0 = 1 Mev, we obtain a very rough estimate for $|M|^2$. The value for $|M|^2$ is on the average equal to ~ 1.3 for E1-transitions, and it is equal to ~ 0.2 for M1-transitions. The $|M|^2$ values for actual M1-transitions are given in Table 2.

The degree of forbiddenness of M1-transitions can be determined also indirectly, namely, by comparing their probabilities with the probabilities of E1-transitions in a given nucleus.

Table 2 provides data on M1-transitions from the initial state in even-odd nuclei. This table* provides the characteristics of states between which the transition takes place, and also the quantity $|M|^2_{M1}/(|M|^2_{E1})_{max}$, where the subscript max in $|M|^2_{E1}$ signifies that this quantity is taken for the E1-transition, which has the highest probability of all E1-transitions from the initial state in a given nucleus.

All M1-transitions are divided into two large groups, which differ by the magnitude of change in the orbital neutron moment in transition. The M1-transition in Si^{29} to the level with an isotropic distribution of protons in the (d, p) reaction was additionally separated. The next to last column of Table 2 gives the magnitude of $|M|^2_{M1}$, which was found, as was indicated above, from Γ_γ and D for D_0 = 1 Mev.

It follows from the last column in Table 2 that if we assume that the probability of the most intensive E1-transition in a given nucleus is equal to the probability of a transition according to the single-particle model, the value of $|M|^2_{M1}$ for M1-transitions will be on the average equal to ~ 0.1. For the three transition types separated in the table, this magnitude will be approximately the same if we exclude transitions into states with l_n=0 in Ca^{41}, since these states are definitely not pure single-particle $2s_{1/2}$ states.

Wilkinson [11] considered the probability ratio of M1- and E1- transitions for light nuclei with A < 20. In this region of atomic weights, M1-transitions mainly take place between p-levels, and consequently these transitions can be considered as l-allowed. Unfortunately, it is not possible to compare the probabilities of E1- and M1-decays of the same state in light nuclei, as we did in the case of disintegration of a state created by the capture of thermal neutrons. The reason for this is either the insufficient investigation of γ-ray spectra or the equal parity of low levels in light nuclei. Therefore, a comparison of probabilities of E1- and M1- transitions can be done only for different states of light nuclei. †

According to [11], by taking into account the movement of the nucleus carcass and for D = D_0, we obtain for the average values:

$$|M|^2_{E1} = 0{,}15 \quad \text{и} \quad |M|^2_{M1} = 0{,}15,$$
$$\text{and} \quad |M|^2_{M1} / |M|^2_{E1} \simeq 1.$$

If we further assume that the matrix elements of E1-transitions in nuclei with A < 20 and with A from 20 to 40 do not differ much among themselves and if we consider that we are comparing the $|M|^2_{M1}$ values with the maximum value of $|M|^2_{E1}$, we can arrive at a qualitative conclusion that the probabilities of forbidden M1-transitions and of the l-allowed M1-transitions in light nuclei, which we have observed, do not differ to a great extent.

Causes of Prohibition Removal

In heavy nuclei with odd atomic weights, a large number of forbidden M1-transitions with $\Delta l = 2$ between lower levels is observed. Experimental data on these transitions are considered in more detail in the Appendix.

Possible causes of prohibition removal for such M1-transitions were studied in [12-18]. In particular, the following factors were considered: 1) interaction through the exchange of charges and spins between two nucleons; 2) a spin-orbital connection; 3) connection between nucleons and nucleus surface oscillations; 4) an admixture of other nucleon configurations in a given single-particle state.

---

* We consider that the $1/2^+ \to 3/2^+$ transitions are pure M1-transitions, since an admixture of E2-transitions can be expected only in the case where M1-transitions are strictly forbidden or if the probabilities of E2-transitions are greatly augmented due to collective effects. From the analysis that we performed, it follows that the forbiddenness of M1-transitions is small, and that the observed probabilities of E2-transitions correspond to single-particle evaluations [10].

† Wilkinson [11] did not consider separately nuclei with different parities of Z and N numbers, since he did not observe sharp differences in $|M|^2$ for different categories of nuclei. E1- as well as M1-transitions, which have been systematized by Wilkinson, can obviously contain various prohibitions (for more details, see [11]), however, we shall abstract them for the moment and consider only the l-prohibition.

TABLE 2. M1-Transitions of Even-Odd Nuclei from the Initial State

Transition type	Nucleus	J^π of the initial state	Final state characteristics			E_γ, Mev	I_γ, %	$\lvert M\rvert^2_{M1}$	$\frac{\lvert M\rvert^2_{M1}}{\left(\lvert M\rvert^2_{E1}\right)_{max}}$
			E, Mev	J^π	l_n				
$\Delta l_n=0$	Mg^{25}	1/2+	0,58	1/2+	0	6,74	2,6	—	0,1
	Mg^{25}	1/2+	2,56	1/2+	0	4,77	1,3	—	0,12
	Si^{29}	1/2+	B.S. *	1/2+	0	8,47	2	0,04	0,025
	S^{33}	1/2+	0,84	1/2+	0	7,80	2,6	0,47	0,15
$(s_{1/2}-s_{1/2})$	Ca^{41}	1/2+	2,68	1/2+	0	5,70	1,4	—	1
	Ca^{41}	1/2+	3,40	1/2+	0	4,94	3	—	1,5
$\Delta l_n=2$	Mg^{25}	1/2+	0,98	3/2+	2	6,36	4,3	—	0,2
	Mg^{25}	1/2+	2,81	3/2+	2	4,52**	<2**	—	<0,25
$(s_{1/2}-d_{3/2})$	Si^{29}	1/2+	1,28	3/2+	2	7,22	7,5	0,24	0,15
	S^{33}	1/2+	O. c.	3/2+	2	8,64	1,8	0,24	0,08
$1/2^+ \to 3/2^+$	Si^{29}	1/2+	2,43	3/2+	Isotr.	6,04	1,2	0,07	0,04

*B.S. – basic state of nucleus.

**The existence of this γ line has not been established; only an estimate of its intensity is given.

A study of causes indicated under 1) to 3) shows that they cannot augment the probability of M1-transitions from the (n, γ) reaction to a considerable extent. We shall not present an analysis of these causes, since it would be similar to the analysis performed, for instance, in [13]. The most natural explanation of the observed probabilities of M1-transitions is apparently the mixing of nucleon configurations in the initial and, possibly, in the final states. In this, it should be kept in mind that only the admixture which, in the corresponding transition, changes the state of only a single particle or changes the bond of a single moment with respect to another is of importance. At the same time, it should be noted that the adjacent states with the same parity will admix. Thus, the $s_{1/2}$, $d_{3/2}$, and $d_{5/2}$ states will be admixed to the $s_{1/2}$ and $d_{3/2}$ states with the greatest probability. For instance, in Si^{29}, M1-transitions can correspond to the following changes in neutron configurations:

For the $1/2^+ \to 3/2^+$ transitions, in the case of admixtures in the initial state,

$$[(d_{5/2}\, d_{7/2})_{J=2}\, d_{3/2}]_{1/2^+} \to [(d^2_{5/2})_{J=0}\, d_{3/2}]_{3/2^+},$$

and in the case of admixtures in the final state

$$[(d^2_{5/2})_{J=0}\, s_{1/2}]_{1/2^+} \to [(d_{5/2}\, d_{3/2})_{J=2}\, s_{1/2}]_{3/2^+};$$

for $1/2^+ \to 1/2^+$ transitions

$$[(d^2_{5/2}\, d_{3/2})_{J=1}\, s_{1/2}]_{1/2^+} \rightleftarrows [(d^2_{5/2})_{J=0}\, s_{1/2}]_{1/2^+}.$$

In the last case, the transition direction depends on the presence of admixtures in the initial or in the final state.

The appearance of mixed configurations of nucleons in the initial state is possible if a compound nucleus is formed. In this, the nucleon configuration energy can be concentrated in a whole number of possible nucleon configurations.

However, the assumption of the formation of compound nuclei in the initial state is contradicted by data on E1-transitions, in particular, by the correlation between the matrix elements of E1-transitions and the reduced widths of levels toward which these transitions are oriented [4].

Data on probabilities of E1- and M1-transitions from the state created by the capture of thermal neutrons can be coordinated without resorting to the conception of a compound nucleus. For this, it is sufficient to assume that in the capture of a neutron by the nucleus a small number of nucleon configurations are excited in the initial state, for instance, the configurations indicated above for Si^{29}. The probability of a direct transition of the captured neutron must be several times greater than the probability of the excitation of such configurations.

This assertion does not contradict the data on $|M|^2_{M1}$ values, since they are definitely smaller than $(|M|^2_{E1})_{max}$ for Mg^{25}, Si^{29}, and S^{33} nuclei.

M1-Transitions in Odd-Odd Nuclei

Data on M1-transitions in Na^{24}, Al^{28}, P^{32}, and Cl^{36} nuclei are given in Table 3. As in Table 2, the transitions are divided into groups in correspondence with changes in Δl_n. The transition to the energy level

of 0.47 Mev in Na^{24} is given separately. This transition apparently corresponds to the $s_{1/2} \rightarrow d_{5/2}$ change in the state of the last neutron, whereby the small transition probability can be explained. The presence of j-j-multiplets in odd-odd nuclei, which are caused by different mutual orientations of angular moments of odd neutrons and protons, leads to a considerably greater number of M1- transitions and, correspondingly, of levels with $l_n = 0$ and $l_n = 2$ in odd-odd nuclei with respect to even-odd nuclei [3].

It follows from data given in Tables 2 and 3 that the magnitude of $|M|^2_{M1}/(|M|^2_{E1})_{max}$ for odd-odd nuclei is considerably greater than that for the corresponding even-odd nuclei. However, we cannot accurately establish whether the increase in this ratio is connected with an increase in the probability of M1-transitions or with a decrease in the probability of E1-transitions.

On the one hand, there is no reason for assuming that the values of $(|M|^2_{E1})_{max}$ remain unchanged in the transition from odd-odd to even-odd nuclei. Table 1 provides approximate evaluations for $(|M|^2_{E1})_{max}$ obtained for Γ_γ and D values which are given in Table 1 and for $D_0 = 1$ Mev.

It follows from Table 4 that $(|M|^2_{E1})_{max}$ decreases on the average approximately 30-fold in the transition from even-odd to odd-odd nuclei, while $|M|^2_{M1}$ (see Tables 2 and 3) decreases only approximately three-fold. However, this comparison is not reliable, since the values of $\Gamma\gamma$ and D which we used are very inaccurate.

On the other hand, an increase in the probability of M1-transitions can be expected. This can be enchanced by the bond between an odd neutron and an odd proton. For instance, in certain transitions with $\Delta l_n = 0$, as was indicated in [19], a reorientation of the neutron angular moment with respect to the odd proton angular moment can take place, which would augment the probability of M1-transitions. Such transitions would be somewhat similar to the $^1s_0 \rightarrow {}^3s_1$ transition in a deuteron or to transitions between members of a j-j-multiplet, which is determined by different mutual orientations of angular moments of odd neutrons and protons. As is known, the matrix elements of such transitions are large [20-23].

Considering Table 3, it can be easily noticed that some of the transitions with $\Delta l_n = 0$, in particular, transitions with energies of 6.40 Mev in Na^{24}, 7.72 Mev in Al^{28}, 6.76 Mev in P^{32}, and 7.41 Mev in Cl^{36}, are actually distinguished by a great number of quanta per single neutron capture (0.1-0.7) as well as by the magnitude of $|M|^2_{M1}/(|M|^2_{E1})_{max}$ (it is equal to ~ 1.5 on the average).

APPENDIX

On M1-Transitions Between Slightly Excited States of Heavy Nuclei

A considerable amount of information on probabilities of M1-transitions between lower states of heavy nuclei with odd atomic weights is available in literature. In [12, 13, 24, and 25] the following regularity has been recently established for the forbidden M1-transitions with $\Delta l_n = 2$: the matrix elements have a small scatter in nuclei with an odd number of protons as well as in nuclei with an odd number of neutrons. In the first case, they are 300 times smaller, and in the second case, they are 60 times smaller than the respective values for M1-transitions which are allowed with respect to the single-particle model.

The indicated regularity is illustrated in Fig. 1. The lifetimes $\tau_\gamma E^3_\gamma$ for M1-transitions with $\Delta l = 2$ are given here. They are given separately for nuclei with an odd number of neutrons (left-hand side) and with an odd number of protons (right-hand side). The value for τ_γ was found from the following equation:

$$\tau_\gamma = 1{,}44\,(1+\alpha_{tot})\left(1+\frac{E2}{M1}\right)T_{1/2}.$$

The term E2/M1 takes into account the presence of an E2 admixture in a given transition. The results given in Fig. 1 have been, for the most part, published earlier in [12, 13, and 24]. The difference consists only in the fact that we found that our point for Tl^{203} ($E\gamma$ = = 0.279 Mev) lies considerably higher in correspondence with the new value for $\tau\gamma$, and that, in the left-hand side, the values for Cd^{111} ($E\gamma$ = 0.432 Mev) and Cd^{113} (E = 0.300 Mev) are added, which can be reliably calculated on the basis of data on Coulomb excitation.

The small scatter of matrix element values can be related to the fact that, within limits of each group of odd nuclei, all the transitions under consideration belong to the same type. In the case of an odd number of neutrons, we deal with $2d_{3/2} - 3s_{1/2}$ transitions, and in the case of an odd number of protons, we are concerned with $1g_{7/2} - 2d_{5/2}$ transitions, with the exception of Au^{197}, Tl^{203}, and Tl^{205}, where the transitions belong to the $2d_{3/2} - 3s_{1/2}$ type. In all probability, the attenuation of the forbiddenness in M1-transitions with $\Delta l = 2$ and $\Delta j = 1$ is connected with configuration mixing [18]. Naturally, it will manifest itself in different ways in different transition types. This explains the different degrees of forbiddenness in M1-transitions in odd-neutron and odd-proton nuclei.

The spin-orbital interaction must play a certain role in the attenuation of forbiddenness, in M1-transitions in odd-proton nuclei. In order to determine the influence of configuration mixing on the probability of M1-transitions in nuclei of this category, the contribution of the spin-orbital interaction should be evaluated more accurately than it was done in [13].

Beside l -forbidden M1-transitions, we considered also other relatively reliably established M1-transitions in heavy odd nuclei (A > 90) with measured τ_γ values.

TABLE 3. M1-Transitions of Odd-Odd Nuclei from Initial States

Transition type	Nucleus	J^π of the initial state	Final state characteristics			E_γ, Mev	I_γ, %	$\lvert M\rvert^2_{M1}$	$\frac{\lvert M\rvert^2_{M1}}{(\lvert M\rvert^2_{E1})_{max}}$
			E, Mev	J^π	l_n				
$\Delta l_n=0$ $(s_{1/2}-s_{1/2})$	Na^{24}	$1^+, 2^+$	0,56	2^+	0	6,40	22	0,059	1,2
	Na^{24}	$1^+, 2^+$	1,34	1^+	0	5,61	4,5	0,023	0,6
	Na^{24}	$1^+, 2^+$	1,84	$1^+, 2^+$	0	5,12	0,8	0,004	0,1
	Al^{28}	$2^+, 3^+$	B.S.	3^+	0	7,72	24	0,17	1,5
	Al^{28}	$2^+, 3^+$	0,03	2^+	0	(7,70)	<5	—	<0.3
	Al^{28}	$2^+, 3^+$	0,97	2^+	0	6,76	1,7	0,017	0,2
	Al^{28}	$2^+, 3^+$	2,14	$2^+, 3^+$	0	5,60	1,2	0,022	0,2
	Al^{28}	$2^+, 3^+$	2,49	$2^+, 3^+$	0	4,73	<8	—	—
	Al^{28}	$2^+, 3^+$	3,29	$2^+, 3^+$	0	4,42	1	0,037	0,4
	Al^{28}	$2^+, 3^+$	3,35	$2^+, 3^+$	0	(4,38)	<0,3	—	<0,12
	Al^{28}	$2^+, 3^+$	3,67	$2^+, 3^+$	0	4,06	2	0,094	1
	Al^{28}	$2^+, 3^+$	3,70	$2^+, 3^+$	0	(4,03)	<0,5	—	<0,25
	Al^{28}	$2^+, 3^+$	4,24	$2^+, 3^+$	0	2,98	<8	—	—
	P^{32}	$0^+, 1^+$	0,51	$0^+, 1^+$	0	7,42	4	—	0,6
	P^{32}	$0^+, 1^+$	1,15	$0^+, 1^+$	0	6,76	10	—	2
	Cl^{36}	$1^+, 2^+$	1,16	$1^+, 2^+$	0	7,41	10	0,19	7
	Cl^{36}	$1^+, 2^+$	1,60	$1^+, 2^+$	0	6,96	1,9	0,05	2
$\Delta l_n=2$ $(s_{1/2}-d_{5/2})$	Al^{28}	$2^+, 3^+$	1,63	—	2	6,13	3	—	0,5
	P^{32}	$0^+, 1^+$	O. c.	1^+	2	7,94	0,3	—	0,03
	P^{32}	$0^+, 1^+$	0,08	2^+	2	7,85	0,9	—	0,1
	Cl^{36}	$1^+, 2^+$	O. c.	2^+	2	8,56	2,8	0,035	1,5
	Cl^{36}	$1^+, 2^+$	0,79	—	2	7,78	7,8	—	5
$\Delta l_n=2$ $(s_{1/2}-d_{5/2})$	Na^{24}	$1^+, 2^+$	0,47	1^+	2	(6,49)	<0,1	—	<0,03

Remarks: 1) B.S. – basic state of nucleus. 2) The figures in brackets denote the energies of undetected γ lines; their intensity is estimated. 3) For excited levels of odd-odd nuclei, as a rule, only l_n is known, but, regardless of the indeterminancy of J values, we can state that the transitions to levels with $l_n = 0$ are M1-transitions; the transition corresponding to $(\lvert M\rvert^2_{E1})_{max}$ is the most probable transition of all the transitions oriented to levels with $l_n = 1$.

TABLE 4. Evaluation of $(\lvert M\rvert^2_{E1})_{max}$ Values

Parity of Z and N nos.	Nucleus	E_γ, Mev	I_γ, %	Characteristics of states			$(\lvert M\rvert^2_{E1})_{max}$
				J^π of the init. state	final		
					J^π	l_n	
Even-odd nuclei	Si^{29}	2,10	16	$1/2^+$	$1/2^-$	1	1,66
	S^{33}	2,97	13	$1/2^+$	$1/2^-$	1	2,95
Odd-odd nuclei	Na^{24}	2,41	10,5	$1^+, 2^+$	—	1	0,04
	Al^{28}	2,28	5,1	$2^+, 3^+$	—	1	0,11
	Cl^{36}	4,98	6	$1^+, 2^+$	—	1	0,025

The reduced lifetimes for these transitions are given in Fig. 2. The left-hand side of the figure shows the results which we borrowed from the exhaustive article on Coulomb excitation by McGowan and Stelson, which has appeared recently. In this work, reduced probabilities of M1-transitions were mainly obtained only for odd-proton nuclei. The values for $\tau_\gamma E_\gamma^3$ which have been calculated from these data, are given in the left-hand side of Fig. 2. The right-hand side displays the $\tau_\gamma E_\gamma^3$ values of M1-transitions for odd-neutron nuclei, which were calculated on the basis of data from [28].

Before we consider Fig. 2, it is necessary to say something about the separation of M1-transitions which entered Figs. 1 and 2. If reliably established transitions with $\Delta l = 2$ are represented in Fig. 1, Fig. 2 shows all the remaining transitions, the ones that are forbidden due to various causes as well as the allowed transitions. In particular, a small part of transitions with $\Delta l = 2$ can happen to be in Fig. 2. It should be noted that only transitions of the $nd_{3/2}-nd_{5/2}$, $ng_{7/2}-ng_{9/2}$, etc., types are allowed transitions in the single-particle model.

Passing to the left-hand side of Fig. 2, we shall note that the majority of transitions in odd-proton nuclei have a considerably greater probability than the transitions represented in the right-hand side of Fig. 1. It is also important that M1-transitions in Tl^{203} (0.400 Mev) and in Tl^{205} (0.410 Mev), which are allowed with respect to the single-particle model, have matrix elements which are close to single-particle evaluations, while M1-transitions with $\Delta l = 2$ in Tl^{203} (0.279 Mev) and in Tl^{205} (0.205 Mev) are much more severely forbidden than in other odd-proton nuclei (see right-hand side of Fig. 1).

A much smaller amount of data is available on M1-transitions for odd-neutron nuclei (right-hand side of Fig. 2). In this, for almost all of them, no information is available on the M1 + E2-transition mixtures. It should be emphasized that if the E2 admixture were taken into account, the points on the diagram would be shifted upwards. In the case under consideration, the majority of M1-transitions has very small matrix elements. The absence of matrix elements of M1-transitions which would be close to single-particle evaluations remains unexplained in the case of odd-neutron nuclei. This could be, perhaps, explained by the fact that this type of nuclei has not been sufficiently studied or by some other cause.

LITERATURE CITED

1. A. V. Shut'ko and D. F. Zaretskii, Zhur. Éksp. i Teor. Fiz. 29, 866 (1955).
2. A. Lane and J. Lynn, Report No. 4, submitted by Great Britain to the Second International Conference on the Peaceful Use of Atomic Energy (Geneva, 1958); J. Lynn, Proc. Intern. Conf. on the Neutron Interaction with the Nucleus, (New York, September, 1957).

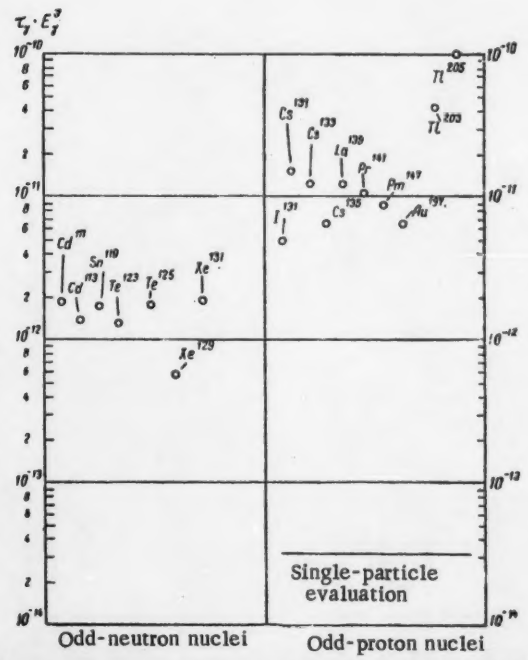

Fig. 1. Reduced lifetimes with respect to l-forbidden M1-transitions.

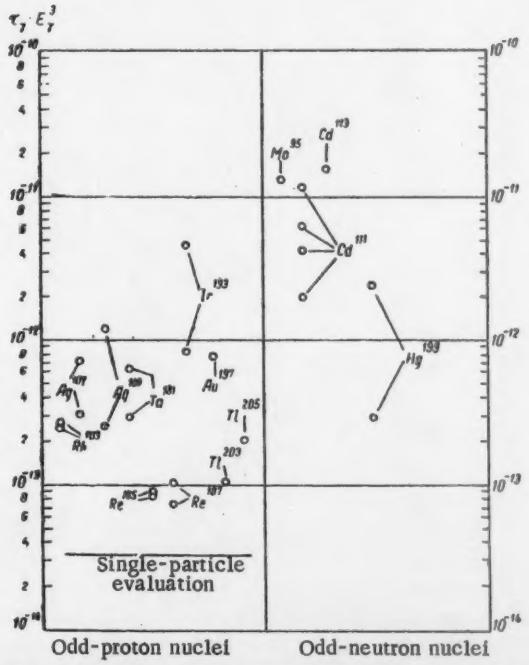

Fig. 2. Reduced lifetimes with respect to M1-transitions which are not related to l-forbidden transitions.

3. L. V. Groshev and A. M. Demidov, Atomnaya Énergiya 3, 8, 91 (1957). ‡
4. L. V. Groshev, A. M. Demidov, V. N. Lutsenko, and V. I. Pelekhov, Transactions of the Second International Conference on the Peaceful Use of Atomic Energy (Geneva, 1958), Vol. 1: Nuclear Physics [in Russian] (Atomizdat, Moscow, 1959) p. 281.
5. S. Moskowski, Phys. Rev. 89, 474 (1953).
6. L. Levin and D. Hughes, Phys. Rev. 101, 1328 (1956).
7. R. Brugger, J. Evans, E. Ioki, and R. Shankland, Phys. Rev. 104, 1054 (1956).
8. C. Hibdon, Report No. 2426, submitted by the USA to the Second International Conference on the Peaceful Use of Atomic Energy (Geneva, 1958).
9. D. Hughes and R. Schwartz, "Neutron cross sections," US AEC report BNL-325 (1958).
10. G. Bartholomew, P. Campion, J. Knowles, and G. Manning, Proc. Intern. Conf. on the Neutron Interaction with the Nucleus (New York September, 1957).
11. D. Wilkinson, Phil. Mag. 1, 127 (1956).
12. R. Graham and R. Bell, Canad. J. Phys. 31, 377 (1953).
13. H. De-Waard and T. Gerholm, Nuclear Phys. 1, 281 (1956).
14. R. Sachs and M. Ross, Phys. Rev. 84, 379 (1951).
15. A. Russek, Phys. Rev. 99, 834 (1955).
16. E. Feenberg, Shell Theory of Nuclei (Princeton, 1955) p. 211; P. Goldhammer, Phys. Rev. 101, 1375 (1956).
17. A. Volkov, Phys. Rev. 94, 1664 (1954).
18. A. Arima, H. Horie and M. Sano, Progr. Theoret. Phys. 17, 567 (1957).
19. D. P. Grechukhin, Zhur. Eksp. i Teor. Fiz. 33, 183 (1957).
20. J. M. Blatt and V. F. Weisskopf, Theoretical Nuclear Physics (John Wiley, N. Y., 1952).
21. J. Severins and S. Hanna, Phys. Rev. 100, 1254 (1955).
22. A. DeShalit, Phys. Rev. 105, 1537 (1957).
23. M. Goldhaber and W. Weneser, Annual Rev. Nucl. Sci. 5, 1 (1955).
24. T. Alvager, B. Iohansson, and W. Zuk, Arkiv fysik 14, 373 (1958).
25. T. Lindqvist and I. Marklund. Nuclear Phys. 1, 281 (1956).
26. K. Way et al., Annual Rev. Nucl. Sci. 6, 129 (1956).
27. F. McGowan and P. Stelson, Phys. Rev. 109, 901 (1958).
28. D. Strominger, J. Hollander and G. Seaborg, Rev. Mod. Phys. 30, 585 (1958).

‡Original Russian pagination. See C. B. translation.

GROWTH OF URANIUM RODS IN AN AGGRESSIVE GASEOUS MEDIUM

I. V. Batenin, A. N. Rudenko, and B. V. Sharov

Translated from Atomnaya Énergiya, Vol. 7, No. 4, pp. 329-332
October, 1959,
Original article submitted February 13, 1959

This article describes the growth (increase in length) of uranium specimens which takes place when heated specimens are exposed to air, nitrogen, and carbon dioxide. The dependence of this growth on temperature, pressure of the medium, the rod diameter, and on the degree of initial uranium surface oxidation was determined. Also the growth of copper wire specimens was detected. A possible mechanism of the growth of uranium rods is suggested.

We investigated rods of technically pure uranium (diameter: 2-4 mm; length: up to 100 mm), where the deformation texture was removed by hardening, which was checked by dilatometric and roentgenographic methods.

The elongation of rods was measured with respect to the distance between the end faces, which were previously polished to a metallic sheen, or with respect to the change in distance between two notches that were made beforehand on the cylindrical surface. In certain cases the elongation was measured directly during experiments by means of an indicator system. Bent specimens were straightened out before measurements.

The rod specimens were placed in a quartz test tube 35 mm in diameter, which was connected to an auxiliary ~ 50-liter vessel. The gas pressure in this system could be varied from 10^{-2} mm Hg to atmospheric pressure. The test tube with the specimen was heated in an electric furnace. The specimen temperature was controlled by means of a thermocouple.

Growth of uranium rods on heating in air. When specimens 4 mm in diameter were heated at atmospheric pressure, their length changed (Table 1).

Figures 1, 2, and 3 show the growth of rods in relation to pressure in the system at temperatures of the α-, β-, γ-phases, respectively. Figure 4 shows the dependence of the growth rate of rods on their diameters. All other conditions being equal, specimens with a thin film of oxide on their surface grow faster than specimens with a clean surface. This fact was detected in the following manner. Rods in the γ-phase were first oxidized in air under a pressure of 100 mm Hg. Then, the formed oxide film was taken off some rods by pickling, and it was left on the other rods. The end faces of all specimens were cleansed. The rods were heated in a vacuum of 10^{-2} mm Hg to a temperature of 820°C and then, in order to prevent the formation of a thick film of oxides on pickled specimens, air (under a pressure of 100 mm Hg) was supplied for a short time (~ 1 min), after which the system was again evacuated. At the end of the experiment, the dimensions of pickled specimens did not change, while specimens with an oxide film were elongated by 0.4%.

Additional experiments on specimens with an axial deformation texture [010] showed that their growth rate at 500°C somewhat exceeds the growth rate of hardened rods (experiments were conducted over a period of 25 hr).

Growth of uranium rods on heating in nitrogen. The previously evacuated system was filled with nitrogen, from which oxygen was eliminated by passing it through

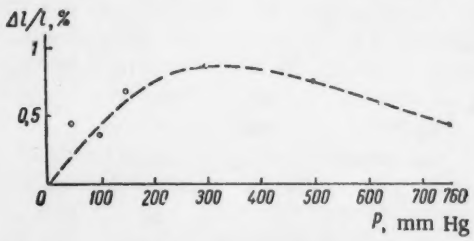

Fig. 1. Growth of uranium rods (d = 2 mm; l = = 100 mm) in relation to air pressure at 600°C for an exposure time of 6 hr.

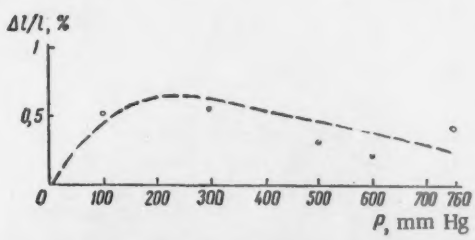

Fig. 2. Growth of uranium rods (d = 4 mm; l = = 100 mm) in relation to air pressure at 700°C for an exposure time of 15 min.

TABLE 1.

Specimen length before experiment, mm	Temperature, °C	Exposure time, min	Specimen length after experiment, mm
106.00	800	10	110.50
98.76	700	15	98.90
98.65	600	15	98.60

TABLE 2.

Specimen length before experiment, mm	Temperature, °C	Specimen length after experiment, mm
61.5	700	61.7
89.7	800	91.8

molten uranium. At normal pressure and temperatures corresponding to the β- and γ-phases, the rods became elongated. The growth of specimens 4 mm in diameter for an exposure time of 30 min is shown in Table 2.

Growth of uranium rods on heating in carbon dioxide. In experiments at atmospheric pressure, a growth of rods at temperatures corresponding to the γ-, β-, and α-phases was detected. Thus, at 800°C a rod 4 mm in diameter and 100 mm long was elongated by 6% in 10 min, at 700°C the rod was elongated by 3% and in the α-phase the growth begins with temperatures of ~ 500°C at a rate equal to one hundredth of a percent per hr.

Investigation of grown uranium specimens. The density of metal after growing remained practically constant with respect to the initial density. For instance, a specimen 4 mm in diameter and 83.63 mm long had a density of 18.60 g/cm^3. After exposure for 1.5 hr at 820°C in air under a pressure of 100 mm Hg, it was elongated by 15% and its density (after removing the surface film by pickling) was 18.57 g/cm^3. The growth of rods at the temperatures of β- and α-phases does not cause any changes in the density of specimens.

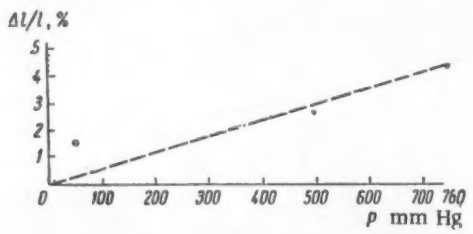

Fig. 3. Growth of uranium rods (d = 4 mm; l = = 100 mm) in relation to pressure at 800°C for an exposure time of 10 min.

The end faces of uranium rods which lengthened, to a great extent assumed the shape shown in Fig. 5 (fine longitudinal cracks were observed on the cylindrical surface; as a rule, the rods were bent). The surface of the uranium rods which grew, after the film was removed by pickling was heavily pitted. The depth of the narrowest cavities attained ~ 0.3 mm.

An x-ray analysis revealed cubic face-centered lattices with a parameter of 5.31 A on the surface of a uranium rod grown by heating in air. Such lattices correspond to a UO_2* structure.

If we assume that the film is continuous and uniform after the growth of uranium rods on heating in air, the film thickness depends on the medium pressure and temperature at which the growth occurred, and it hardly depends on the exposure time. For instance, at 800°C and under normal air pressure, the film thickness is equal to 0.13-0.14 mm. The thickness of a film formed at 700°C and under a pressure of 1 atmos is equal to 0.026 mm. However, if the air pressure is reduced the film thickness considerably increases for the same temperature, and the time required for its formation is, of course, longer.

The density of the film which was formed on the uranium surface in air during its growth varies between

* J. J. Katz and E. Rabinowitch, Chemistry of Uranium [Russian translation] (IL, Moscow, 1954).

11.6 and 13.2 g/cm^3 depending on the temperature and pressure under which the growth took place. This dependence has a rather complicated character. The density tends to increase with a decrease in pressure. The film density was determined by weighing oxidized specimens and specimens that were pickled in cold concentrated nitric acid (for the purpose of removing the oxide film) in air and alcohol.

Growth of copper wires. A 0.5-1 mm ϕ copper wire which is heated at 900°C in air for 30 min becomes elongated by several percent. All other conditions being equal, the growth rate of this wire is inversely proportional to its diameter, as in the case of the growth of uranium rods (see Fig. 4). For the same heating in a vacuum of 10^{-4} mm Hg the copper wire length did not change.

The state of the wire surface also affects its growth. For instance, copper wire specimens were oxidized at 900°C. Then the oxide film of some specimens was removed by pickling, and other specimens remained oxidized. All specimens were heated in vacuum to 900°C. As in the case of uranium rods, air was admitted in the vacuum system for a short time, after which the system was again evacuated. At the end of the experiments the oxidized specimens became elongated, and the dimensions of specimens with a clean surface did not change.

A possible mechanism of the growth of uranium rods. The available experimental data suggest the following possible mechanism in the growth of rods heated in an aggressive medium (oxygen and other gases). Oxygen diffuses the heated uranium rod, then a film of lower oxides ($UO+UO_2$) is formed on the rod. The oxidation is not uniform (it depends on the crystallographic directions). Thus, a color mosaic was observed on the electropolished surface of uranium which had been exposed to air. By the x-ray method, we were able to establish that the (020) planes in α-uranium are most intensively oxidized, and the (002) planes are oxidized least.

In the course of time, the oxidation of lower oxides takes place simultaneously with the diffusion processes.

It was shown by experiments that the growth of rods is caused by oxygen which diffuses in the film and oxidizes the lower oxides. The film penetrates to a depth of 0.3 mm. Since the density of higher oxides is smaller than the density of lower oxides, large tensile stresses appear in the rod; however, the density of the rod core does not change. During the oxidation process, the layer which contains both the metal and its oxides gradually crumbles and is transformed into higher oxides, which secures a constant thickness of the stretching layer. It was experimentally established that the rod growth is inversely proportional to its diameter. This agrees with the proposed mechanism, since the amount of the diffused gas, all other conditions being equal, is proportional to the rod surface (i.e., to its diameter), and the tensile resistance of the rod is proportional to the rod cross section (i.e., to the square of the diameter). Since no balancing forces are present at the junction between the end face and the cylindrical surface, the edge is pushed away from the rod (Fig. 5).

As was shown by experiments, oxygen participates most actively in the growth process of uranium rods if suitable conditions for the formation of lower oxides are maintained. An optimum pressure region exists for the maximum growth of uranium for a given temperature (for the temperature regions of α- and β-phases). Excess oxygen, which causes vigorous oxidation and the formation of higher uranium oxides, can reduce the growth in certain cases since the lower oxide film does not reach a thickness necessary for the growth of rods. For instance, if a uranium rod 4 mm in diameter is heated in open air at 600°C, it does not grow and its

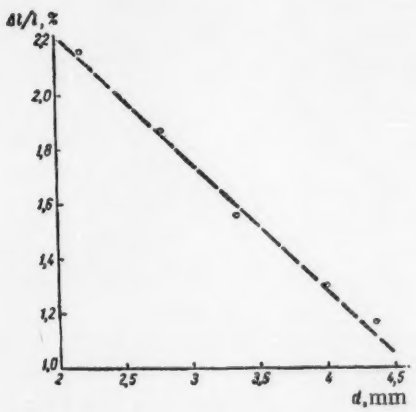

Fig. 4. Growth of uranium rods in relation to their diameter. The specimens were heated for 30 min at 710°C in air under a pressure of 300 mm Hg.

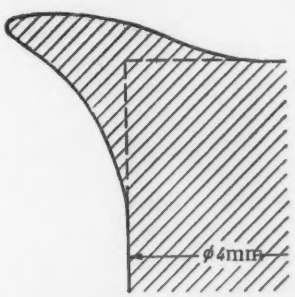

Fig. 5. Axial cross section of a uranium rod elongated by 5%, heated in air at 800°C over a period of 10 min.

length decreases because of oxidation. However, the formation of lower oxides on the uranium surface in the γ-phase is so vigorous that even the oxidation of this film in air cannot materially reduce its thickness, and the rods become elongated.

For the sake of simplicity, we have considered the growth mechanism of uranium rods which was brought about by the interaction between the rods and oxygen. However, in growth in a nitrogen atmosphere or at a sufficiently high temperature in an air atmosphere, uranium mononitride which can develop into higher nitrides, can play the role of monoxides. In growth in an atmosphere of carbon dioxide, the latter, as is known, is decomposed in the presence of uranium, and oxides and carbides are formed on its surface. The growth of copper wires can also be explained by the transition of the Cu_2O oxide on their surface into the higher CuO oxide.

The growth effect should be taken into account in producing thin uranium rods by heat treatment in air (and in other aggressive media) and also in experiments where thin uranium rods are used.

In conclusion, the authors extend their gratitude to P. A. Petrov for his guidance in the work.

EXPERIMENTAL INVESTIGATION OF THE CONDITIONS OF THE REDUCTION AND PRECIPITATION OF URANIUM BY MINERALS

R. P. Rafal'skii and K.F. Kudunova

Translated from Atomnaya Énergiya, Vol. 7, No. 4, pp. 333-337
October, 1959,
Original article submitted February 18, 1959

The article gives the results of an experimental investigation of the processes of reduction and precipitation of uranium by certain minerals widely distributed in hydrothermal uranium deposits. It is assumed that iron, sulphur, and arsenic, which are included in the composition of these minerals, reduced U(VI) present in hydrothermal solutions, as a result of which primary uranium minerals were deposited. The experimental investigation of these processes, which has been almost uninvestigated hitherto, is of great practical importance because it extends present representations of the physicochemical conditions favorable to the localization of uranium mineralization.

The experimental data obtained indicates that as a result of the reduction of U (VI) to U(IV) in acid solutions at temperature of 100-350° C, crystalline uraninite, collomorphic uranium "pitch", and sooty uranium blacks are formed. The character of the accessory minerals depends on the composition of the mineral-precipitant, the reaction temperature and, in some cases, the initial uranium concentration in the solution.

The results of the experiments confirm the working possibility of the formation of primary uranium minerals under natural conditions as a result of the reaction of solutions containing U (VI) with ore and vein minerals.

Introduction

According to present representations, oxidation reduction processes play an important role in processes of uranium transfer and the formation of primary uranium minerals during the formation of hydrothermal deposits. It is assumed that the reduction and precipitation of uranium was able to take place as a result of the reaction of uranium-bearing solutions with minerals and rocks containing reducing agents [1, 2]. The present work is devoted to the results of an experimental investigation of these processes.

A plate of mineral-precipitant of thickness 0.2-0.4 mm was placed in a quartz ampoule and several milliliters of a solution of UO_2SO_4 were introduced. After the ampoule had been evacuated and sealed, it was heated at the predetermined temperature, which up to 200°C was maintained with an accuracy of ± 5°C, while at higher temperatures the accuracy was ± 10° C. At the end of the experiment the ampoule was cold-water cooled. The accessory minerals were investigated using a microscope and x-ray analysis, which was carried out by the polycrystalline method using unfiltered Fe-radiation. The photographs were taken with a URS-55 camera in RKZ cells (φ = 57.3 mm). The conditions for taking the photographs were: 35 kv, 12 ma. When the constants were calculated (accuracy 0.005 A) the variation in the thickness of the sample was taken into account because in certain cases the amount of material was limited and the thickness of the sample reached 0.1 mm. For this reason, the exposure was increased from 3 to 5 hours.

The uranium precipitants were native minerals, with the exception of pyrrhotine which was synthesized in the laboratory. Chalcopyrite contained individual inclusions of quartz, while native arsenic contained a very fine emulsion dissemination of arsenides (?). Chemical analysis of the siderite* gave the following results (%): FeO 45.76; MgO 8.59; CaO 0.24; MnO 1.42; Fe_2O_3 0.75; CO_2 39.00; insoluble residue 3.94; total 99.70.

Results of the Experiment

At elevated temperatures uranium was reduced and precipitated from acid uranyl sulfate solutions by pyrite, pyrrhotine, galena, chalcopyrite, siderite, smaltine, and native arsenic, the composition of which included

* The analysis was carried out by B. M. Eloev.

TABLE 1. Relation Between the Lattice Constant of UO_2 and the Conditions of Formation.

Mineral-precipitant	Uranium content in the initial solution, g/liter	Temperature, °C	Heating time, hours	Lattice constant, A
Pyrite	2	150	120	(U_3O_8)
"	2	200	113	5.46
"	2	250	113	5.46
"	2	350	116	5.47
Siderite	2	100	72	5.39*
"	2	150	120	5.38*
"	2	200	113	5.35* (5.46)
"	2	250	113	5.40 (5.46)
"	2	350	116	5.42
"	10	100	72	5.40
"	10	200	118	5.45
"	10	300	100	5.46
Galena	2	150	120	5.44
"	2	200	113	5.45
"	2	250	113	5.46
"	2	350	116	5.46

* The constant was determined approximately because of the high degree of diffusion of the lines.

Fe, S, or As in their lower valence states. As a result of oxidation-reduction actions, a coating of UO_2 was formed on the mineral-precipitant, hematite was precipitated on the walls of the ampoule or in a mixture with UO_2, and an emulsion of elemental sulfur was formed on the surface of the solution. The character of the UO_2 formed depends mainly on the composition of the mineral-precipitant and the heating temperature.

The influence of the composition of the mineral-precipant was expressed very markedly in certain cases. If the uranium concentration in the initial solution of UO_2SO_4 was 2 g/liter, crystalline uraninite which completely covered the plate, was formed on pyrite, galena, chalcopyrite, and smaltine† at a temperature of 250° C in 70-80 hours (Fig. 1). The diameter of the individual cystals of uraninite did not usually exceed 0.005 mm, and was sometimes 0.001 mm or less. The most widely distributed forms of the crystals were octahedrons and cuboctahedrons. Concretions were often observed. Large crystals with a diameter of up to 0.05 mm formed accumulations covering ~ 50-60% of the area of the plate in some cases.

That these accessory minerals are associated with uraninite is confirmed by the data of x-ray analysis and also by the fact that their character is independent of the composition of the above-listed mineral-precipitants.

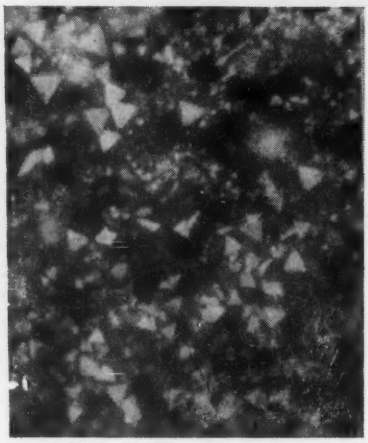

Fig. 1. Uraninite associated with galena: concentration of uranium in the initial solution 2 g/liter; T = 250° C; heating time 27 hours; magnification 600.

† The nature of the precipitate with pyrrhotine was not determined because the initial preparation was only of fragmental size.

The character of UO_2 precipitated by siderite is quite different. Under these conditions siderite was covered with a velvet-black powdery coating (very similar to uranium black), the relationship of which with UO_2 can be accurately established only by x-ray analysis.

The very fine collomorphic deposits of uranium pitch, similar in reflecting power to uraninite, occupies an intermediate position between crystalline uraninite and the powdery uranium blacks. A compact coating of collomorphic uranium pitch was formed during the reduction of uranium by native arsenic.

X-ray analysis showed that synthetic uraninite has a very high lattice constant (5.46 A), which remains unchanged when it is precipitated under similar conditions on pyrite, pyrrhotine, chalcopyrite, galena, and smaltine. The lattice constant of collomorphic uranium pitch was somewhat higher (5.47 A). On the other hand, a low constant, not exceeding 5.40 A is characteristic for UO_2 precipitated on siderite. In this case, splitting up of the diffraction lines – indicating the formation of a secondary amount of the second phase with a higher constant (~ 5.46 A) – was observed on the powder diagrams. In contrast to the fairly clear lines of uraninite, the lines of uranium pitch and uranium black on the powder diagrams are very diffuse.

The influence of temperature. A very fine-grained aggregate, in which the presence of U_3O_8 was established by x-ray analysis, was formed at 150° C in 120 hours on pyrite. Under similar conditions a precipitate having a crystal lattice of UO_2 was formed on galena. At 200-350° C crystalline uraninite was obtained on pyrite and galena.

The influence of temperature was most clearly shown during the precipitation of uranium by siderite. If the uranium concentration in the initial solution was 2 g/liter, at 100-200° C siderite was covered with a powdery velvet-black sooty coating. The indistinct outlines of the deposits were distinguished with difficulty under the microscope. With an increase in temperature, the deposits became more compact and changed color. The deposits obtained at 350° C were fairly compact and had a dark-gray color. The surface of the plate became shagreen-like as a result of the formation on it of nodular deposits of UO_2; these deposits were distinguished under a binocular magnifier at low magnification. The rounded or irregular outlines of the individual deposits were visible under the microscope with a very low reflecting power.

If the uranium concentration in the initial solution was 10 g/liter, at 100° C the siderite was covered with a coating of UO_2, the surface of which also had a nodular structure but of a finer character than in the previous case. An investigation of the deposit with an

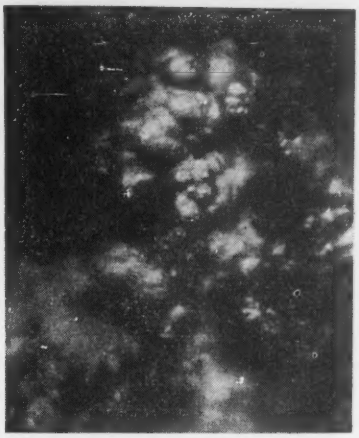

Fig. 2. Uranium pitch on siderite: concentration of uranium in the initial solution 5 g/liter; T = 200°C; heating time 41 hours; magnification 1800.

TABLE 2. Relation Between the Lattice Constant and the Initial Concentration of the Solution.

Mineral-precipitant	Uranium content in the initial solution, g/liter*	Temperature, ° C	Heating time, hours	Character of the UO_2 precipitate	Lattice constant, A
Siderite	2	200	41	Sooty coating of uranium blacks	5.37
"	5	200	41	Fine-grained aggregate with areas of collomorphic structure	5.41
"	10	200	41	Crystalline uraninite	5.44
Pyrite	0.5	250	27	" "	5.46
"	2	250	27	" "	5.45
"	10	250	27	" "	5.46

*The pH of the UO_2SO_4 solution at uranium concentrations of 2, 5 and 10 g/liter is 3.6, 2.9, and 2.7, respectively.

immersion lens showed that the individual nodules consisted of very fine crystals with a diameter of less than 0.001 mm, among which crystals with the faces of an octahedron could be distinguished. Thus, as a result of the reduction of siderite by ferrous iron, crystalline UO_2 is already formed at a temperature of 100° C.

If the reduction and precipitation of uranium takes place at a temperature of 100° C or more, relatively large cubic and octahedral crystals of uraninite are formed.

With an increase in temperature the lattice constant of UO_2 increases appreciably (Table 1). This relation is shown very markedly for UO_2 precipitated from siderite, which fully agrees with the data of microscopic observations. The fact that a second phase with a constant of 5.46 A is formed on siderite at temperatures of 200-250° C, in addition to the phase with a constant close to 5.40 A, is also of interest. Its formation is detected by the appearance of additional lines, using high angles on the powder diagrams.

The influence of the UO_2SO_4 concentration in the initial solution is noted during the precipitation of uranium by siderite. With a uranium concentration of 2 g/liter, powdery uranium blacks are formed on siderite; the individual deposits of these blacks being indistinguishable under the microscope. If the concentration is increased to 5 g/liter, a fine-grained aggregate is formed at 200° C; at high magnification, areas with a typical collomorphic structure can be readily distinguishable in this aggregate (Fig. 2). In addition, individual very fine octahedral crystals of uraninite, which evidently grow on the surface of the collomorphic deposits, are found. With a uranium concentration of 10 g/liter in the initial solution, uraninite crystals with a diameter of up to 0.01 mm are formed on siderite. An increase in the crystallinity of the deposit with an increase in concentration is accompanied by an increase in the lattice constant of UO_2.

The influence of the initial concentration was not observed during the precipitation of uranium on siderite (Table 2).

In conclusion it should be noted that a change in the duration of the experiments from 6 to 113 hours (T = = 250° C) did not cause any qualitative changes in the character of UO_2 when it was precipitated on pyrite and galena. Uranium dioxide precipitated at 200-250° C on siderite gives additional lines of the second phase with a higher constant on the powder diagrams only with prolonged heating (76-113 hours).

SUMMARY

1. At elevated temperatures and pressures, U(VI) is reduced in acid solutions by iron, sulfur, and arsenic present in their lower valence states in the composition of natural minerals. As a result of reduction, uranium is precipitated as crystalline uraninite, collomorphic uranium pitch, or sooty coatings of uranium blacks.

2. The character of the UO_2 depends on the composition of the mineral-precipitant, due to the rate of reaction of the solution with the mineral. With siderite, which – like all carbonates – is readily soluble in an acid medium, the reaction takes place rapidly and finely dispersed precipitates of uranium blacks are deposited from the solution. With sulfides, which are slowly dissolving minerals, the solution evidently reacts very slowly. During this process crystalline uraninite is formed.

3. The character of the UO_2 also depends on temperature, an increase of which increases the lattice constant of UO_2. On the basis of the data of the work [4], it may be assumed that a more complete reduction of U(VI) occurs with an increase in temperature.

It is of interest that crystalline uraninite can be formed easily at 100° C whereas uranium pitch and even uranium blacks are precipitated at 250° C.

4. At a considerable velocity of the reaction of the solution with the mineral (precipitation on siderite), the character of the UO_2 depends on the uranium concentration in the initial solution. The formation of more coarsely dispersed precipitates with an increase in the concentration may be due to the slowing down of the reaction after the deposition of the first portions of the precipitate on the surface of the mineral-precipitant. It is also possible that the influence of the concentration is due to corresponding changes in the pH of the solution. With a reduction in the pH coarser crystals of UO_2 are formed [5].

The results of the experiments, on the whole, confirm the possibility of the deposition of primary uranium minerals under hydrothermal conditions by the reduction of U(VI) by the components of native minerals. It must be emphasized, however, that this by no means excludes the possibility of the transfer of uranium in hydrothermal solutions in tetravalent form. In this latter case the correlation of uranium pitch and uraninite with specific minerals and rocks might be explained, not by their reducing action, but by other causes, for example by the higher value of the pH of the solutions at the boundary with these minerals.

LITERATURE CITED

1. V. G. Melkov and L. Ch. Pukhal'skii. Prospecting of Uranium Deposits [in Russian] (Gosgeoltekhizdat, Moscow, 1957).
2. G. Adams and F. Stewart, Reports to the International Conference on the Peaceful Use of Atomic Energy (Geneva, 1955).
3. R. P. Rafal'skii, Geokhimiya No. 7, 67 (1956).
4. G. A. Sidorenko, Geokhimiya No. 1, 22 (1958).
5. R. P. Rafal'skii, Report No. 2067, presented to the Second International Conference on the Peaceful Uses of Atomic Energy (Geneva, 1958).

TECHNIQUES FOR THE PREPARATION AND IDENTIFICATION OF TRANSPLUTONIUM ELEMENTS*

A. Ghiorso

(University of California, Lawrence Radiation Laboratory, Berkeley, California)

Translated from Atomnaya Énergiya, Vol. 7, No. 4, pp. 338-350
October, 1959
Original article submitted May 21, 1959

A short review of the discovery of transuranium elements is given and methods of preparing and identifying them are described. The results of a thorough experimental check of the work of a group of scientists from the USA, Britain, and Sweden on the preparation of element 102 are given.

A radical new method used for preparing isotopes of element 102 is described in detail. Data on the properties of two isotopes of this element are given. The half-life of an isotope of element 102 with a mass number of 254 is 3 sec and the α-particle energy is 8.3 Mev. In 30% of the cases of decomposition, this isotope undergoes spontaneous fission. According to preliminary data, the isotope of element 102 with a mass number of 253 has an α-particle energy of 8.8 Mev.

The agreement of the results of this work with the data obtained by G. N. Flerov et al. is noted. In conclusion, possible ways of preparing and identifying elements with an atomic number Z above 102 are examined briefly.

Over the last 15 years we have witnessed the discovery of ten transuranium elements. The techniques employed in this field of investigation have changed greatly and reflect, in general, the developments in a number of other scientific directions. In the present article, most attention is paid to techniques for preparing and identifying elements 101 (mendelevium) and 102 and the possibility of applying the methods developed to elements with higher atomic numbers. Obviously, a short review of the discovery of all the transplutonium elements is of interest as it illustrates the gradual change in the experimental methods, starting from the time when chemical methods were particularly important to the present, when one can hardly limit oneself to purely chemical investigations. The synthesis of each new heavy element usually depended on the preparation of appreciable amounts of elements with lower atomic numbers and thus the discovery of new elements occurred more or less in jumps. It was necessary to acquire new knowledge and improve the old method before attempting to prepare the next transuranium elements. The knowledge obtained with the new method that differed radically from the old one was the key to the discovery of mendelevium and element 102. It is possible that the preparation and identification of elements beyond element 102 will require methods which differ even more in principle.

After the discovery of plutonium in 1940 by Seaborg et al. [1], no attempts were made for several years to prepare any heavier elements. During this time the technology of plutonium separation was developed and the required investigation of the chemistry of the actinides carried out; at the same time the procedures for work with lethal amounts of plutonium were being put into practice. It is possible that in the first years appropriate safety measures for work with this element were not always applied.

The first of the transplutonium elements discovered was element 96 (curium). In 1944, only after many unsuccessful attempts, Seaborg et al. [2] finally obtained the 160-day isotope Cm^{242}, by irradiating Pu^{239} with α particles on the 60-inch cyclotron of the Crocker Laboratory. A very thorough chemical analysis was required to identify the new element. This discovery was very useful; numerous chemical experiments were carried out with tracer amounts of the new element. Soon after this, in 1945, Seaborg et al. [3] discovered element 95 (americium). The isotope Am^{241} with a half-life of 500 years was isolated from plutonium irradiated in a reactor. It was established that americium is formed from the β-active isotope Pu^{241}. The chemical properties of americium and curium were found to be so similar that a method for completely separating these elements was only deve-

* Report read at the Eighth Mendeleev Congress in Moscow (March, 1959).

loped several years after their synthesis. The separation of these two elements was based on Seaborg's hypothesis that they belonged to a series of elements with chemical properties similar to those of the rare-earth elements. He named this series the actinides.

The equipment used for the discovery of Cm^{242} and Am^{241} was very simple. At that time the techniques of pulse analysis with an ionization chamber were not well developed and inaccurate counting methods had to be used to detect α activity. In order to determine the radiation energy, absorption curves of the radiation in mica were plotted and thus a relatively high activity was required for reliable measurements.

In the following years a new technique was developed successfully. At the same time several milligrams of Am^{241} were isolated and then irradiated with α particles in the cyclotron at Berkeley.

In 1949 element 97 (berkelium) was prepared by Thompson et al. [4] by the reaction $Am^{241}(\alpha, 2n)Bk^{243}$. The isotope Bk^{243} (K-capture, half-life 4.3 hours) was prepared in amounts sufficient to identify the new element. However, at that time there were no scintillation counters and it was therefore very difficult to investigate the characteristic x radiation of this element. Only the α decay could be measured and this was 0.001 of the total activity of Bk^{243}.

By this time, ionization chambers were so improved that they could be used to detect small amounts of α particles of a given energy. The ion-exchange method of chemical separation, used for rare-earth elements, was applied quite successfully to the chemical isolation and identification of berkelum. This method made it possible to separate the new element rapidly from the target material (Am^{241}). The high level of α activity in the target made thorough safety measures necessary.

Several months later, in 1950, on the basis of the work that lead to the discovery of berkelium, Thompson et al. [5] prepared element 98 (californium) by bombarding several micrograms of Cm^{242} with α particles. The isotope Cf^{245}, with half-life of 45 minutes was identified by its α activity. The number of californium atoms prepared was insignificant (approximately 5000 atoms), but as the chemical properties and electronic configuration of californium and curium were found to be different, it was possible to determine absolutely accurately the atomic number of the new element. It was established that the element was eluted from a cation-exchange column by a predicted solution volume.

It was considered that after the synthesis of californium, element 99 or the next one would be prepared only after several years. Two years were devoted to preparing other heavy element isotopes and increasing the knowledge of their nuclear properties. It was planned to synthesize elements with $Z > 98$ by irradiating plutonium in a reactor with a powerful neutron flux.

The discovery of elements 99 (later named einsteinium, E, in honor of Albert Einstein) and 100 (named fermium, Fm, in honor of Enrico Fermi) is an outstanding example of the unexpected in science. Both these elements were discovered in the products formed as a result of a thermonuclear explosion in November 1952 (operation "Mike"). The explosion products were collected on filter paper by special airplanes which flew through the cloud of radioactive dust and the products were delivered to a number of laboratories in the USA. Chemical investigations at the Argonne National and Los Alamos Scientific Laboratories showed that the explosion products contained several new, heavy isotopes of plutonium. From this it was concluded that new elements may also have been formed during the explosion as a result of numerous successive neutron captures by uranium. When these conclusions became known, we made an attempt to find heavy isotopes of transuranium elements with $Z > 98$ in the explosion products.

The new elements could be isolated by the ion-exchange method. Hundreds of kilograms of coral were collected from the atoll close to the test site; after the corals had been processed, einsteinium and fermium, that is, their isotopes E^{253} and Fm^{255}, were identified successfully. We carried out the preparation of these elements in 1953, but the work was only published in 1955 [6].

It is interesting to note that the amount of fermium first obtained was approximately 200 atoms. Essentially new techniques were not used then in experiments. The discovery was made possible by painstaking work based on long experiments.

At the beginning of 1954, plutonium that had been irradiated with a powerful neutron flux in a reactor for several years yielded isotopes of berkelium, californium, einsteinium, and fermium, which had previously been found in the rock taken from the region of the thermonuclear tests in 1952. As the amount of heavy elements obtained in the reactor was considerably greater than the amount of elements isolated from the explosion products, it was possible to irradiate 20-day E^{253} with helium ions in a cyclotron to obtain element 101. At that time, on the cyclotron in Berkeley we obtained heavy ion beams of relatively low currents with a continuous energy spectrum in the final radius. It was found that the yield of reactions in which only neutrons were emitted was very low and, therefore, it was useless to irradiate plutonium with nitrogen ions to obtain element 101.

Having obtained a sufficient amount of E^{253} by 1955, we attempted to synthesize the new element. We had 10^9 atoms of the isotope E^{253} and estimated that by using a helium ion beam (with a strength of

about 200 $\mu a/cm^2$), we would obtain approximately one atom of element 101 in the experiment, if the cross section of the predicted isotope of element 101 with a mass of 255 was ~ 1 mbarn. These calculations were based on the hypothesis that the half-life of the isotope of element 101 was several minutes.

We had to work extremely rapidly to isolate the minute amounts of the expected element 101 from the target material. We could not use the usual methods. Even if we were able to carry out the chemical isolation sufficiently rapidly, a new target had to be made for each repeated irradiation. As several irradiations were needed to detect an isotope with a half-life of the order of several minutes, the minute amounts for the targets would be used up rapidly during washing. Luckily, just before we started the experiments, a new method based on the use of recoil nuclei formed during the reactions was proposed and tested. It was thought that if a very pure target was made sufficiently thin, then the atoms of the new elements would be ejected from it and they could then be collected in a vacuum on a separate collecting foil. During a test irradiation of Cm^{244} to prepare Cf^{246}, it was found that high californium yields could actually be obtained if the target was carefully prepared electrolytically. As the track of a recoil atom is very short (approximately 50 $\mu g/cm^2$), the yield could vary greatly from one target to another.

Small amounts of Cm^{244} were introduced into the target in order to have an internal indicator of the yield. The focus of the internal beam of the Berkeley cyclotron was intensified so as to obtain a very high helium ion current density at the target. Then a probe was developed with a design such that rapid removal of the recoil nuclei collector was possible. After numerous tests in which the apparatus was adjusted, the experiments began.

The first experiments were limited to an examination of short-lived α activities. Many experiments gave no results and we were planning to terminate them. However, during one experiment a strong pulse from spontaneous fission was recorded. When this result was repeated in another experiment, we were convinced that the apparatus was sufficiently reliable. It could be assumed that a new isotope was obtained which underwent spontaneous fission with considerably greater probability than in the case of isotopes found previously. It seemed that Fm^{256} could be an isotope with such a high rate of spontaneous fission. It could form either directly by an (α, p) reaction or as a result of K-capture by an isotope of element 101 with a mass of 256. As the expected half-life of this isotope must be greater than that of the isotope of element 101 with a mass of 255, we assumed that by increasing the irradiation time we would be able to increase the yield of the element and this would make chemical operations possible. A chemical separation was necessary as the ion beam produced a high α activity in the gold foil collector and this hindered registration of radiations in an ionization chamber. The collector foil was rapidly dissolved and all the actinide elements were separated on an ion-exchange column. This usually required 5-10 minutes.

Then new experiments with a longer irradiation time were begun. Almost immediately we were rewarded by obtaining an average of one spontaneous fission per experiment.

Chemical separation showed that the spontaneous fission was caused by the actinides. In order to differentiate element 101 from fermium, we carried out additional chemical operations to separate different elements of the actinide group. Cation-exchange columns were used for this. The results of the first experiments were confirmed by the fact that cases of fission were observed in the transfermium and fermium fractions. In some experiments, spontaneous fission was observed in both fractions. For a more accurate determination of the position of the element undergoing spontaneous fission during its chromatographic elution from the column, more accurate experiments were set up.

Several experiments were carried out to extend the data obtained. The reaction products after each 3-hour irradiation were rapidly separated on an ion-exchange column. Isotope E^{253} was added and this, together with isotope Cf^{246} formed during the irradiation, made it possible to calibrate the column. Five spontaneous fission counters were used so that it was possible to investigate simultaneously the drops of eluent corresponding to the fractions of elements separated. As the elution curve shows, spontaneous fission was observed in both the fractions corresponding to element 101 and fermium.

We synthesized the isotope of element 101 with a mass of 256, which was converted by K-capture (with a half-life of ~ 30 min) into the isotope Fm^{256}, that fissioned spontaneously with a half-life of ~ 3 hours. As a result of eight experiments we then isolated only 17 atoms of element 101, but due to the original character of the experiment we decided to publish the results. The report on the discovery of element 101 was published in 1955 [7]. We named this element mendelevium (symbol Mv) in honor of the great Russin chemist Dmitri Ivanovich Mendeleev, who was the first to use the Periodic Law to predict the chemical properties of as yet undiscovered elements.

The discovery of mendelevium required particularly sensitive apparatus for recording the activity, as at first this element was identified by counting the number of atoms and was synthesized by conversion in a target which itself contained an unweighable amount of material. In investigating the other members of this series of previously unknown elements, we worked with small amounts of material, but never as little as in this case. Of course, by then the preparation of new

elements was quite familiar to us; it was based mainly on the possibility of detecting α radiation of heavy elements with high efficiency and reliability. Investigations of this type depend essentially on the possibility of identifying isotopes by α-particle energy. It is true that the alpha background did not fall to zero, but in this case it was practically absent as we were recording spontaneous fission.

Spontaneous fission was first discovered by G. N. Flerov and K. A. Petrzhak in 1940 for U^{238}. They established that spontaneous fission was a very rare phenomenon. After new elements with higher atomic numbers had appeared in the periodic table, it was shown that the probability of spontaneous fission increases rapidly with an increase in the atomic number of the element. For example, with the isotope Cf^{252} 3% of all decay cases were spontaneous fission; this means that its spontaneous fission half-life is 66 years. Until recently, Cf^{254} was the isotope with the shortest spontaneous fission half-life (60 days). It is known that Fm^{254} has a half-life of ~6 months. For this reason the 3 hour half-life found for Fm^{256} was so unexpected. This phenomenon made the discovery of mendelevium possible.

The results of the first work on the synthesis of mendelevium were later confirmed several times in our laboratory with the use of thicker targets; this made it possible to measure the half-life of mendelevium with great accuracy. It was found [8] that Mv^{256} has a half-life of 1.5 hours and that a more accurate value for the half-life of Fm^{256} is 2.7 hours. Furthermore, an α-active isotope with a half-life of 45 min was discovered (it probably formed during the decay of Mv^{255}).

The use of these methods allowed us to prepare and identify mendelevium; it was only two years later that work was published on the subject of new elements. As einsteinium was the heaviest of all the elements that the experimentors had in amounts sufficient for irradiation, the only method by which elements with atomic numbers above mendelevium could be obtained was by irradiation with ions with more than two protons. Thus, an attempt could be made to prepare isotopes of element 102 by irradiating curium with carbon ions.

Such experiments were carried out in Stockholm in 1957 by a group of scientists from the USA, Britain, and Sweden. In a series of very complicated experiments, curium was irradiated with C^{13} ions, accelerated in a cyclotron; a very low α activity was observed and this was ascribed to an isotope of element 102. This α-active product with a half-life of 10-15 minutes was eluted in chromatographic separation in the fraction corresponding to element 102.

An experiment consisted of irradiating a Cm^{244} target, ~1 mg/cm^2 thick, which was covered with a thin aluminum foil (50-100 μg/cm^2) and placed in a vacuum. The recoil nuclei passed through the aluminum foil and stopped in a thin plastic collector. Although they gave poorly reproducible results, nonetheless, numerous irradiations of a large number of targets showed that the observed activity had the characteristics mentioned above. The number of other radioactive elements obtained in the experiments was insignificantly small. In the work then published [9] it was reported that for five cases of decay, hypothetically assigned to the element 102, there was only about 1/10 count/min of Cf^{246} and a very small amount of Fm^{250}. The number of observed cases of decay assigned to element 102 was always found to be very small and, therefore, it was difficult to check this activity reliably. The C^{13} ion beam used in the experiments was 0.03 – 0.1 μa and the ion energy was ~90-100 Mev.

At approximately the same time, experiments were begun in Berkeley on the heavy ion linear accelerator HILAC in order to confirm the results of the Stockholm group. However, at first the ion beams from the HILAC accelerator were too weak and the Stockholm experiments could not be repeated. Making a test was impossible for a year. It soon became clear that we could not confirm their conclusions [10]. In 1957 we spent many months carrying out experiments of a different type and putting considerable effort into repeating what was found in Sweden. At first we bombarded several targets simultaneously with a recoil nucleus collector behind each. Since the beam intensity which we had was greater than that used in Stockholm, heating of the target by the beam was the whole problem. It soon became clear that it was impossible to irradiate the target in a vacuum and, therefore, we placed the target in a helium atmosphere and put the collector foils right against the targets. In order to be sure that we did not lose recoil nuclei in the protective foils, at first we did not use them at all. Later, in order to reduce the amount of curium ejected from the target, aluminum foils 100 μg/cm^2 thick were used.

In the first experiments a chemical method was used to separate the small amounts of curium ejected from the target by the bombarding beam. Many experiments were carried out with C^{12}, C^{13}, and O^{16} ions of various energies. However, our attempts to find a 10-minute activity with an α-particle energy of 8.5 Mev, which was ascribed to element 102, were unsuccessful, though we obtained ~100 counts/min for Cf^{246} and approximately the same activity for Cf^{245} and Fm^{250}. These amounts were hundreds of times greater than the amounts of the isotopes obtained in the Stockholm experiments. Not once did we observe pulses corresponding to an α-particle energy of 8.5 Mev, apart from those which were caused by the extremely low background of our apparatus.

In order to be sure that there were no errors, we continued our investigations. Palladium foils, 0.9 mg/cm^2 thick, were first used as collectors. Immediately after the irradiation, which usually lasted for about 30 minutes, we dissolved the palladium and

separated the actinide fraction from it. Approximately 5 min after the end of irradiation, we were able to record α particles of the actinide fraction on the analyzer.

It might have been expected that like californium, which evaporates readily from metallic uranium, element 102 would be even more volatile and, being held by a metallic foil, would evaporate when the foil was heated by the beam. To test this hypothesis we tried to collect recoil nuclei on a Mailar (a special plastic) collector. The collectors were cooled with helium to prevent them from burning. It was assumed that a recoil nuclei held in the collector would be oxidized and this would prevent their evaporation. The collectors were then burned on a platinum plate. In this way we were able to examine the reaction products on a pulse analyzer directly, without chemical operations, 1 min after the end of irradiation.

Again, though we obtained large amounts of Cf^{245}, Cf^{246}, and Fm^{250} we did not observe activities which could be ascribed to element 102.

We also used a method by means of which, it seemed to us, it would definitely be possible to record the 10-minute α-activity with an energy of 8.5 Mev, assigned to the isotope of element 102. This method, which is based on collection of recoil nuclei with an electrostatic field, was used for the first time to identify a short-lived isotope of element 102 (the method will be described later). After the successful preparation and identification of the short-lived isotope of element 102, we were sure that the method made it possible to detect the existence of isotopes with considerably longer half-lives. The recoil nuclei of element 102 were collected on a negatively charged aluminum plate placed near the target in a helium atmosphere. The aluminum plate could be analyzed on a pulse analyzer immediately after a short irradiation. We observed large amounts of Cf^{245}, Cf^{246}, and Fm^{250} on the plates, but did not detect any long-lived isotope of the element 102. Experiments with a beam whose intensity reached 0.25 μa were carried out over a wide range of energies.

A new method was used quite recently; in it the recoil products were collected on a continuous belt and analyzed almost immediately in a grid ionization chamber, placed next to the target system (the method will be examined at the end of the article). These experiments could also have demonstrated readily the existence of the hypothetical long-lived isotope of element 102.

Out doubts on the reliability of the Stockholm experiments, from which conclusions were drawn on the discovery of element 102, may be formulated in the following way:

1. We used curie targets of the same isotopic composition and irradiated them with monoenergetic C^{12}, C^{13}, and O^{16} ions over a wide range of energies. The intensity of our beam was ten times greater than that of the Stockholm cyclotron with a wide energy spectrum.

2. We used four different methods of collecting the recoil nuclei – the products of nuclear reactions. They all made it possible to detect only large amounts of actinide elements (reaction products), but a 10-minute activity with an energy of 8.5 Mev could not be obtained.

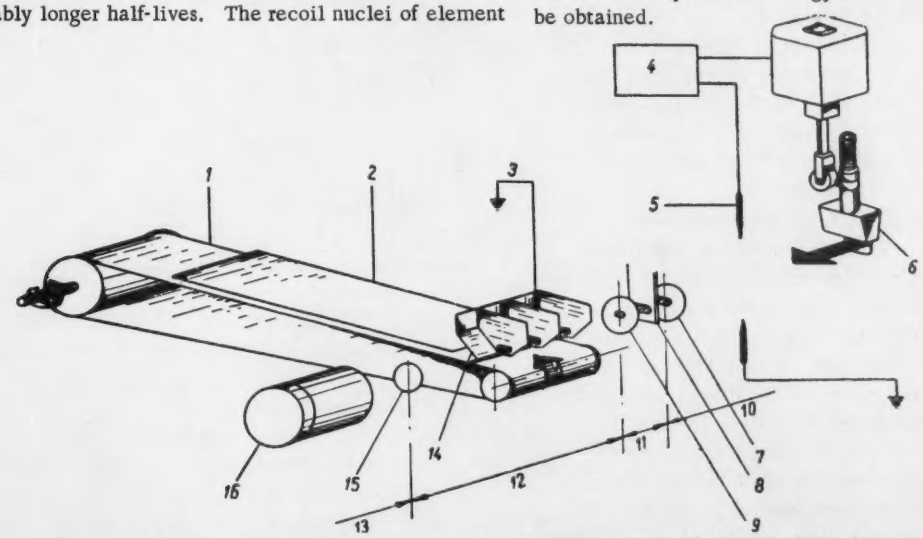

Fig. 1. Scheme of continuous experiment used in the discovery of element 102: 1) conveyor belt (-400 v); 2) collecting foil (-600 v); 3) target; 4) thyratron relay; 5) discharge gap; 6) shield; 7) foil separating helium space from vacuum system; 8) set of foils to reduce the energy of the primary beam; 9) foil of collimator; 10) vacuum; 11) helium cooling; 12) helium at atmospheric pressure; 13) vacuum; 14) teflon shield; 15) foil separating helium space from vacuum system; 16) Faraday cylinder

3. The conditions of our experiments and the Stockholm experiments were identical. In most of the latter experiments it was necessary to use thin aluminum foils for protection against curium ejected from the target. It seems to us that we can compare the amounts of Cf^{246}, Cf^{245}, and Fm^{250} obtained in our experiments with the amounts of the same elements, obtained in the experiments of the Stockholm group. We consider that this comparison of the irradiation conditions is more accurate than a comparison of the beam intensities.

4. In our experiments the unknown activity pertaining to element 102 would have been fixed as the method of collecting recoil nuclei with an energy field was applied successfully to the identification of the short-lived isotope of element 102.

The failure of our attempts to reproduce the Stockholm results can probably be explained by the following circumstances. Experiments on the cyclotron were extremely complicated as they were carried out on the internal beam of the cyclotron. The activity obtained was extremely low and varied sharply. In the best case in one experiment several decays were observed, but in most experiments nothing was observed. Of 50 irradiations, only 12 were successful. It is extremely probable that under these difficult experimental conditions the unknown activity is explained by the presence of impurities or other circumstances.

It should be noted that in most experiments on the cyclotron the energy of the C^{13} ions was 90 Mev; this corresponds to reactions with the evaporation of six or more neutrons and therefore the mass of the isotope 253 or less is most probable. It is quite probable that isotopes of element 102 with a mass of 257 or 259 will have a half-life of 10 min, but these isotopes may be obtained only by irradiation of heavier curium isotopes or by the use of bombarding ions of lower energies. It may also be expected that an isotope of element 102 with a half-life of 10 min would be more likely to have an α-particle energy of 8.0 Mev rather than 8.5 Mev.

The only conclusion from the data presented is that the activity found in the Stockholm experiment cannot be assigned to element 102.

After four months of unsuccessful searching for a 10-minute isotope of element 102, we attempted to record shorter-lived isotopes. A radically new method was needed for this purpose. It had been established [11] that under suitable conditions recoil nuclei (reaction products) may be collected almost completely on an electrically charged plate in a gas atmosphere. Long-range reaction products (with a range of 1 cm in helium at atmospheric pressure) may be slowed first in the gas and then collected on the surface of a conducting foil. If such products form a thin layer on the foil surface, then with α decay the daughter nuclei will be ejected from the foil due to recoil. Thus, in principle, it is possible to perform an experiment in which there is continuous separation of the daughter fermium, formed by decay of element 102.

Fig. 1 shows the scheme of an experiment for the preparation of element 102.

The target consisted of a mixture of curium istopes (95% Cm^{244} and 4.5% Cm^{246}), deposited on a very thin nickel foil 0.5 mg/cm^2 thick. It was covered with aluminum 75 μg/cm^2, for protection against ejection of curium. The curium was irradiated with a monoenergetic beam of C^{12} ions with an energy of 60-100 Mev. The atoms formed were stopped in helium. It was found that when the energy field had a sufficient voltage, practically all the positively charged atoms could be collected on a moving and negatively charged metal belt, arranged directly underneath the target.

Atoms of element 102 were transferred on the conveyor belt under a foil, negatively charged relative to the belt. Approximately half of the daughter atoms, formed by α decay of atoms of element 102, were ejected from the belt surface due to recoil and collected on the foil. After each irradiation the collecting foil was cut perpendicular to the direction of movement of the belt into five parts of equal length. After a delay corresponding to the half-life of the daughter product, each of the five foils was simultaneously analyzed for α decay with the aid of five chambers with a Frisch grid, fitted with amplifiers and analyzers with recording equipment. With this arrangement we could readily make all necessary measurements for identifying atoms collected on the foil and thus measure the half-life of the primary atoms. The method was first used successfully for identifying the new isotope Fm^{248}, obtained by irradiation of Pu^{240} with C^{12} ions. By determining the amount of 20-minute Cf^{244} transferred to the collecting foil it was established that the half-life of Fm^{248} equals 0.6 min.

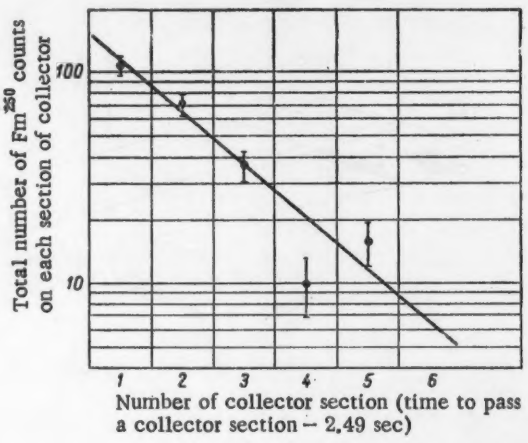

Fig. 2. Over-all result of many experiments showing the α decay of the 3-second isotope of element 102 with mass 254 into Fm^{250}.

After the reliability of the method had been proved, experiments were begun to detect short-lived isotopes of element 102. It could be expected that the most probable isotope would be that with a mass of 254. We considered that the half-life of this isotope, which yields 30-minute Fm^{250} that emits α particles with an energy of 7.43 Mev, would be a few seconds. From the nature of the distribution of the Fm^{250} activity on the moving belt we came to the conclusion that the half-life of the mother substance equaled 3 sec (Fig. 2). These nuclei were formed by the reaction $Cm^{246}(C^{12}, 4n)102^{254}$.

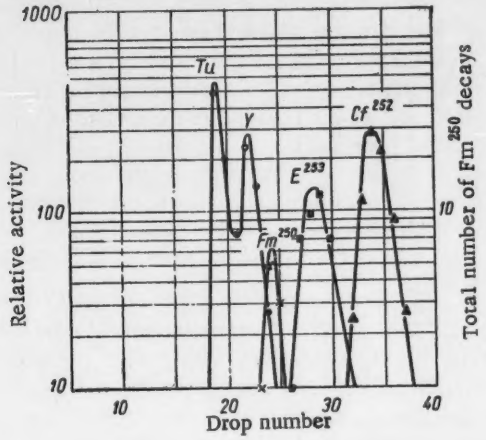

Fig. 3. Chemical identification of Fm^{250} obtained by α decay of the isotope of element 102 with a mass 254.

Similarly it was found that the excitation function for the formation of Fm^{250} has a sharp maximum at an energy of 70 ± 5 Mev and corresponds to a (C^{12}, 4 n) reaction, which agrees with recent calculations of the effective cross sections of this reaction. The collected atoms were ejected from the belt as a result of recoil during α decay; this was shown by the fact that neither Cf^{246} nor Cf^{245}, which were usually collected in very large amounts on the belt, were found on the collector. It was found that a change in the rate of motion of the belt led to a change in the distribution of Fm^{250} on the collecting foils, whose nature corresponded to a 3-second half-life. The number of Fm^{250} counts in a single experiment reached 40 and, hence, it follows that the maximum cross section of the reaction on Cm^{246} was approximately a few microbarns.

Conclusive chemical identifications of the atoms ascribed to Fm^{250} was carried out by a solution of the radioactive substance obtained on the collecting foil and its separation from other actinide elements by elution from a column of the cationite Dowex-50 with ammonium α-hydroxyisobutyrate. In the fractions corresponding to fermium, in one experiment we detected two and in another nine atoms of Fm^{250} (Fig. 3), which gave us confidence in the identification of element 102 in these experiments as a result of the extraction of its daughter element (fermium).

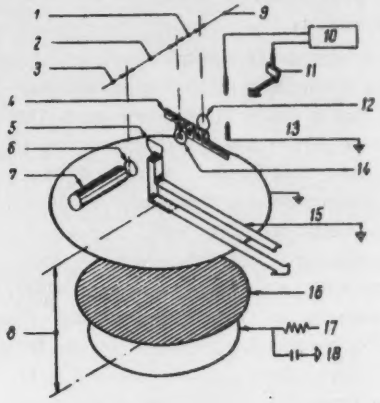

Fig. 4. Belt transporter and ionization chamber used for measuring the energy of α particles directly at the target: 1) helium cooling; 2) helium at atmospheric pressure; 3) vaccum for Faraday cylinder; 4) set of foils to reduce the energy of the primary beam; 5) target (+250 v); 6) foil separating helium space from vacuum system; 7) Faraday cylinder; 8) argon and 7% methane (at atmospheric pressure); 9) vacuum of linear accelerator; 10) thyratron relay; 11) shielding shutter; 12) foil separating helium space from vacuum system; 13) discharge gap; 14) collimator and window; 15) Mailar belt covered with aluminum; 16) Frisch grid (+830 v); 17) collecting electrode (+2500 v); 18) signal to preamplifier.

The work was published in July 1958 [12]. Somewhat later we learned of the excellent work of G. N. Flerov and his group [13, 14]. The method which they used, though it was quite different from ours, made it possible to demonstrate readily the existence of an isotope of element 102 with a mass less than 254. These experimenters reported that they did not observe any long-lived α activity with an energy of 8.5 Mev which could be ascribed to element 102, but they observed a short-lived activity with a half-life measured in seconds and with an α-particle energy of 8.8 Mev. These experiments were very difficult and complicated by the presence of a background caused by contamination of the target with a small amount of

lead. The target consisted of Pu^{241} and the bombarding particles were O^{16} ions, accelerated on the cyclotron of the Atomic Energy Institute of the Academy of Sciences of the USSR in Moscow. However, although it is very sensitive, this method did not make it possible to determine unequivocally the atomic number of the new α-activity.

After experiments demonstrating the existence of the isotope of element 102, we modified our apparatus so that it was possible to determine the energy of the α particles of this or other isotopes which could have been formed. In these experiments we used the method described previously, but with some important changes (Figs. 4-6). Instead of a continuously moving looped metal belt, we used a Mailar conducting belt 0.025 mm thick, which was made conducting on both sides with a thin film of aluminum. The recoil nuclei were slowed in helium and attracted to the belt by an electrostatic field. The belt was then drawn into a grid ionization α chamber, arranged near the target, and the decay products analyzed with a 100-channel pulse analyzer.

There were two methods of using this apparatus: 1) the belt was moved continuously from the target to the ionization chamber; 2) after a short irradiation, the belt was rapidly moved into the chamber and analyzed there while the next section was prepared for measurement.

The advantage of the second method was that the grid ionization chamber could be placed further from the target and thus shielded from the very intense α- and β-radiations produced by the beam of heavy ions. The other advantage of this method was the possibility of simultaneously measuring the half-lives of many isotopes by means of an addition counter connected to an α-particle pulse analyzer and an apparatus determining the time succession of pulses.

After 8 months of continuous refinements, we obtained an apparatus which was capable of registering short-lived α-active isotopes directly at the target with high reliability and excellent resolution. Although difficulties were encountered in the use of this method, its application was found to be extremely valuable. One of the many factors complicating the method was its sensitivity to the purity of the helium used in the target chamber. This was connected with the fact that on the one hand, we had to use a mixture of argon and methane in the grid α chamber for pulse analysis and, on the other, the belt had to be moved rapidly from the target chamber to the grid chamber. The fulfillment of both conditions required complex mechanical equipment. However, as a result of a series of modifications we constructed a quite satisfactory apparatus; with its aid we measured the α-particle energy of Fm^{248} (E_α = 7.8 Mev), whose 30-second half-life was established at the beginning of 1958 by continuous separation of Cf^{244} in experiments with a conveyor belt.

Quite recently we attempted to irradiate curium targets to detect α-active isotopes of element 102. We immediately encountered great difficulties due to the fact that very small amounts of lead in the target led to the formation of α particles with energies of 8.3 and 8.8 Mev and half-lives of 5-22 sec. By careful purification of the material of a new target

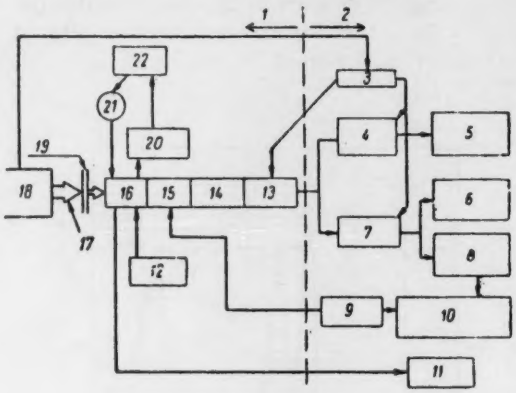

Fig. 5. Block scheme of electronic part of transport system: 1) target zone; 2) counting zone; 3) manipulator; 4) amplifier for pulses from fission fragments; 5) 100-channel amplitude analyzer of fission fragments; 6) 100-channel amplitude analyzer of α particles with wide channels; 7) α-particle pulse amplifier; 8) 100-channel amplitude analyzer of α particles with narrow channels; 9) synchronization regulator; 10) five 10-channel time analyzers; 11) beam current measurer; 12) source of target potential; 13) preamplifier; 14) grid ionization chamber; 15) transport belt; 16) target support; 17) beam; 18) heavy ion linear accelerator; 19) foils reducing energy of ions; 20) helium purifier; 21) helium; 22) gas imput regulator.

and electrolytic deposition of the target on pure nickel foil, we were able to reduce the background to an insignificant value. Unfortunately, our apparatus did not operate long and therefore we were unable to obtain conclusive results. We observed the formation of a 3-second isotope of element 102 whose α-particle energy was 8.3 Mev and also spontaneous fission, possibly of the same isotope of element 102 with a mass 254. The fraction of decays by spontaneous fission was unexpectedly high (30%), many orders higher than predicted. The activity obtained in these experiments did not exceed 10-20 counts/hr. Due to the difficulty and the complexity of the conditions of counting close to the target, we cannot be sure that this activity was actually caused by element 102 until new experiments are done.

In the experiments described we did not record appreciable numbers of α particles with an energy of 8.8 Mev, which were expected from the decay of the isotope of element 102 with mass 253. One of the most probable of the reactions observed in the Moscow experiments could have been the reaction $Pu^{241}(O^{16}, 4n)102^{253}$. In our case the same isotope must have been obtained by the reaction $Cm^{246}(C^{12}, 5n)\,102^{253}$. To increase the yield of this isotope we attempted to bombard curium targets with C^{13} ions. In this case the isotope of element 102 with mass 253 should be obtained by the reaction $Cm^{244}\,(C^{13},\ 4n)\,102^{253}$. The higher Cm^{244} content of our targets should have raised the yield of this reaction by a factor of at least 15. In these very recent experiments we observed short-lived α-particles with an energy of 8.8 Mev, which could have been caused by the isotope of element 102 with mass 253. If this effect is also observed in future experiments, it can be regarded as independent confirmation of the Moscow work. Our data are preliminary and some time will be required to obtain conclusive results.

I hope that we are able to investigate many isotopes of element 102. Other target materials which we will probably use soon are Cf^{250} and Cf^{252}. These will apparently make it possible to obtain isotopes of element 102 as their reactions with carbon ions proceed with a much greater effective cross section. They will also have the advantage of making it possible to obtain a number of heavier isotopes of element 102 and thus to determine many nuclear characteristics of the new element (Fig. 7). Then it may be possible to obtain isotopes (such as the isotope of element 102 with mass 259) which will be quite long-lived and make a chemical identification possible.

The way to apply this new method to the preparation and identification of elements beyond element 102 is clear, but the solution of this problem involves great difficulties. We now know that the cross section of the formation of very heavy elements is extremely small. Since only small amounts of target material may be used and we have comparatively low intensity ion beams available, it will probably be some time before success is achieved in any laboratory. To these difficulties is added the complication of the short half-life of decay by spontaneous fission. This is indicated by our very preliminary data showing the very great rate of spontaneous fission of the isotope of element 102 with mass 254. Under these conditions it will be very difficult to demonstrate that a new element has been found.

Spontaneous fission does not have sufficient characteristics for distinguishing between one element and another by this method as is done with α-particle radiation. However, even in this case, apparently it may be possible to obtain isotopes with an odd number of neutrons which are quite stable as regards spontaneous fission so that the α-particle energy of these isotopes may be determined.

It is extremely probable that elements 103 and 104 will be prepared after some time. The purpose of one

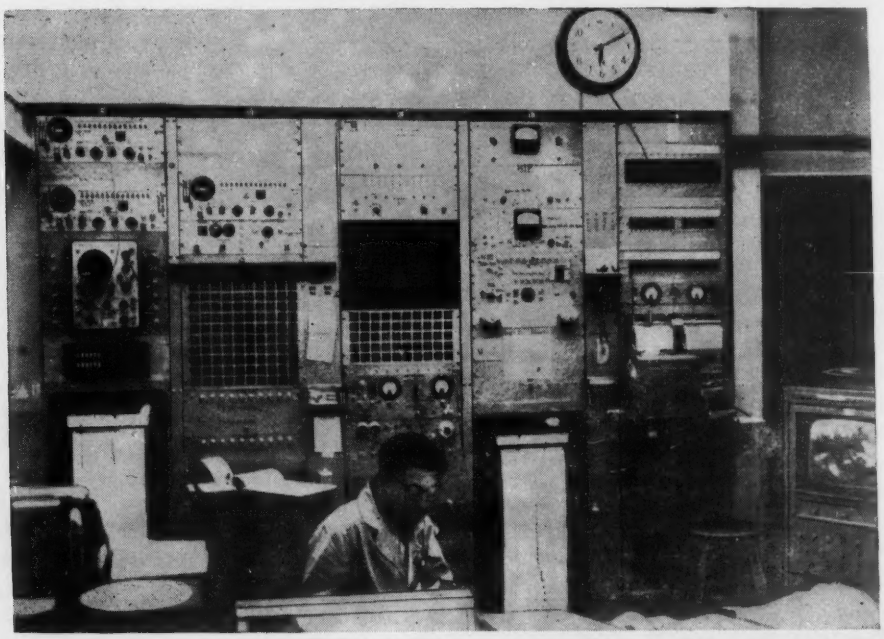

Fig. 6. Counting equipment (various analyzing apparatus can be seen).

of the main experiments which should be carried out when element 104 is discovered will be to show that it differs from element 103 and other elements of the actinide series. Element 103 represents the end of the actinide series, and therefore it will be very important to show that element 104 is an analog of hafnium.

I would like to examine a possible method by which this may be done, even with half-lives of the order of a few milliseconds. In the method proposed, the time of motion of an ion in a gas, moving under an electrical field, is measured. If an ion, after being slowed to thermal rates in the gas, is attracted by an electrical field of constant gradient, then it is possible that the time of motion of an ion of element 104 will be less than that of an ion of element 103 with approximately the same mass number. This follows from the fact that the ionic radius (which determines the rate of motion) of element 104 will be, according to expectations, 13% less than that of element 103. The changes in radius of other elements of the actinide series are very small. Thus, if it is possible to develop a method of separating ions with an appropriate resolution by using the difference in the time of motion, it may be possible to show an essential chemical difference between elements 103 and 104. We have considered several possible methods of carrying out such an experiment but have not had the time for testing them.

Another method which, it seems to me, has a real chance of success would make it possible to identify the mass number of a few reaction products. In this method use would be made of the fact that recoil nuclei, reaction products, may be slowed in a gas and drawn toward a small opening by an electrostatic field of suitable form. By means of differential evacuation it would be possible to transfer an atom through a small opening from a volume with a relatively high gas pressure, necessary for slowing the recoil nuclei, into a volume under high vacuum. After the single-charged ion has been introduced into the vacuum, a strong electric field must accelerate it to a high energy so that an analysis can be carried out with a magnetic field by the usual method. The ion may then be directed immediately into a counter for determination of its radioactive properties or detected with an electron multiplier and recorded as an ion of given mass.

Naturally, considerable difficulties will be encountered in putting these methods into practice, but I think that the great possibilities of these methods will completely justify the efforts made.

Another method may be used in the synthesis of elements of very great atomic number. It is possible that it will require the combined efforts of scientists of such countries as the USA and USSR. I am thinking of the irradiation of very large amounts of the heaviest elements in suitable containers with high neutron fluxes produced by nuclear explosions. If 10 g of Cf^{252} were irradiated in this way one would expect to obtain very heavy isotopes which would decay to form nuclei lying in a region of new stability and, as a result, obtain superheavy elements. These possibilities do not lie

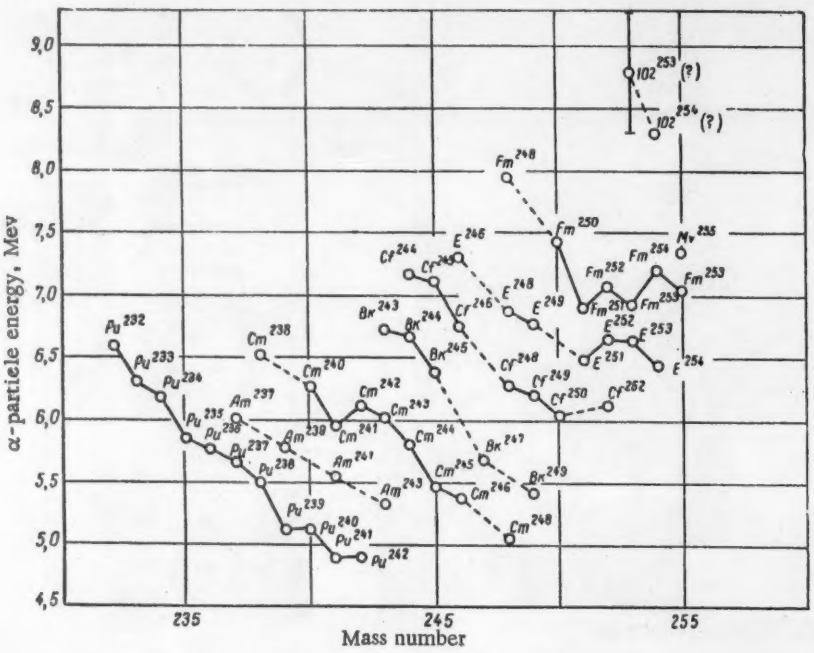

Fig. 7. Relation between α-particle energy and mass number, including new data for isotopes of element 102 with masses 253 and 254.

beyond the bounds of reality. In any case, it is evident that the field of transuranium elements will remain a very interesting and profitable field of investigation for the next decade or more.

LITERATURE CITED

1. G. Seaborg, E. McMillan, J. Kennedy and A. Wahl, Phys. Rev. 69, 366 (1946); G. Seaborg, A. Wahl and J. Kennedy, Phys. Rev. 69, 367 (1946).
2. G. Seaborg, R. James and A. Ghiorso, "The transuranium elements," Natl. Nuclear Energy Ser. 14B, 1554 (1949).
3. G. Seaborg, R. James and L. Morgan, "The transuranium elements," Natl. Nuclear Energy Ser. 14B, 1525 (1949).
4. S. Thompson, A. Ghiorso and G. Seaborg, Phys. Rev. 77, 838 (1950).
5. S. Thompson, K. Street and A. Ghiorso, Phys. Rev. 80, 790 (1950).
6. A. Ghiorso, S. Thompson, G. Higgins et al., Phys. Rev. 99, 1048 (1955).
7. A. Ghiorso, B. Harvey et al., Phys. Rev. 98, 1518 (1955).
8. Phillips, R. Gatti et al., Phys. Rev. Letters 1, 215 (1958).
9. P. Fields, A. Friedman et al., Phys. Rev. 107, 1460 (1957).
10. A. Ghiorso, T. Sikkeland, J. Walton, and G. Seaborg, Phys. Rev. Letters 1, 17 (1958).
11. A. Ghiorso. Unpublished data.
12. A. Ghiorso, T. Sikkeland, J. Walton, and G. Seaborg, Phys. Rev. Letters 1, 18 (1958).
13. G. N. Flerov, S. M. Polikanov, A. S. Karamyan et al., Doklady Akad. Nauk SSSR 120, 73 (1958).
14. G. Flerov, Proceedings of the Conference on Reactions between Complex Nuclei, Gatlinburg, Tennessee, May 5-7, 1958, p. 384.

THE NEUTRON TISSUE DOSE

A. M. Kogan, G. G. Petrov, L. A. Chudov, and
P. A. Yampol'skii

Translated from Atomnaya Énergiya, Vol. 7, No. 4, pp. 351-362
October, 1959
Original article submitted April 2, 1959

This paper is devoted to the determination of dosimetric characteristics of intermediate-energy neutrons. A calculation of the interaction of neutrons with paraffin for the normal incidence of an extended beam of neutrons in the energy interval from 100 ev to 1 Mev, which has been performed by means of an electronic computer, is given here. The computation results are used for calculating the components of the neutron tissue dose resulting from the moderation process in the tissue. The dose resulting from the neutron capture is calculated on the basis of the authors' data on the distribution of slow neutrons in paraffin and on neutron reflection from the surface of a hydrogenous medium. The depth distributions of neutron dose components for thermal neutrons and neutrons with energies of 100 ev, 1, 30, 240, 500 kev, and 1 Mev were obtained. The depth distributions of the biological dose for neutrons of the same energy and the biological dose values pertaining to the unit neutron flux were obtained.

In recent years, neutron protection and the dosimetry of neutron fluxes have assumed a great importance. With the development of the atomic industry and the appearance of a large number of nuclear accelerators of various types, it became necessary to develop safety norms for workers in the atomic industry.

While γ radiation dosimetry is a relatively well-developed dosimetry field with established irradiation norms which require only certain revisions and improvements, in neutron dosimetry, however, certain important characteristics have not yet been established or they have been determined only approximately.

Up to the present time, the dosimetric characteristics of intermediate-energy neutrons (10 ev – 500 kev) had been barely investigated. However, protection from neutrons with energies in this interval is necessary. Actually, thermal neutrons (for which irradiation norms are available) can be easily absorbed, however, the absorption of intermediate-energy neutrons requires considerable protective devices, which, in practice, cannot absorb all neutrons, due to which mainly intermediate-energy neutrons are accumulated around reactors. In connection with this, the problem of the dosimetry of intermediate-energy neutrons is of great importance today.

A number of papers has been devoted to the calculation of the neutron tissue dose corresponding to the unit flux of neutrons with a given energy. The surface tissue dose of neutrons with energies from 0.5 to 20 Mev was calculated in 1947 [1]. The dose was calculated with respect to the initial collision, and the radiations arising in the capture of neutrons in tissue were not taken into account. The depth distribution of a fast neutron dose was first calculated for energies between 0.5 and 5 Mev [2]. In [2], the Boltzmann kinetic equation was solved on the basis of the crude assumption that the path of neutrons in tissue is independent of the energy. In this calculation, as in [1], the energy region below 500 kev was not considered, and the effects of neutron capture in tissue were not taken into account. The maximum allowable flux of thermal neutrons was calculated [3] on the basis of the experimentally obtained absorption curve for thermal neutrons in paraffin. A calculation of the thermal neutron dose was presented in [4]; the obtained curve for neutron absorption in tissue was in good agreement with measurement results obtained in [3]. The latest and most complete work on the calculation of the tissue dose was presented in [5]. In this paper, the tissue dose for neutrons with energies equal to 10, 5, 2.5 Mev, 500, and 5 kev was calculated by the statistical Monte Carlo method.

The determination of the tissue dose for thermal neutrons and for neutrons with energies equal to 100 ev, 1, 30, 240, 500 kev, and 1 Mev on the basis of the results obtained by means of a computer and experimental data from [6 and 7] is presented below. Assume that an extended beam of monoenergetic neutrons falls perpendicularly on a flat surface in semiinfinite space filled with biological tissue. The neutrons incident to the tissue surface are partially reflected or scattered and absorbed in the tissue,

TABLE 1. Average Tissue Composition.

Element	Weight %	Atom/ cm^3 ($\times 10^{22}$)
Hydrogen	10.1	6
Carbon	12.1	0.6
Nitrogen	4.0	0.17
Oxygen	73.6	2.7

transmitting their energy to it. Below we shall accurately define the tissue dose which results from the processes of interaction of neutrons with the tissue. The fact that instead of a phantom of limited dimensions, we assume a semiinfinite space filled with tissue does not affect the results to a great extent. Actually, the greatest part of neutrons is scattered and absorbed in the first 10-15 cm of tissue.

The tissue composition which we used in our further calculations, in correspondence with data from [8], is given in Table 1.

Other elements which are present in noticeable quantities in the tissue, for instance, phosphorus (2.2×10^{20} atom/ cm^3) or sulfur (2.6×10^{19} atom/ cm^3), can be neglected, since their contribution to the interaction of neutrons is negligible [1].

The following reactions of neutrons with energies up to 1 Mev with the tissue elements are possible: 1) elastic scattering on hydrogen nuclei, 2) elastic scattering on heavy nuclei (carbon, nitrogen, and oxygen), 3) absorption in hydrogen nuclei with emission of γ quanta with an energy of 2.19 Mev, 4) absorption in nitrogen nuclei according to the $N^{14}(n,p)C^{14}$ reaction (the proton energy is 0.62 Mev), and 5) radiation capture on nitrogen according to the $N^{14}(n,\gamma)N^{15}$ reaction, where an energy of 10.8 Mev is emitted in each capture [9].

1. Energy Transmitted by Neutrons to the Tissue in Elastic Scattering.

In order to determine the energy lost by neutrons in unit volume of a tissue-equivalent material in the scattering process, the kinetic Boltzmann equation was solved numerically by the electronic computer of the Academy of Sciences, USSR. The distribution of the recoil nucleus energy released in paraffin, which was obtained numerically, defined the magnitude of the tissue dose created by fast neutrons in the scattering process. For the over-all neutron dose, it was necessary to take into account the neutron dose resulting from the capture of neutrons.

Calculation of Neutron Distribution. Assume that a flat monoenergetic neutron beam with an energy E falls perpendicularly on a flat paraffin plate with a finite or infinite thickness l and whose other two dimensions are infinite.

Let us introduce a notation where: $u = \ln(E_0/E)$ (where E is the neutron energy in the medium), v is the neutron velocity, x, y, and z are the Cartesian coordinates pertaining to the plate, θ, φ ($\mu = \cos\theta$) are the angles defining the direction of the neutron velocity vector, and $N(u, \mu, \varphi, x, y, z)$ is the density of neutrons in the phase space (u, μ, φ, x, y, z). In the latter case, N is independent of φ, y, and z, and, therefore, we shall use the quantity

$$N(u, \mu, x) = 2\pi N(u, \mu, \varphi, x, y, z).$$

Let us consider the interaction of neutrons with energies of 1 Mev and less. In calculations, it was assumed that the interaction of neutrons with hydrogen and carbon nuclei in paraffin can be reduced to elastic scattering and capture. The thermal motion of atoms was not taken into account, which was obviously of no importance as long as the neutron energy was large in comparison with the thermal motion energy.

The total cross sections were borrowed from [1]. For the collision density $\varphi(u, \mu, \varphi) = Nv\Sigma_{tot}$, the following kinetic equation is valid:

$$\mu d\frac{\partial\varphi}{\partial x} + \varphi = \int_{-1}^{1}\int_{0}^{u}\left[\frac{d}{d_s^H} w_H(u, \mu, u', \mu') + \frac{d}{d_s^C} w_C(u, \mu, u', \mu')\right]\varphi(u', \mu')\, du'\, d\mu', \quad (1)$$

where $d = \frac{1}{\Sigma_{tot}}$, $d_s^H = \frac{1}{\Sigma_s^H}$, $d_s^C = \frac{1}{\Sigma_s^C}$,

w_H and w_C are the probability densities of the transition from the (u', μ') state into the (u, μ) state in scattering in hydrogen and carbon, respectively.

The boundary conditions will be written in the following form:

$$\varphi(u, \mu, 0) = A\delta(\mu - 1)\delta(u) \text{ for } \mu > 0; \quad (2)$$

$$\varphi(u, \mu, l) = 0 \text{ for } \mu \leqslant 0. \quad (3)$$

The A coefficient is determined by normalizing the incident neutron flux. The boundary conditions signify that neutrons with an energy less than E_0 only can leave the plate.

The calculation results are normalized per unit incident flux. The incoming flux (per cm^2) is equal to

$$\int\limits_{\mu>0} \int\limits_{0}^{\infty} N(u, \mu, 0)\, v\mu\, du\, d\mu = \int\limits_{\mu>0} \int\limits_{0}^{\infty} d\mu\varphi(u, \mu, 0)\, du\, d\mu = Ad_0,$$

where d_0 is the path length corresponding to energy E_0. Hence,

$$A = \frac{1}{d_0}. \tag{4}$$

In the expression for the collision density, let us separate the part φ_1, which is determined by the directly transmitted neutrons that did not experience a single collision:

$$\varphi = \varphi_1 + \psi.$$

From (2) and (4), it follows that

$$\varphi_1 = \frac{1}{d_0}\delta(\mu - 1)\,\delta(u)\, e^{-\frac{x}{d_0}}. \tag{5}$$

By substituting (5) in (1), (2), and (3) for the function ψ, which we calculated, we obtain the following nonhomogeneous equation:

$$\mu d\frac{\partial\psi}{\partial x} + \psi = \int\limits_{-1}^{1} \int\limits_{0}^{u} \left[\frac{d(u')}{d_s^H(u')} w_H(u, \mu, u', \mu') + \frac{d(u')}{d_s^C(u')} w_C(u, \mu, u', \mu')\right] \psi(u', \mu')\, du'\, d\mu' + \left[\frac{1}{d_s^H(0)} w_H(u, \mu, 0, 1) + \frac{1}{d_s^C(0)} w_C(u, \mu, 0, 1)\right] e^{-\frac{x}{d_0}}, \tag{6}$$

and the homogeneous boundary conditions

$$\psi(u, \mu, 0) = 0 \quad \text{for} \quad \mu > 0; \tag{7}$$

$$\psi(u, \mu, l) = 0 \quad \text{for} \quad \mu \leqslant 0. \tag{8}$$

If the scattering is isotropic in a center-of-mass coordinate system, then

$$w_H = e^{-(u-u')}\,\delta\left(\gamma - e^{-\frac{u-u'}{2}}\right); \tag{9}$$

$$w_C = 3{,}52083\, e^{-(u-u')} \times \times \delta\left(\gamma - 6{,}5e^{-\frac{u-u'}{2}} + 5{,}5e^{\frac{u-u'}{2}}\right), \tag{10}$$

where γ is the cosine of the scattering angle. In the energy region under consideration, i.e., for $E_0 \leq 1$ Mev, these equations are satisfied.

Considering the relatively small contribution of carbon to the total cross section (6-20%), for the sake of simplicity, we assume that the scattering on carbon is isotropic in a laboratory system. An approximate solution of (6) with the boundary conditions found from (7) and (8) was found by the difference method. The calculation was performed by means of a fast electronic computer.

The calculation of $\psi_m^n(i)$ ($\underline{n}$, $\underline{m}$, and $\underline{i}$ are the energy, space, and angle indices respectively) was performed for each layer with respect to the $\underline{n}$ index, i.e., $\psi_m^n(i)$ was determined after $\psi_m^k(i)$ values for $k < n$ for all $\underline{n}$ and $\underline{i}$ were calculated. However, also ψ_m^k for $k = n$ entered the right-hand part of the difference analog of (6). In connection with this, $\psi_m^{n-1}(i)$ was used instead of $\psi_m^n(i)$ with subsequent conversions, where the newly found values of $\overline{\psi_m^n(i)}$ were taken into account. After the integrals in the right-hand part were calculated, (6) could be written in the form

$$\mu d\frac{\partial\psi}{\partial x} + \psi = S(x) + q(u, \mu)\, e^{-\frac{x}{d_0}}, \tag{11}$$

where S(x) is the already known grid function, and

$$q(u, \mu) = \frac{1}{d_s^H} w_H(u, \mu, 0, 1) + \frac{1}{d_s^C(0)} w_C(u, \mu, 0, 1). \tag{12}$$

In integrating (11), S(x) was approximated in each calculation interval by a function of the form $(Ax + B) \cdot e^{-\frac{x}{d_0}}$ where A and B are different constants for each calculation interval.

The lengths of the steps along $\underline{x}$ were chosen in such a manner that the maximum allowable error in interpolating S(x) according to the indicated interpolation formulas did not exceed 0.5%. The steps along $\underline{u}$ were chosen to be equal to the maximum logarithmic energy loss in collision with carbon for the convenience in passing through the discontinuity in collision density. The sufficient smallness of this step was checked by means of a model equation:

$$\psi = \int\limits_{0}^{u} \frac{d(0)}{d_s^H(0)} e^{-(u-u')}\psi(u')\, du' + 3{,}52083 \int\limits_{0}^{u} \frac{d(0)}{d_s^C(0)}\psi(u')\, du' + \frac{d(0)}{d_s^H(0)} e^{-u} + \frac{d(0)}{d_s^C(0)} f(u), \tag{13}$$

for $f(u) = \begin{cases} 3.52083\, e^{-u} \text{ for } u < \xi\ (\xi = 0.33412 \text{ is the maximum logarithmic energy loss}). \\ 0 \text{ for } u \geq \xi. \end{cases}$

The exact solution can be written for (13). For the step under investigation, the approximate solution differed from the actual solution by less than 5%.

In solving the infinite problem, S(x) was continued beyond the extreme right-hand calculation point x_{rh} in the following approximate form:

$$S(x_{rh}) = e^{-\frac{x-x_{rh}}{d_0}}.$$

By means of this approximate value, (11) was solved for the $x > x_{rh}$ region for the $\psi(\infty) = 0$ condition. The exact solution of this problem at the point x_{rh} is in the following form

$$\psi(x_{rh}) = \frac{S(x_{rh})}{1-\mu d}. \qquad (14)$$

The obtained value for $\psi(x_{rh})$ was used as the right-hand boundary condition. The exact solution at the point x_{rh} could differ to a great extent from the solution found according to (14), however, this discrepancy became smaller in passing to the left-hand boundary (the same applied to $e^{-\frac{x_{rh}-x}{|\mu| d}}$).

The calculations were verified by checking the balance of particles, which was obtained after integrating both parts of (6) with respect to μ and x. The ratio of the integral of the left-hand side of (6) to the integral of its right-hand side for each energy level differed from unity by not more than 0.04.

The calculations were performed for two series: the basic and the additional series.

The additional series, which consisted of three variants, had a methodical significance. For evaluating the error in solving (11) in the additional series, reduced steps with respect to x were used. Moreover, the error in the approximate right-hand boundary conditions was evaluated. This evaluation showed that the solution for a plate with a thickness equal to nine initial paths hardly differed from the solution for an infinite plate. By error evaluation and methodical calculations, it was established that the total error in ψ with respect to the exact solution did not exceed 10%.

The basic series consisted of six variants with initial energies equal to 1 Mev, 500, 240, 30, 1, and 0.1 kev. The plate thickness in all variants of the basic series was assumed to be infinite. The layer thickness, according to which the actual calculations were performed, was equal to nine initial path lengths i.e., it was 20.4 cm for E_0 = 1 Mev, and 5.04 cm for E_0 = 0.1 kev.

Table 2 shows the spatial distributions of thermal neutron fluxes for different initial energies. These data were obtained by using the diffusion approximation for the spatial distribution of moderated neutrons. It is of interest to compare the obtained data with the experimental results.

In Figs. 1a, b, and c the data in Table 2 for neutrons with initial energies equal to 240, 30, and 100 ev are compared with the distribution of the absorption density of slow neutrons, found by measurements for neutrons with initial energies of 220, 25 kev and ~5 ev [6], respectively. A good agreement

TABLE 2. Thermal Neutron Flux

Initial energy											
1 Mev		500 kev		240 kev		30 kev		1 kev		100 ev	
depth,cm	flux	depth,cm	flux	depth,cm	flux	depth,cm	flux	depth,cm	flux	depth,cm	flux
0	0,382	0	0,351	0	0,317	0	0,231	0	0,284	0	0,353
0,34	0,867	0,24	0,661	0,17	0,521	0,100	0,316	0,08	0,374	0,8	0,475
0,68	1,32	0,47	0,959	0,34	0,721	0,19	0,401	0,17	0,459	0,17	0,571
1,0	1,74	0,71	1,23	0,51	0,911	0,29	0,481	0,25	0,545	0,25	0,687
1,4	2,13	0,95	1,50	0,69	1,09	0,39	0,559	0,34	0,628	0,34	0,78
2,0	2,80	1,4	1,97	1,0	1,42	0,58	0,709	0,50	0,784	0,50	0,97
2,7	3,32	1,9	2,36	1,4	1,71	0,78	0,846	0,67	0,930	0,67	1,15
4,1	3,90	2,8	2,90	2,1	2,16	1,2	1,09	1,00	1,180	1,0	1,44
5,4	3,92	3,8	3,11	2,8	2,44	1,6	1,28	1,3	1,38	1,3	1,65
6,8	3,57	4,7	3,1	3,4	2,63	1,9	1,41	1,7	1,53	1,7	1,81
8,2	3,01	5,7	2,81	4,1	2,53	2,3	1,50	2,0	1,62	2,0	1,88
9,5	2,41	6,6	2,46	4,9	2,40	2,7	1,54	2,4	1,66	2,4	1,90
10,9	1,85	7,6	2,07	5,5	2,20	3,1	1,54	2,7	1,66	2,7	1,86
12,3	1,37	8,5	1,69	6,2	1,95	3,5	1,50	3,0	1,62	3,0	1,78
13,6	0,984	9,5	1,33	6,9	1,67	3,9	1,43	3,4	1,55	3,4	1,68
15,0	0,691	10,4	1,03	7,6	1,42	4,3	1,33	3,7	1,46	3,7	1,56
16,3	0,474	11,4	0,779	8,3	1,17	4,7	1,73	4,0	1,35	4,0	1,42
17,7	0,312	12,3	0,576	8,9	0,948	5,0	1,12	4,4	1,22	4,4	1,28
19,0	0,201	13,2	0,414	9,6	0,746	5,560	0,99	4,7	1,09	4,7	1,14
20,4	0,121	14,2	0,286	10,3	0,570	5,8	0,85	5,0	0,960	5,0	0,998

TABLE 3. Absorbed Energy Distribution and the Energy Albedo

Initial energy											
1 Mev		500 kev		240 kev		30 kev		1 kev		100 ev	
depth, cm	energy, Mev/cm^3	depth, cm	energy, Mev/cm^3	depth, cm	energy, Mev/cm^3	depth, cm	energy, Mev/cm^3	depth, cm	energy, Mev/cm^3	depth, cm	energy, Mev/cm^3
0	0,053	0	0,0328	0	0,0214	0	0,00330	0	0,000111	0	10^{-4}·0,110
0,34	0,112	0,24	0,0714	0,017	0,0443	0,1	0,00838	0,08	0,000299	0,08	10^{-4}·0,297
0,70	0,147	0,47	0,0954	0,34	0,0605	0,19	0,0118	0,17	0,000431	0,17	10^{-4}·0,429
1,0	0,168	0,71	0,110	0,52	0,0749	0,29	0,0142	0,25	0,000521	0,25	10^{-4}·0,518
1,4	0,180	0,95	0,119	0,69	0,081	0,39	0,0157	0,34	0,000580	0,34	10^{-4}·0,578
2,0	0,185	1,4	0,124	1,0	0,0848	0,58	0,0170	0,50	0,000635	0,50	10^{-4}·0,632
2,7	0,176	1,9	0,119	1,4	0,0816	0,78	0,0168	0,67	0,000633	0,67	10^{-4}·0,631
4,1	0,140	2,8	0,0955	2,1	0,0664	1,2	0,0143	1,0	0,000546	1,0	10^{-4}·0,544
5,4	0,101	3,8	0,0696	2,8	0,0489	1,6	0,0112	1,3	0,000426	1,3	10^{-4}·0,425
6,8	0,069	4,7	0,0484	3,4	0,0341	1,9	0,00802	1,7	0,000314	1,7	10^{-4}·0,314
8,2	0,046	5,7	0,0318	4,1	0,0229	2,3	0,00562	2,0	0,000224	2,0	10^{-4}·0,223
9,5	0,029	6,6	0,0205	4,8	0,0149	2,7	0,00386	2,3	0,000156	2,3	10^{-4}·0,155
10,9	0,018	7,6	0,013	5,5	0,00954	3,1	0,00259	2,7	0,000107	2,7	10^{-4}·0,106
12,2	0,011	8,5	0,00808	6,2	0,00600	3,5	0,00172	3,0	10^{-4}·0,722	3,0	10^{-5}·0,720
13,6	0,007	9,5	0,00496	6,9	0,00373	3,9	0,00112	3,4	10^{-4}·0,486	3,4	10^{-5}·0,483
15,0	0,004	10,4	0,00302	7,6	0,00228	4,3	0,000738	3,7	10^{-4}·0,324	3,7	10^{-5}·0,322
16,3	0,0025	11,4	0,00182	8,3	0,00138	4,7	0,000478	4,0	10^{-4}·0,215	4,0	10^{-5}·0,213
17,8	0,0015	12,3	0,00108	9,0	0,000841	5,1	0,000308	4,4	10^{-4}·0,141	4,4	10^{-5}·0,141
19,1	0,0009	13,3	0,000643	9,7	0,000504	5,5	0,000197	4,7	10^{-5}·0,937	4,7	10^{-6}·0,927
20,4	0,0005	14,2	0,000378	10,3	0,000300	5,8	0,000126	5,0	10^{-5}·0,617	5,0	10^{-6}·0,606

Initial energy					
1 Mev	500 Mev	240 Mev	30 kev	1 kev	100 ev
0,032	0,0285	0,0286	0,0231	0,0217	0,0213

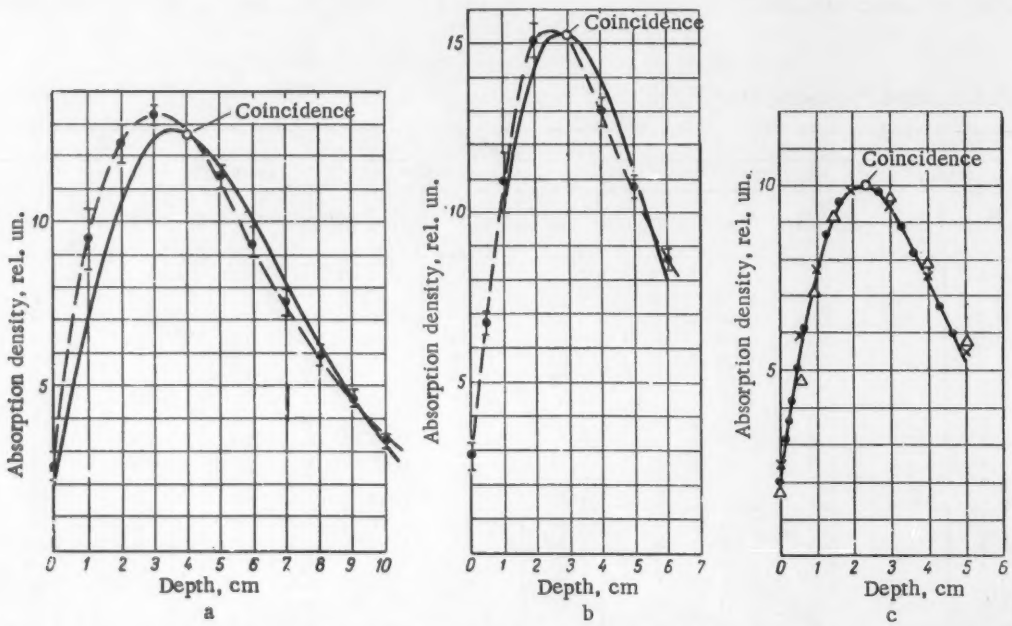

Fig. 1. Distribution of the absorption density of slow neutrons with the following energies: a) ——:220 kev (experiment); – – – –: 240 kev (calculation); b) ——: 25 kev (experiment); – – – –: 30 kev (calculation); c) –●– – –: 100 ev; Δ: 1 kev (calculation); ×: ~ 5 ev (experiment).

between experimental and calculation data on the spatial distribution of fluxes of moderated neutrons was observed.

Table 3 gives the absorbed energy distribution and the energy albedo for all six initial energy values. The depth and the initial energy serve as the entrance data. The density values of the energy absorbed in unit volume at different depths, which are given in the table, characterize the part of the tissue dose created by fast neutrons in their scattering in a tissue-equivalent material.

If we assume that the molecular composition of paraffin is $C_{24}H_{50}$ and that its density is 0.87 g/cm^3, we obtain $n^H_{par} = 7.75 \times 10^{22}$ hydrogen atoms and $n^C_{par} = 3.72 \times 10^{22}$ carbon atoms per cm^3 of paraffin. The average logarithmic energy loss ξ per single collision is equal to 1 for hydrogen, 0.158 for carbon, 0.136 for nitrogen, and 0.12 for oxygen. By using the values from [10] for the effective scattering cross sections σ, which are averaged with respect to energy, the ratio of the moderating power $\xi_H n_H \sigma_H$ of hydrogen in tissue to the over-all moderating power $\sum_i \xi_i n_i \sigma_i$ of all nuclei entering the tissue composition can be calculated for different neutron energies:

E, Mev	1	0,5	0,1	0,001	0,0001
$\xi_H n_H \sigma_H / \sum_i \xi_i n_i \sigma_i$	0,955	0,950	0,980	0,985	0,985

Thus, the scattering of neutrons with energies of 1 Mev and less in tissues occurs mainly on hydrogen. The spatial distributions of recoil proton energies in 1 cm^3 of paraffin and of tissue in units of path lengths coincide, and the absolute values are proportional to the density of hydrogen nuclei in these substances.

Consequently,

$$\Delta E_t\ (x) = 0{,}78 \Delta E_{par}\ (0{,}78x),$$

where ΔE_{par} (x) are energy losses (Table 2), and x is the tissue depth.

2. Tissue Dose Due to Protons from the N^{14} (n, p) Reaction.

In the capture of a neutron by a nitrogen nucleus according to the N^{14} (n, p) reaction, a 620-kev proton is released, the path of which in the tissue is equal to $\sim 10^{-3}$ cm. In connection with the smallness of proton paths in tissue, it can be assumed that the proton is absorbed at the same point where the neutron is captured. Consequently, the depth distribution of the absorption density of neutrons, which is given in [6], corresponds to the distribution of the portion of a neutron dose which is due to protons from the N^{14} (n, p) reaction.

The density curves φ (x) for neutron absorption in a tissue-equivalent material are given in [6]. The values of α (x) for the unit neutron flux are normalized in such a manner that $\int_0^\infty \varphi(x)dx = 1 - \alpha$ (α is the reflection coefficient). In the case where the unit neutron flux phantom falls on the surface, the number of neutrons absorbed in 1 cm^3 at the maximum of the absorption curve will be $\varphi(x_{max})(1-\alpha) = \kappa$ (x_{max} is the depth for which the curve has the maximum value). Correspondingly, $[\varphi(x)/\varphi(x)_{max}]\kappa$ denotes the portion of the unit flux incident on the surface which is absorbed in 1 cm^3 at the depth x. The absorption with respect to the N^{14} (n, p) reaction amounts to 12.7%, and the remainder is almost entirely absorbed by hydrogen in the tissue, since the absorption by carbon, oxygen, phosphorus, and sulfur can be neglected.

Thus, the expression for the neutron tissue dose due to protons from the N^{14} (n, p) reaction at the depth x can be written thus (erg/cm^3):

$$0{,}127 \frac{\varphi(x)}{\varphi(x_{max})} \kappa 0{,}62 \cdot 1{,}6 \cdot 10^{-6} = 1{,}26 \cdot 10^{-7} \frac{\varphi(x)\kappa}{\varphi(x_{max})}.$$

The value for κ is determined by using the relative neutron absorption curves [6] and the albedo values [7]. The results are given in Table 4.

TABLE 4. Spatial Distribution of Neutron Absorption

Proton energy	φ_{max}	α	κ
Thermal	0,32	0,58	0,135
100 ev	0,178	0,56	0,078
1 kev	0,178	0,47	0,094
30 kev	0,178	0,38	0,11
240 kev	0,132	0,19	0,105
500 kev	—	—	0,1
1 ev	0,11	0,12	0,097

As follows from [6], the spatial distribution of the neutron absorption density in paraffin depends only slightly on the initial energy of incident neutrons. In particular, the relative curves for 5 ev and 25 kev are almost identical, and therefore, we assign the same shape to curves for 100 ev and 1 kev as to the curves for 5 ev or 25 kev. We also consider that the energies for which the moderation was calculated, i.e., 30, 240 kev and 1 Mev, can be assigned to distributions obtained in experiments with neutron energies equal to 25, 220, and 830 kev, respectively. No experimental data on absorption are available for the 500 kev energy, and

therefore, the average of the values for 220 and 830 kev was used in determining the form of the absorption density distribution for 500 kev and for κ corresponding to this energy. Such interpolation leads to an error of ~ 7% for the tissue dose and an error of 2% for the biological dose of 500 kev neutrons.

3. The Dose Resulting from Capture γ Radiation

In calculating the dose resulting from capture γ radiation, the radiation capture of neutrons in carbon and oxygen can be neglected due to the smallness of their cross sections. The radiation capture of neutrons by nitrogen also provides a small contribution in comparison with the capture of neutrons by hydrogen. The energy of capture radiation on nitrogen constitutes ~ 5% of the energy of capture γ quanta on hydrogen. By taking into account the great hardness of capture radiation on nitrogen and, consequently, the small electron transformation coefficient, it can be assumed that the capture γ radiation on nitrogen constitutes less than 5% of the over-all capture radiation dose.

In considering the propagation of γ rays in a semi-infinite tissue volume, the multiple-scattering effect should be taken into account by introducing the accumulation factor. In this, it is important to obtain the dose distribution of capture γ radiation in the first 20 cm from the tissue surface. It was demonstrated by experiment [11] that the attenuation of γ rays in water (if the source is located at a depth approximately equal to a single free γ-quantum path or less) follows the exponential law with an absorption coefficient equal to the electron transformation coefficient. We assume that the electron transformation coefficient of γ rays with an energy of 2.2 Mev in tissue is the same as that in water, i.e., it is equal to 2.5×10^{-2} cm^{-1} [12].

If a γ-radiation source in the shape of an infinite plane (where the source density is ρ quantum / cm^3) is placed at the depth x in a medium with an absorption coefficient μ, the flux of γ quanta at the depth x_0 will be expressed by the relation

$$\Pi_\gamma(x, x_0) = \frac{\rho}{2}\left[-Ei(-\mu|x-x_0|)\right],$$

where

$$-Ei(-a) = \int_a^\infty \frac{e^{-t}}{t}\,dt.$$

The γ-ray dose is calculated for an infinite cylinder with a radius of 15 cm (a length of 20 cm is sufficient for practical purposes, since the density of capture γ-radiation sources approaches zero at great depths). For these conditions, the flux of γ quanta at the point X_0 on the cylinder axis is expressed in the following form:

$$\Pi_\gamma(x, x_0) = \frac{\rho}{2}\left\{\left[-Ei(-\mu|x-x_0|)\right] - \left[-Ei\left(-\mu\sqrt{R^2+|x-x_0|^2}\right)\right]\right\}.$$

If the expression inside the large brackets in this equation is denoted by $F(|x-x_0|)$, the capture γ-radiation dose at the point x_0, normalized per unit neutron flux, will be equal to

$$D_\gamma(x_0) = \frac{0{,}873}{2}\mu E_\gamma \int_0^\infty \frac{\varphi(x)}{\varphi_{max}}\varkappa F(|x-x_0|)\,dx.$$

By substituting the numerical values

$$\mu = 2{,}5\cdot 10^{-2}\ cm^{-1}$$

and $E\gamma = 2.2 \times 1.6 \times 10^{-6}$ erg (0.873 is the portion of neutrons absorbed by the tissue hydrogen), we obtain the expression for the γ-ray dose at the point x_0 (erg/g):

$$D_\gamma = 3{,}84\cdot 10^{-8}\int_0^\infty \frac{\varphi}{\varphi_{max}}\varkappa F(|x-x_0|)\,dx.$$

The energy dose of each initial neutron was determined by numerical integration for a number of points x_0.

The components of the neutron tissue dose, normalized per 1 neutron/cm^2 for different neutron energies and for different tissue depths, were found according to the methods described in sections 1, 2, and 3. The tissue dose components are represented in Figs. 2-8. It is obvious from these figures that the ratio of individual tissue dose components is different for different neutron energies and for different tissue depths. For the maximum values, the tissue dose of recoil nuclei for energies lower than 30 kev is considerably smaller than the capture dose. For 30 kev, the tissue dose created by recoil nuclei will be close to the dose due to protons from capture on nitrogen, but it will still remain smaller than the capture γ-radiation dose.

With an increase in neutron energy, the tissue dose at the curve maximum is determined by recoil nuclei to an ever increasing extent. These ratios change for different depths. At great depths, the specific activity of the capture dose increases, since the dose of recoil nuclei decreases faster than the capture dose with an increase in depth.

The unequal changes in neutron dose components with an increase in depth can lead to the fact that various biological reactions which are caused by neutron irradiation can take place with different biological effectiveness. Where possible (for thermal neutrons and for neutrons with an initial energy of 500 kev), the results from [5] are given in Figs. 2 and 7 for the sake of comparison. For thermal neutrons, we obtained values for the tissue dose created by protons from the capture reaction on nitrogen which were higher than the values obtained in [5]; this could be

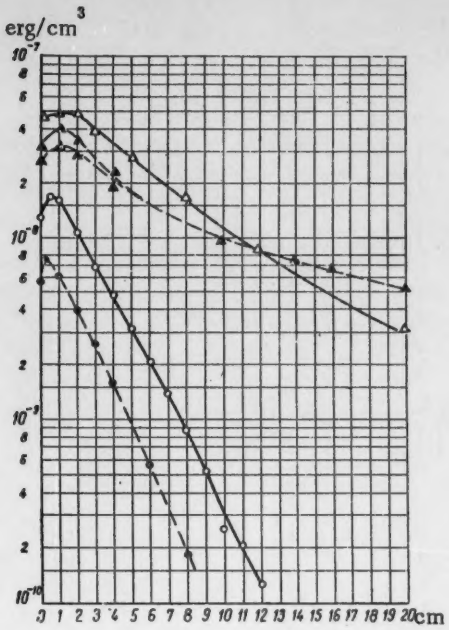

Fig. 2. Distribution of tissue dose components (thermal neutrons). Data obtained in the present work: O) N^{14} (n, p) reaction; Δ) H' (n, γ) capture; data taken from [5]: •) N^{14} (n, p) reaction; ▲) H' (n, γ) capture.

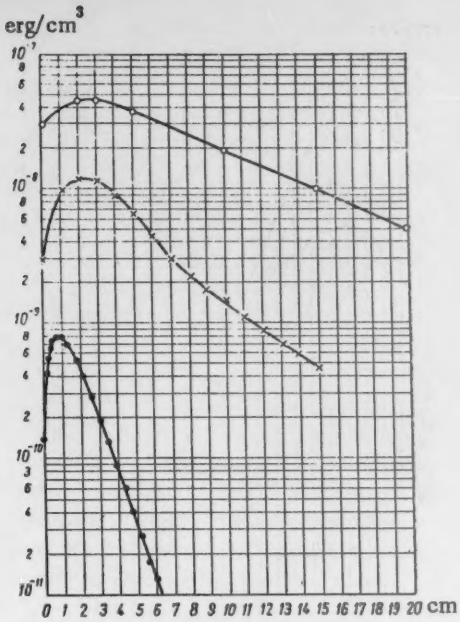

Fig. 4. Distribution of tissue dose components (neutron energy: 1 kev): •) Recoil nuclei; X) N^{14} (n, p) reaction; O) H' (n, γ) capture.

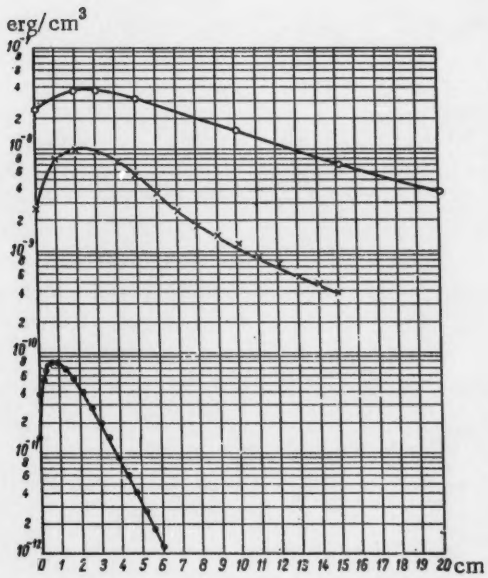

Fig. 3. Distribution of tissue dose components (neutron energy: 100 ev): •) Recoil nuclei; X) N^{14} (n, p) reaction; O) H' (n, γ) capture.

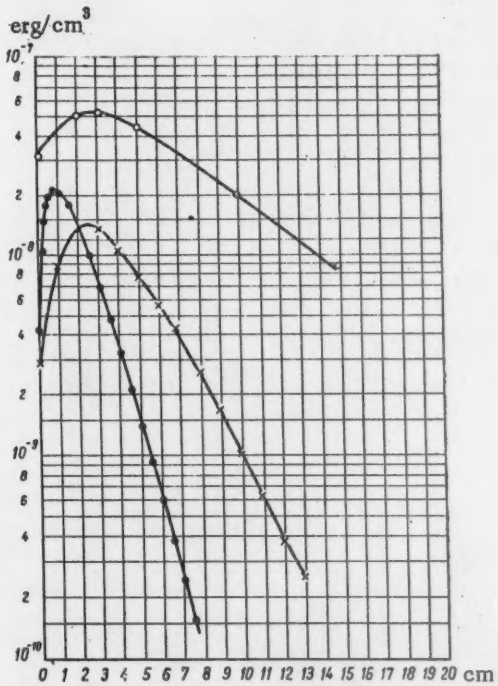

Fig. 5. Distribution of tissue dose components (neutron energy: 30 kev): •) Recoil nuclei; X) N^{14} (n, p) reaction; O) H' (n, γ) capture.

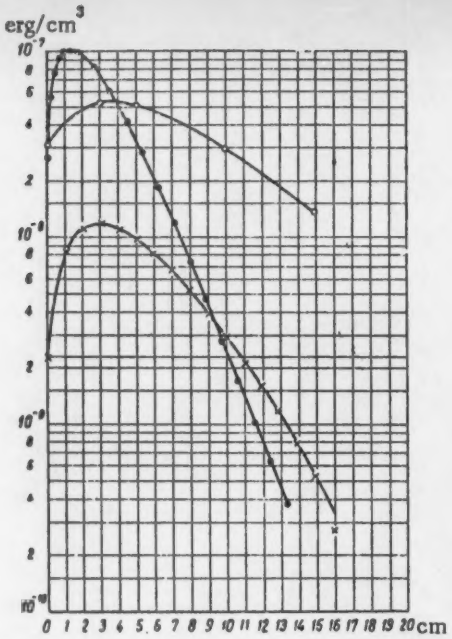

Fig. 6. Distribution of tissue dose components (neutron energy: 240 kev): •) Recoil nuclei; ×) N^{14} (n, p) reaction; ○) H' (n, γ) capture.

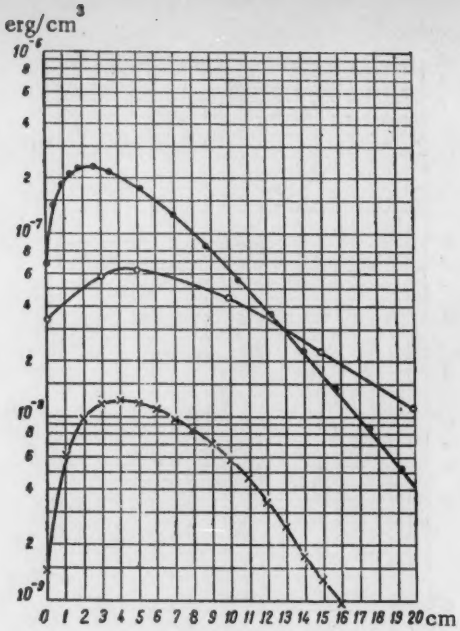

Fig. 8. Distribution of tissue dose components (neutron energy: 1 Mev): •) Recoil nuclei; ×) N^{14} (n, p) reaction; ○) H' (n, γ) capture.

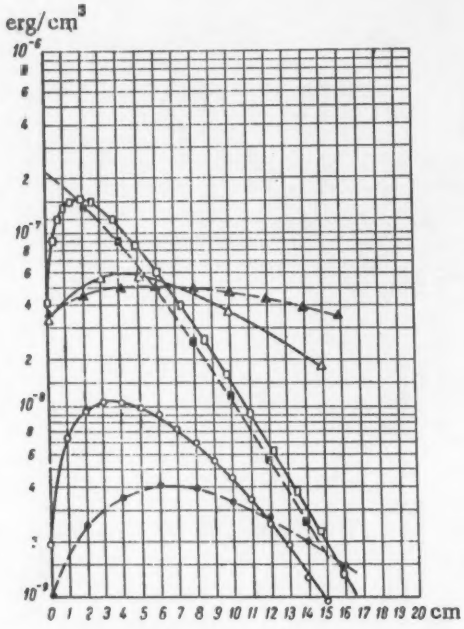

Fig. 7. Distribution of tissue dose components (neutron energy: 500 kev). Data obtained in the present work: □) recoil nuclei; ○) N^{14} (n, p) reaction; △) H' (n, γ) capture; data borrowed from [5]: ■) recoil nuclei; •) N^{14} (n, p) reaction; ▲) H' (n, γ) capture.

explained by the fact that the albedo of thermal neutrons in normal incidence is less than the albedo for the angular distribution considered earlier [7], due to which the greater part of neutrons is absorbed in the tissue. A comparison of capture components of a dose for the 500-kev energy shows that the maximum of the proton component is shifted towards the surface to a greater extent than it is represented in [5]; with respect to magnitude, the maximum in our case exceeds the maximum obtained in [5] 2.5-fold. The reason for this discrepancy is perhaps the fact that, in [5], the quantitative calculation of moderation and diffusion in the incidence of 500 kev neutrons was performed for a nonmonochromatic beam; moreover, in order to find the absorption densities by purely analytical means, significant simplications, which distort the results, must be introduced in calculations. This can be illustrated by a comparison of curves obtained by means of an electronic computer and by the Monte Carlo method for the energy released in the moderation process (Fig. 7).

4. The Biological Neutron Dose

In order to determine the biological dose, the tissue dose magnitude must be multiplied by the coefficient of the relative biological effectiveness (RBE) that is characteristic for a given radiation type.

In order to find the biological dose values on the basis of the above values, we must use the RBE coeffi-

cient which is obtained in different experiments with biological objects. The RBE of all electrons is assumed to be equal to unity; the RBE of neutrons is not equal to unity because of the fact that ionizing particles different from electrons and having an RBE larger than unity appear in the action of neutrons on the tissue. For neutrons with an energy of up to 1 Mev, such particles consist almost exclusively of protons. Therefore, in passing from tissue doses to biological doses, the magnitude of the RBE of protons must be known for the neutron energy interval under consideration.

The recoil protons and the reaction of capture by nitrogen determine 83% of the tissue dose of neutrons with an energy of 1 Mev; the remaining part of the dose (17%) is due to capture γ rays, i.e., due to electrons in the final consideration. With an increase in neutron energy, the share of the tissue dose which is due to protons increases even more, and therefore, it can be considered, without committing large errors, that the RBE of neutrons with the energy $E \geq 1$ Mev is the RBE of protons.

In recent years, a large number of papers devoted to the RBE of different types of radiation have appeared in foreign literature. An expecially large number of papers are devoted to the RBE of neutrons. With regard to the magnitude of the RBE of fast neutrons, obtained with respect to acute biological effects, these papers can be divided into two groups. In the first group [13-17], where the results gravitate toward the value RBE = 5, the investigations were performed on mice, where, as a rule, fission neutrons were used. In the second group [13, 15 and 17-20], RBE $\simeq$ 2 values were obtained; these experiments were also performed on mice, which were irradiated with neutrons with an energy of not less than 10 Mev, although RBE $\simeq$ 2 values were obtained for fission neutrons in certain cases.

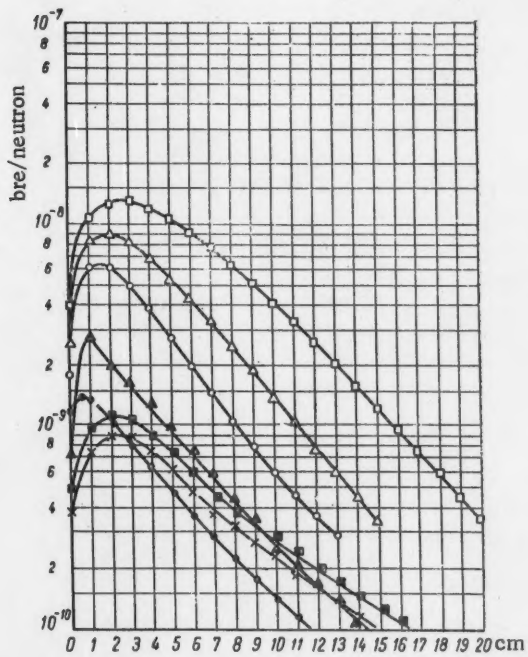

Fig. 9. Depth distribution of the biological dose for RBE = 5. Neutron energies: o) thermal neutrons; ×) 100 ev; □) 1 kev; Δ) 30 kev; ○) 240 kev; Δ) 500 kev; □) 1 Mev.

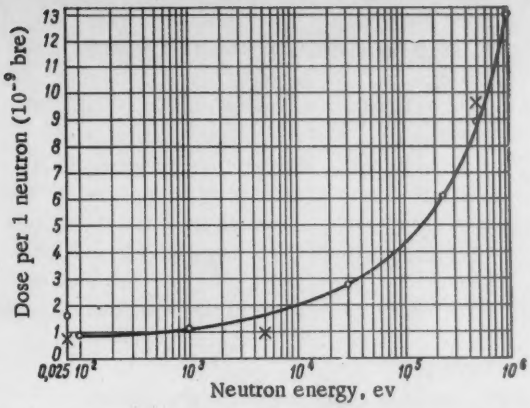

Fig. 10. Biological dose per unit neutron flux. ○) Data obtained in the present work; ×) data borrowed from [5].

It seems to us that RBE = 5 is a reasonable choice in calculations for protons, since in the first place, this value was obtained in experiments with neutrons which were close with respect to energy to those which we investigated, and in the second place, since a larger value for the RBE leads to smaller magnitudes of the maximum allowable dose, which guarantees a larger degree of safety in work with neutrons.

The biological doses which were calculated for RBE = 5 are given in Fig. 9. The relative values of biological damage per unit flux of neutrons of different energies were calculated with respect to the maximum values of depth biological doses (Fig. 10). Also the values borrowed from [5] are shown in this figure.

LITERATURE CITED

1. J. Mitchell, Brit. J. Radiol. 20, 177 (1947).
2. J. Tait, Brit. J. Radiol. 23, 282 (1950).
3. P. C. Capron, M. Faes, and G. C. Tavernier, Nature 162, 129 (1949).
4. W. Snyder, Nucleonics 6, 46 (1950).
5. W. Snyder and J. Neufeld, Brit. J. Radiol. 28, 342 (1955).
6. A. M. Kogan, G. G. Petrov, L. A. Chudov, and P. A. Yampol'skii, Atomnaya Énergiya present issue, translation page 865.
7. A. M. Kogan, G. G. Petrov, L. A. Chudov, and P. A. Yampol'skii, Atomnaya Énergiya present issue, translation page 867.

8. E. Tochilin and S. Ross, Radiation Research 4, 158 (1956).
9. P. Mittelman and R. Liedtke, Nucleonics 13, 50 (1955).
10. Atlas of Effective Neutron Cross Sections of Elements [in Russian] (Izd. AN SSSR, Moscow, 1955).
11. V. N. Sakharov, Dissertation [in Russian] (Institute of Chemical Physics, Academy of Sciences, USSR, 1955).
12. N. G. Gusev, Manual for Radioactive Radiation and Radiation Protection [in Russian] (Medgiz, Moscow, 1956) p. 7.
13. D. Jordan, J. Clark, and H. Vogel, Radiation Research 4, 77 (1956).
14. D. Jordan, J. Clark, and H. Vogel, Radiation Research 6, 460 (1957).
15. T. Evans and Yu Ying-fu, Radiation Research 5, 477 (1956).
16. V. Bond et al., Radiology 67, 650 (1956).
17. A. Upton, F. Conte, G. Hurst and W. Mills, Radiation Research 4, 117 (1956).
18. J. Storer, B. Rogers, F. Boone, and P. Harris, Radiation Research 8, 71 (1958).
19. P. Harris and W. Langham, Radiation Research 3, 417 (1955).
20. R. Rothermel, K. Woodward and J. Storer, Radiation Research 5, 433 (1956).

BEHAVIOR OF REACTORS WITH TEMPERATURE SELF-REGULATION

V. N. Andreev, O. D. Kazachkovskii, and N. V. Krasnoyarov

Translated from Atomnaya Énergiya, Vol. 7, No. 4, pp. 363-366
October, 1959
Original article submitted January 8, 1959

Investigations of the physics of reactors with fast neutrons [1 and 2] indicate that changes in reactivity with an increase in the reactor power level can be divided into relatively fast changes, which are mainly connected with mechanical deformations of fuel elements and an expansion of the coolant, and into slow changes, which are connected with the temperature expansion of reactor structural parts. For a number of processes, the power coefficient of reactivity can be separated into the instantaneous power coefficient $\underline{p}$ and the delayed power coefficient $\underline{k}$ with the average lag time τ. This applies also to intermediate and thermal reactors. The $\underline{p}$ and $\underline{k}$ coefficients can be positive as well as negative. A number of papers [3-6] is devoted to reactor behavior problems connected with temperature effects.

We performed a general investigation of the behavior of a reactor, the control of which was connected only with the above-mentioned temperature effects. The neutrons were divided into two groups: prompt neutrons (lifetime equal to zero) and delayed neutrons (lifetime equal to τ_0). It was assumed that, if the reactor is shut down, the contribution of the delayed power effect decreases exponentially with time. Under these assumptions, the reactor kinetics equations are of the following form: *

$$W(t)=\frac{\beta}{\tau_0[\beta-\rho(t)]}\int_{-\infty}^{t}W(t')\exp\left(-\frac{t-t'}{\tau_0}\right)dt', \quad [\rho(t)<\beta]; \tag{1}$$

$$\rho(t)=\rho_0+pW(t)+\frac{k}{\tau}\int_{-\infty}^{t}W(t')\exp\left(-\frac{t-t'}{\tau}\right)dt', \tag{2}$$

where W(t) is the reactor power level, $\rho(t)$ is the reactivity, β is the effective portion of delayed neutrons, and ρ_0 is the reactivity of the cooled-down reactor (for W(t) = 0).

This system of equations is reduced to a nonlinear differential equation for W(t) (or for $\rho(t)$), which, by substitutions W(t) = x and τ W'(t) = y, is reduced to the following form:

$$\frac{dy}{dx}=\frac{A_1y^3+A_2y^2x+A_3yx^2+A_4x^3+A_5y^2+A_6yx+A_7x^2}{A_8yx^2+A_9yx}, \tag{3}$$

where A_1-A_9 are constant coefficients, which depend on $\underline{k}$, $\underline{p}$, τ, τ_0, β, and ρ_0. Since the behavior of integral curves in the X, Y plane strongly depends on the character of their behavior in the vicinity of singular points, we investigated all the six singular points of (3).†

The singular points x = 0, y = 0 and $x=-\rho_0/(k+p)$, y = 0 are of the greatest interest. The neighborhood of the first singular point determines the character of the reactor power level rise from the zero power level, and the second singular point determines the reactor behavior in the region of power levels close to the steady-state power level, for which the reactivity ρ_0, which is introduced by regulating devices, is compensated by temperature effects. The conditions for the existence of such a point is $k + p < 0$ (for $\rho_0 > 0$). By investigating the solution of (3) in the neighborhood of the zero singular point, it was shown that, in all cases for $0 < \rho_0 < \beta$, the reactor power level rises from the zero level according to the law given by

$$W(t)=W_0\exp\left(\frac{\rho_0 t}{(\beta-\rho_0)\tau_0}\right).$$

More varied solutions of (3) were obtained in the neighborhood of the steady-state point: aperiodically stable (AS) and aperiodically unstable solutions (AU) (the singularity is a nodal point), oscillatory stable (OS) and oscillatory unstable solutions (OU) (the singularity is a focal point), and a special type of unstable solutions (U), which differs from the former by the fact that, if, in the preceding cases, an infinite number of

* See, for instance, [3].

† See, for instance, [7].

integral curves passes through the singular point, in the latter case, only two curves pass (the singularity is a saddle point). Figure 1 shows the general aspect of existence regions for the enumerated solutions, which are given in ρ_0/β vs. $p/k + p$ coordinates. The I-IV curves satisfy the equation

$$\left(\frac{\rho_0}{\beta}\right)_{I,\,II} = \frac{-1-ac+2a \pm \sqrt{(1+ac-2a)^2-(1-ac)^2}}{(1-ac)^2};$$

$$\left(\frac{\rho_0}{\beta}\right)_{III} = -\frac{1}{c}; \quad \left(\frac{\rho_0}{\beta}\right)_{IV} = -\frac{1}{1+ac},$$

where $a = \tau/\tau_0$ and $c = p/(k+p)$. For $\tau < \tau_0$, the OS, OU, and AU regions vanish.

In the case of oscillatory solutions, small power oscillations have a sinusoidal character with the period

$$T = \frac{4\pi\tau\,(\beta + c\rho_0)}{\sqrt{4\rho a\,(\beta + c\rho_0) - (\beta + \rho_0 + ac\rho_0)^2}}$$

and the logarithmic damping decrement

$$\delta = -\frac{\beta + \rho_0 + ac\rho_0}{2\,(\beta + c\rho_0)}\,T.$$

An investigation of special properties of (1) and (2) and of the other singular points made it possible to explain the general behavior of integral curves. Only that portion of the X, Y phase plane for which the solutions of (1) had a physical sense was considered. These regions were limited by the straight lines

$$y = (1-a)\,x \text{ and } y = \frac{x}{c} + \frac{(1-a)\,\beta - \rho_0}{p},$$

on which $\rho\,(t) = -\infty$ and $\rho\,(t) = \beta$.

In dependence on the constant coefficients in (1) and (2), the following four types of regions were obtained:

a) a single-bond region, which includes the neighborhoods of the zero and the steady-state points;

b) two regions touching at a single point, where the neighborhoods of the zero and the steady-state singular points are located in one of the two regions;

c) two regions similar to the b-type regions, where the neighborhoods of the zero and the steady-state singular points are located in different regions;

d) two isolated single-bond regions, where the neighborhoods of the zero and the steady-state singular points are located in different regions.

The steady-state point is always stable, and the transition from the zero power area to the steady-state power area always takes place in a-type regions. In the case of b-type regions, the transition from the zero-power area to the steady-state area is possible and takes place if the solutions at the steady-state point are stable (AS or OS). In the case of c-type regions, the integral curves pass from the zero-power area into the steady-state point area, and they enter this area under the same conditions that are valid for the b-type regions. In the opposite case, the curves from the zero-power area pass into infinity without entering the region containing the steady-state point. It is obvious that, in the case of d-type regions, it is impossible to pass from the zero-power to the steady-state power level by using only temperature self-regulation of the reactor and preserving the $\rho\,(t) < \beta$ relation.

For $p < 0$, all integral curves end at the steady-state point, and for $p > 0$, only the integral curves from a certain given portion of the phase space (including the zero-power area) can enter the steady-state point. Beyond this portion, all integral curves (sometimes with the exception of one curve) bypass the steady-state point region and pass into infinity. The limits of these regions are, in particular, segments of the straight line $x = (\beta - a\beta - \rho_0)/(2p - pa + k)$. If the steady-state point is unstable, all integral curves pass into infinity.

Figures 2-4 show examples of characteristic cases of the behavior of integral curves. Figure 2 shows AS solutions for regions of the types a and c which end at the steady-state point; Fig. 3 shows OS solutions at the steady-state point for the b-type region (the boundaries which separate solutions that converge to the steady-state point are set off from the remaining solutions). Figure 4 shows an example of an unstable solution U for the d-type region. The lines for which $\rho\,(t) = 0$ are shown by dotted lines. It is obvious from Fig. 4 (right-hand top corner) that the reactor power level progress-

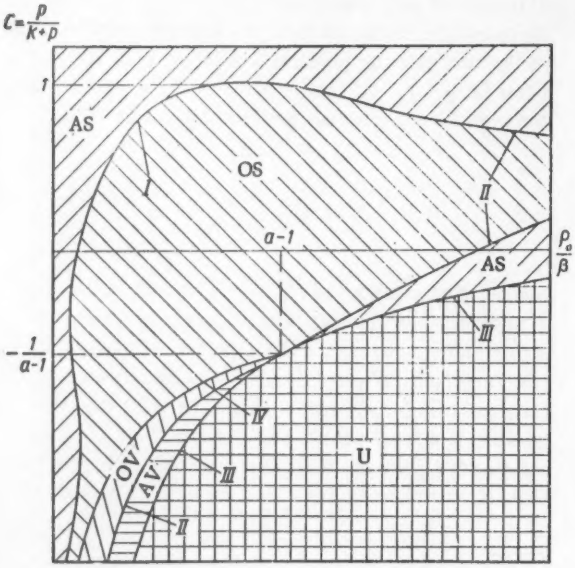

Fig. 1. Existence regions for different solutions of (3) in the neighborhood of the steady-state point.

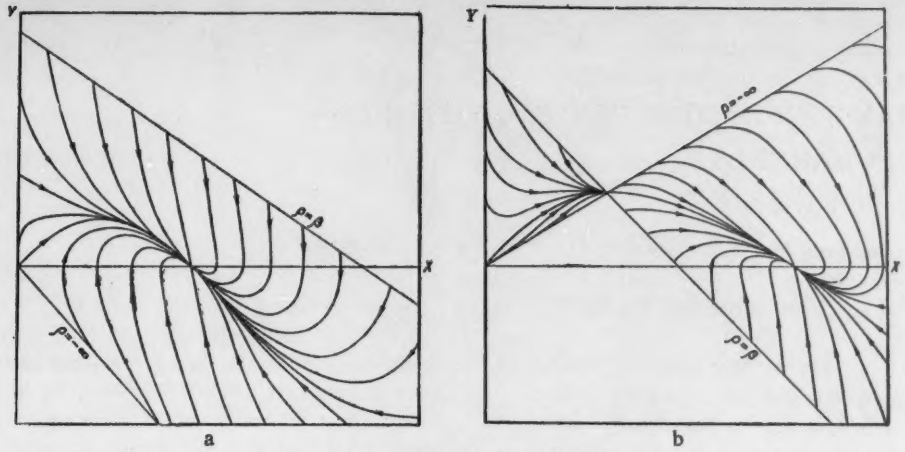

Fig. 2. Aperiodically stable solutions of (3) which end at the steady-state point. a) solutions in the a-type region; b) solutions in the c-type region.

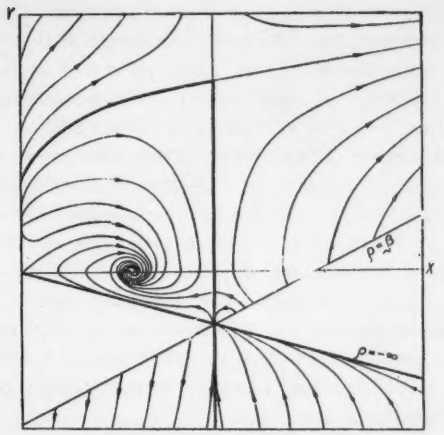

Fig. 3. Oscillatory-stable solutions of (3) at the steady-state point for the b-type region.

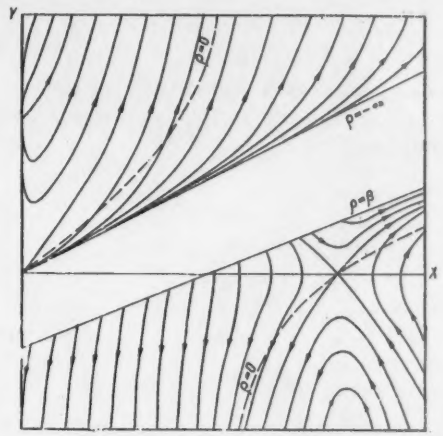

Fig. 4. Unstable solutions of (3) for the d-type region.

ively rises (tending to a certain limit), while ρ (t) is always negative. This regimen, which is caused by a positive temperature bond, sometimes arises for $p > 0$.

If we restrict our consideration to a single group of neutrons with an average lifetime (which is valid for slow processes), the region of solutions consists of an X, Y semiplane. The number of singular points is reduced to two: the zero and the steady-state points; in the steady-state point area, solutions of the following types remain: AS, OS, OU, and AU as the power increases for $p > 0$, and AS, OS, and AS for $p < 0$.

The authors extend their thanks to A. I. Leipunskii for his interest in the work.

LITERATURE CITED

1. A. I. Leipunskii et al., Transactions of the Second International Conference on the Peaceful Uses of Atomic Energy (Geneva, 1958). Vol. 2, Nuclear Reactors and Nuclear Engineering [in Russian] (Atomizdat, Moscow, 1959) p. 215.
2. F. Thalgott, Report No. 1845, presented by the USA to the Second International Conference on the Peaceful Uses of Atomic Energy (Geneva, 1958).
3. T. A. Velton, Experimental Reactors and Reactor Physics [in Russian] (Gostekhizdat, Moscow, 1956) p. 481.
4. R. Ackroyd, G. Kinchin, J. Mann, and T. McCullen, Report No. 1462, submitted by England to the Second International Conference on the Peaceful Uses of Atomic Energy (Geneva, 1958).
5. M. Schultz, Regulation of Nuclear Power Reactors [Russian Translation] (Il, Moscow, 1957).
6. W. Ergen and A. Weinberg, Physica 20, 413 (1954).
7. V. V. Nemytskii and V. V. Stepanov, Qualitative Theory of Differential Equations [in Russian] (Gostekhizdat, Moscow-Leningrad, 1947).

HEAT TRANSFER IN MERCURY FLOW THROUGH ANNULAR CHANNELS

V. I. Petrovichev

Translated from Atomnaya Énergiya, Vol. 7, No. 4, pp. 366-369
October, 1959
Original article submitted May 25, 1959.

At the present time, the heat transfer in the flow of liquid metals in annular channels is calculated in the first approximation according to heat-transfer equations which are valid for cylindrical tubes (with smooth surfaces), where the equivalent hydraulic diameter is introduced [1-4]:

$$Nu = 4{,}8 + 0{,}014\, Pe^{0{,}8}. \tag{1}$$

In this case, on the basis of analytical calculations, Lyon [5] recommends the following equation for an annular channel:

$$Nu_{ac} = 0{,}75 Nu_{tu} \left(\frac{d_2}{d_1}\right)^{0{,}3}, \tag{2}$$

where

$$Nu_{tu} = 7 + 0{,}025 Pe^{0{,}8} \text{ (for tubes).} \tag{3}$$

Here, the Nu and Pe numbers are also determined with respect to the hydraulic equivalent diameter $d_{eq} = d_2 - d_1$.

It is known that, due to the high "molecular" heat conductivity of liquid metals, the thickness of the thermal boundary layer in turbulent flow becomes comparable to the dimensions of the channel. Therefore, (2), which takes into account the geometric properties of the channel, must specify the heat-transfer characteristics under these conditions with greater accuracy. This incompatibility between (1) and (2) was the reason for undertaking the present investigation.

The heat transfer of mercury in turbulent flow in annular channels was investigated in two different experimental devices.

The layout of device No. 1 is shown in Fig. 1. The experimental section, which was 800 mm long, consisted of three tubes (Steel ÉYa1T), which were inserted into each other. The internal diameter of the middle tube was 26.9 mm, and the outside diameters of the two consecutively inserted internal tubes were 17.3 and 13.0 mm. The mercury flowed upward through the internal annular clearance, and cooling water flowed downward through the outer clearance and over the inner tube. Thus, the heat transfer from mercury was measured as it was cooled from the inside or the outside in the annular clearance with the ratios $d_2/d_1 = 1.55$ and $d_2/d_1 = 2.07$ for the boundary condition $q_w = \text{const}$. This condition was secured by maintaining the water equivalents with respect to mercury and water equal in each experiment. The inner tube at the experimental section was sealed with packings on both sides, which prevented its deformation by thermal expansion and permitted the rotation of the tube during measurements for checking against possible eccentricities. The temperatures of mercury and water were measured by means of thermocouples, which were placed in sockets in the inlet and outlet chambers. The maximum difference in the heat balance with respect to mercury and cooling water was 2-4% in experiments. The wall temperature in the annular clearance was measured along its length by means of 14 thermocouples, which were imbedded in the walls inside Steel ÉYa1T capillary tubes with diameters equal to 0.8 mm.

In order to check its reliability in operation, the experimental section was calibrated by means of a special water circuit.

The layout of arrangement No. 2 is shown in Fig. 2. The experiment section consisted of a tube 600 mm long which was made of Steel ÉYa1T and had an outside diameter of 17.5 mm and an inside diameter of 13.5 mm. A displacer, consisting of a tube with an outside diameter of 8.1 mm, was inserted into this tube and was sealed with packing at both ends, thus forming an annular clearance for the passage of mercury The displacer was provided with three narrow locators in order to insure against possible eccentricities in bending.

The external tube was divided into 24 parts by means of narrow annular channels in order to reduce the axial heat overflow. An electric heater, a calorimeter, and a compensation heater were consecutively wound on this tube. The electric heaters were fed a direct current at 130 v from a stable source. The stability of mercury cooling in the cooler was secured by means of a tank for keeping the cooling water at a constant level. The wall temperature was measured

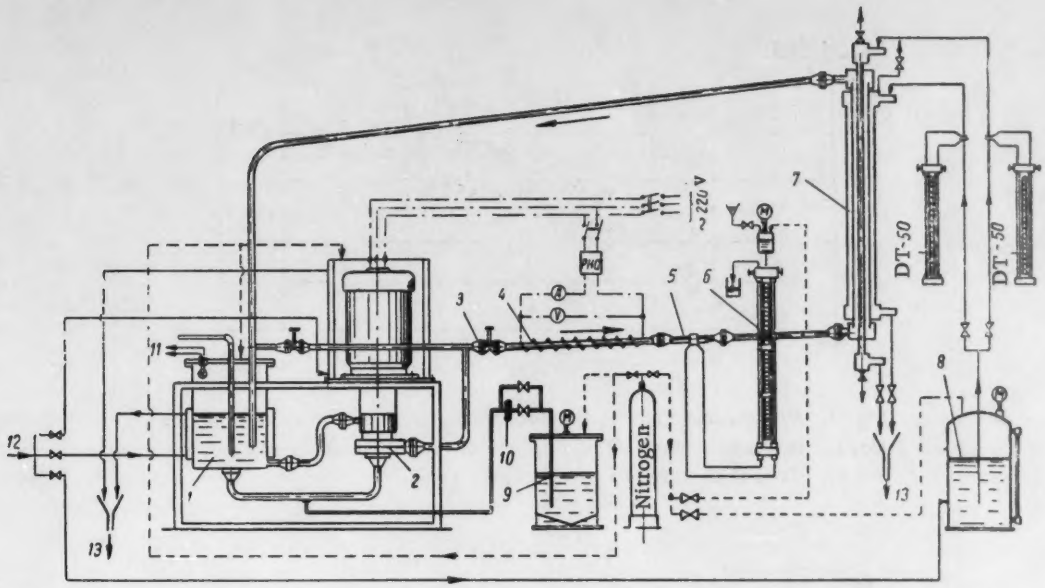

Fig. 1. Layout of experimental arrangement No. 1. 1) Mercury container; 2) circulation pump; 3) regulating valve; 4) electric heater; 5) flowmeter; 6) differential pressure gauge; 7) experimental section; 8) buffer water tank; 9) drainage tank for mercury; 10) filter; 11) level measurement; 12) cooling water; 13) drainage.

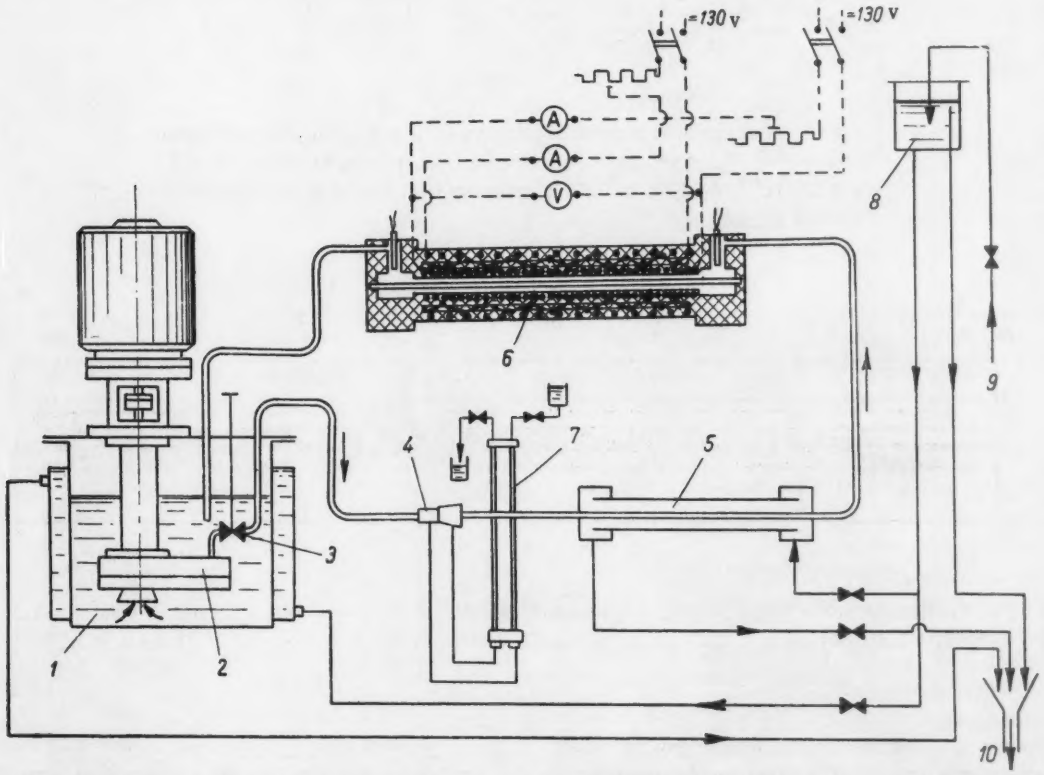

Fig. 2. Layout of experimental arrangement No. 2. 1) Mercury container; 2) circulation pump; 3) regulating valve; 4) throttling flowmeter; 5) cooler; 6) experimental section; 7) differential pressure gauge; 8) tank for keeping the cooling water at a constant level; 9) cooling water supply; 10) drainage.

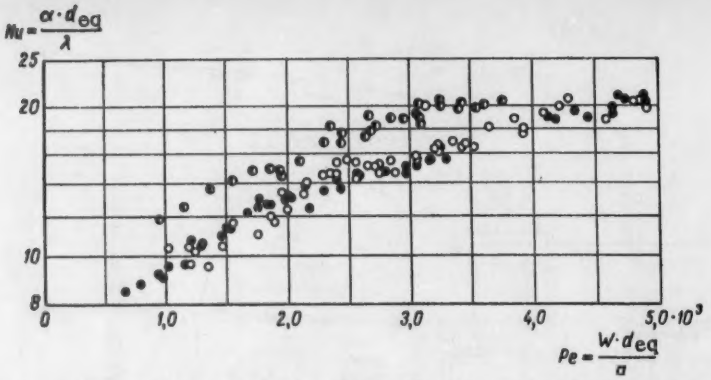

Fig. 3. Average heat transfer in mercury flow in annular channels (device No. 1). External cooling: O) $d_2/d_1 = 1.55$; internal cooling: ●) $d_2/d_1 = 1.55$; external cooling: ◐) $d_2/d_1 = 2.07$.

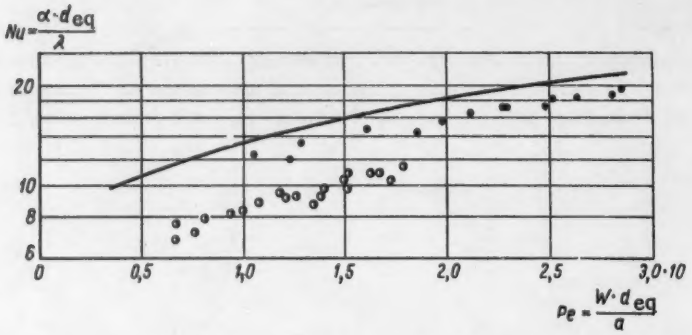

Fig. 4. Average heat transfer in mercury flow in annular channels (arrangement No. 2). ——) Lyon equation for heat transfer in tubes: $Nu = 7 + 0.025\ Pe^{0.8}$; ◐) $d_2/d_1 = 1.67$; ●) mercury heat loss in the tube (without the inner displacer).

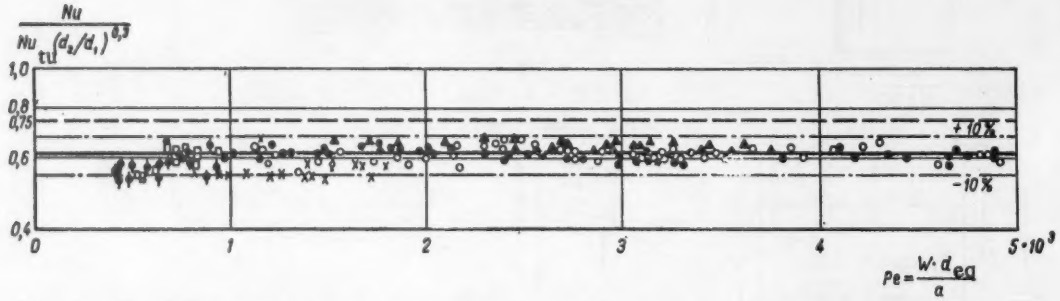

Fig. 5. Comparison of experimental and theoretical data for mercury. Author's data: O) $d_2/d_1 = 1.55$; ●) $d_2/d_1 = 1.55$; ▲) $d_2/d_1 = 2.07$; ×) $d_2/d_1 = 1.67$; data from [4]: ⧫) $d_2/d_1 = 1.42$; □) $d_2/d_1 = 1.77$.

by means of 12 thermocouples, which were imbedded along the tube length. The experimental section also was calibrated with respect to water. All the tubes in experimental sections in both devices were carefully calibrated and ground. Mercury was chemically purified and filtered before pouring it into the device.

Measurement results. All experiments were performed for average mercury temperatures from 30 to 50° C and velocities from 0.3 to 2.25 m/sec.

The dimensionless similarity criteria for heat-transfer processes, calculated with respect to the equivalent hydraulic diameter, were varied within the

following ranges in the experiments: arrangement No. 1: Re = 27×10^3-200×10^3 and Pe = 670-4900; arrangement No. 2: Re = 15×10^3 – 75×10^3 and Pe = 500-1800.

Figures 3 and 4 show the results obtained in measuring the heat loss of mercury in flow in annular channels, given in the form of the generally accepted dependence Nu = f(Pe), where the equivalent hydraulic diameter was used as the characteristic determining dimension. From these figures, it follows that:

1. The experimental data for different d_{eq} cannot be given by a single dependence in such treatment, and therefore, the calculation of heat transfer in turbulent flow of liquid metals in annular channels according to equations for cylindrical tubes cannot yield accurate results;

2. The heat transfer in an annular channel, for the same d_{eq}, is practically identical for external and internal cooling.

In Fig. 5, the experimental data are compared with results obtained by calculation according to (2). It can be seen that the discrepancies between experimental data for different d_{eq} correspond to the correction $(d_2/d_1)^{0.3}$ in (2). These values are somewhat lower than the values obtained by using this equation for the d_2/d_1 ratios which are used in measurements. This can be apparently explained by the presence of a certain contact-thermal resistance at the wall-liquid metal boundary.

Thus, until more accurate data for calculating the heat transfer from heavy liquid metals in turbulent flow in channels with annular cross sections are obtained, the equation

$$Nu = (4{,}3 + 0{,}015\, Pe^{0{,}8}) \left(\frac{d_2}{d_1}\right)^{0{,}3}, \qquad (4)$$

can be recommended, which in the Pe = 500-5000 region, agrees with the obtained data with an accuracy of ± 10%.

LITERATURE CITED

1. L. Trefethen, General Discussion on Heat Transfer (London, 1951).
2. R. Seban and D. Casey, Trans. ASME 79, 1514 (1957).
3. S. S. Kutateladze, V. M. Borishanskii, I. I. Novikov, and O. S. Fedynskii, Liquid-Metal Heat Transfer Media – Suppl. No. 2 to Atomnaya Énergiya [in Russian] (Atomizdat, Moscow, 1958). *
4. V. I. Petrovichev, Collection: Certain Problems in Experimental Physics [in Russian] No. 2 (1959).
5. R. Lyon, Liquid Metals Handbook (2 ed) (1952).

*See C. B. translation.

* * *

GAMMA-RAY ALBEDO OF Co^{60}, Cs^{137}, AND Cr^{51} ISOTROPIC SOURCES FOR SOME SUBSTANCES

B. P. Bulatov

Translated from Atomnaya Énergiya, Vol. 7, No. 10, pp. 369-372
October, 1959
Original article submitted May 5, 1959

In [4], the absolute value of the γ-ray energy albedo of Co^{60} and Au^{198} was experimentally determined for different substances at primary-beam angles of incidence of 0, 45, and 60°.

In the present work, we studied the energy albedo of γ rays emitted by isotropic sources in direct contact with the surface of a scatterer.

METHOD OF MEASUREMENT

The absolute value of the albedo was calculated as the ratio of the total stream of the scattered energy J (Mev/sec) to the total stream of energy J_0 (Mev/sec) of the primary radiation emitted by the sources in a hemisphere.

The experimental arrangement for determining the angular dependence of the intensity of the scattered radiation is shown in Fig. 1a. The γ-ray sources, in the form of cylinders 5 mm in diameter and height, were placed at the center of a scatterer of size 65 × × 65 cm and of practically "infinitesimal" thickness [1]. As sources of monochromatic γ rays we used the radioactive isotopes Cr^{51} (Eγ = 0.320 Mev), Cs^{137} (Eγ = 0.661 Mev), and Co^{60} (Eγ ≃ 1.25 Mev). Carbon, aluminum, iron, and lead were used as scattering material.

By means of a detector placed in a hemisphere of 30 cm radius with its center at the point of contact between the source and the scatterer, the density of the stream of γ-ray energy was measured both with

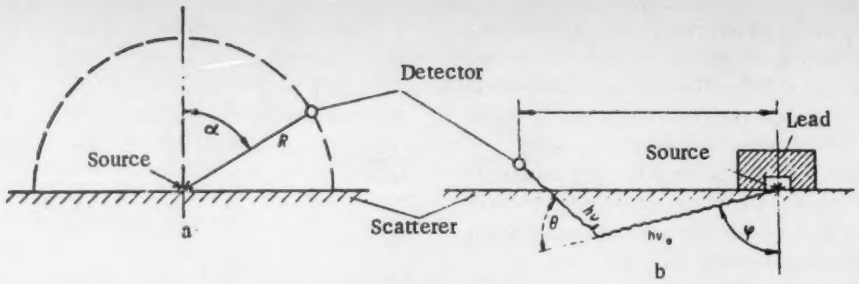

Fig. 1. Experimental setup.

the scatterer and without it. The density of the stream of energy of the scattered radiation was determined from the difference in the readings as a function of the angle α.

The energy J of the total stream of back-scattered radiation and the total stream of energy J_0 of the primary radiation was determined by numerical integration of the corresponding densities of the energy streams over the entire surface of the hemisphere.

The experimental arrangement for determining the dependence of the intensity of scattered radiation and its spectral composition at the distance r between the source and the detector is shown in Fig. 1b. A Co^{60} source in the form of a plate 3.1 × 1.8 × 0.3 cm was placed at the center of a graphite block of size 300 × × 300 × 22 cm. The detector was located above the surface of the scatterer at a height of 5 cm. A lead shield was used to absorb the primary radiation.

During the determination of the spectrum of scattered γ radiation escaping from the scatterer, the radiation was filtered through lead. A counter which had practically constant sensitivity to γ rays of different energy [1, 2] was used in this work. The total error in determining the absolute value of the albedo was ± 15%.

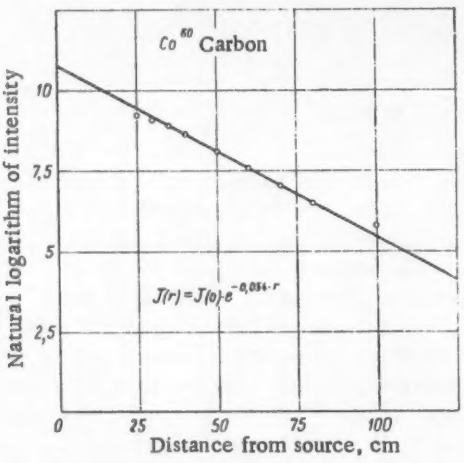

Fig. 2. Relation between intensity of back-scattered radiation and distance between detector and source.

RESULTS OF THE MEASUREMENT

From Fig. 2 it is seen that the intensity of the back-scattered γ-radiation drops exponentially with the distance from the source. This results from the fact that at distances greater than $1.5 - 2\mu_0 r$ the detector records practically only the scattered γ rays from the narrow beam of primary radiation traveling in the direction of the detector, almost parallel to the surface of the scatterer, i.e., at the angle $\varphi \simeq 90°$.

It follows from Fig. 1b that the smaller the angle φ at which the primary radiation is emitted, the smaller the intensity of the escaping scattered radiation, since firstly, with a decrease in the angle φ the scattering angle increases, i.e., the probability of scattering and the hardness of the γ rays decrease [3], and secondly, the path traveled by the scattered radiation in the scatterer increases. The same applies to the γ rays emitted at angles φ close to 90°, but in directions that do not coincide with the source-detector line.

This discussion is confirmed by experiments to determine the spectrum of the radiation escaping from the scatterer. Measurements were made for distances $2\ \mu_0 r$ and $6\mu_0 r$. In both cases, two effective lines of different intensity, with energies of 300-400 and 600-700 kev, were noted in the scattered radiation spectrum. As the distance from the source increased, the contribution of the soft component increases from 70-80% at $r = 2\ \mu_0 r$ to 90% and more at $r = 6\ \mu_0 r$. The hard component of the spectrum was due to single-scattering of the primary γ radiation by angles of $\theta \simeq 40$-60° emitted almost parallel to the surface ($\varphi \simeq 80$-90°). The soft component is produced by the primary γ rays either scattered by angles close to 90° or multiply scattered by small angles of θ.

From Fig. 3 it is seen that the angular distribution of the intensity of the scattered radiation bears an anisotropic character. For the hard γ rays, the maximum intensity occurs at angles φ close to 90°. With a decrease in the energy of the primary radiation, the anisotropy in the angular distribution of the scattered radiation

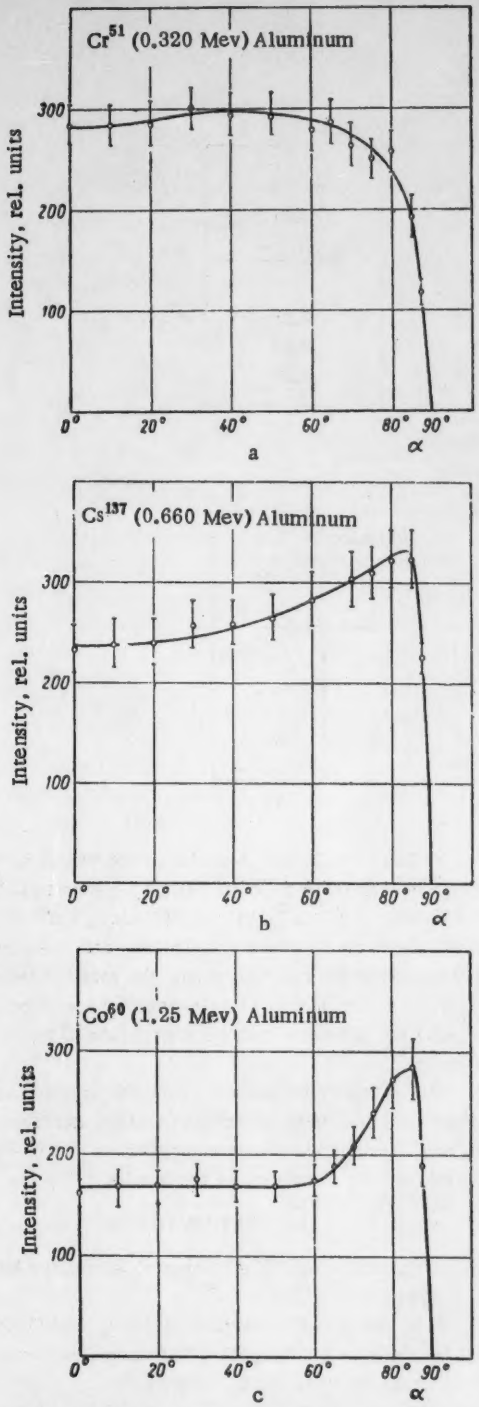

Fig. 3. Relation between the intensity of γ rays from Cr^{51} a), Cs^{137} b), Co^{60} c) scattered by aluminum and the angle α.

intensity decreases, the maximum spreads out and shifts in the direction of the smaller angles. With an increase in the atomic number of the scattering material, the angular distribution becomes more isotropic. All these phenomena are explained by the anisotropy in the angular distribution of Compton scattering and the greater hardness (and also greater path traveled after scattering) of the γ quanta scattered by small angles. The shape of the scattered radiation intensity vs angle α curve is similar to the curve giving the relation between the γ-ray energy albedo (or the quantity [B-1], where B is the accumulation coefficient of the energy with reflection) and the angle of incidence of the primary radiation [4-7] (Fig. 4). As may be seen from Fig. 5, the decrease in the γ-ray albedo of an isotropic source is inversely proportional to the atomic number of the scattering material. With a decrease in the hardness of the primary γ radiation of an isotropic source, the energy albedo increases proportionally to $(E\gamma)^{-1/2}$. The general character of the dependence of the energy

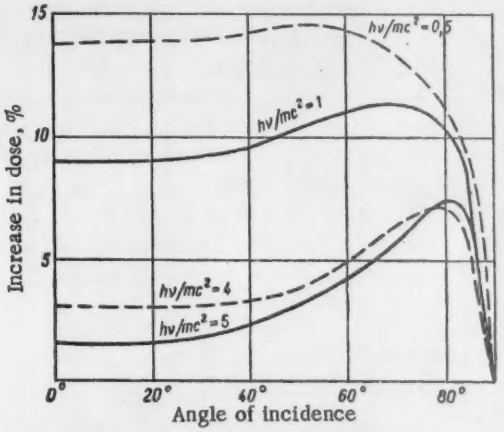

Fig. 4. Relation between quantity [B-1] and angle of incidence of primary radiation.

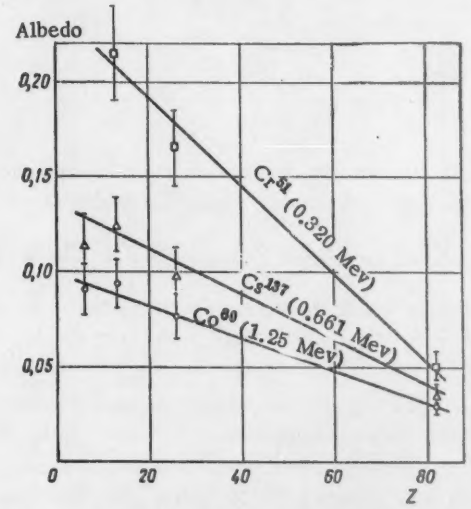

Fig. 5. Relation between energy albedo of γ rays from Cr^{51}, Cs^{137}, and Co^{60} and atomic number of scattering material.

TABLE 1. Cr^{51}

Scattering material	Z	Albedo (exptl.)
Aluminum	13	0.21
Iron	26	0.17
Lead	82	0.05

TABLE 2. Cs^{137}

Scattering material	Z	Albedo	
		exptl.	[6]
Carbon	6	0.12	—
Aluminum	13	0.13	0.124
Iron	26	0.10	—
Lead	82	0.04	—

TABLE 3. Co^{60}

Scattering material	Z	Albedo		
		exptl.	[1,6]	[7]
Carbon	6	0,091	—	0,11 (H_2O)
Aluminum	13	0,094	0,081	0,10
Iron	26	0,077	0,069	0,09
Lead	82	0,029	0,025	0,03

albedo for rays from an isotropic source on the atomic number of the scattering material is described well by the empirical expression $\eta = \frac{4,0}{V\,E_\gamma}\left(1-\frac{Z}{110}\right)$ (E_γ is in kev) within the limits of ± 20%. From this expression and from the shape of the curves of Fig. 5, it follows that at some values $Z = Z_{lim}$ the energy albedo should go to zero. This is explained by the fact that for some substances with $Z > Z_{lim}$ the entire process of interaction with electromagnetic radiation practically reduces to photoelectric absorption alone. The lower the energy of the primary radiation, the smaller the value of Z for which the photoeffect begins to dominate over Compton scattering.

In Tables 1, 2, and 3 are listed the values of the energy albedo of γ rays from isotropic sources Cr^{51} (E = 0.320 Mev), Cs^{137} ($E\gamma$ = 0.661 Mev), Co^{60} ($E\gamma \simeq$ ≃1.25 Mev) obtained experimentally and calculated by integrating the function giving the relation between the value of the albedo and the angle of incidence of the primary radiation over all angles from 0 to 90° as given in [1, 6, 7].

The authors express their profound gratitude to Professor O. I. Leipunskii for his constant attention to this work and for his valuable suggestions and to P. A. Yampol'skii for discussion of the results.

LITERATURE CITED

1. B. P. Bulatov and E. A. Garusov, Atomnaya Énergiya 5, 631 (1958).*
2. B. P. Bulatov, Atomnaya Énergiya 6, 332 (1959).*
3. H. Lohus and J. Laughlin, Radiation Dosimetry (Academy Press, N. Y., 1956) p. 64.
4. J. Corner and R. Liston, Proc. Royal Soc. A. 203, 323 (1950).
5. M. Berger and J. Doggett, J. Research Nat. Bur. Standards 56, 89 (1956).
6. J. Perkins, J. Appl. Phys. 26, 655 (1955).
7. E. Hayward and J. Hubbell, Phys. Rev. 93, 955 (1954).

* Original Russian pagination. See C. B. translation.

DISTRIBUTION OF KINETIC ENERGY OF FRAGMENTS IN TERNARY FISSION OF U^{235} BY THERMAL NEUTRONS

V. I. Mostovoi, T.A. Mostovaya, M. Sovinskii, and Yu. S. Saltykov

Translated from Atomnaya Énergiya Vol. 7, No. 4, pp. 372-374
October, 1959
Original article submitted May 4, 1959

The kinetic-energy distribution of fragments from U^{235} fission with the emission of long-range α particles was first measured by Allen and Dewan [1]. They showed that the kinetic-energy distribution of the fragments in ternary fission was similar to that usually observed in binary fission. The distribution curve had two maxima which corresponded to the two groups of fragments. In comparison with binary fission, the maxima were shifted to the low-energy side by 8 and 10.5 Mev (for the heavy and light fragments respectively).

The distribution curve obtained for ternary fission fragments was strongly distorted and did not permit a more detailed analysis and comparison with binary fission. This distortion, due to the dependence of the recording of the fragment on the angle of emission of the long-range α-particles, was considerable under the experimental conditions of [1], and accurate calculations were difficult.

In the present work, we obtained more accurate information on the kinetic-energy distribution of the fragments in ternary fission.

A double ionization chamber with a grid usually employed for investigating binary fission (Fig. 1) was used to detect the fragments and the long-range α particles. The fragments were detected in one-half of the chamber and the long-range α-particles in the other.

Tin foil (12 μ thick), on which was deposited a thin layer of U^{235} ($\sim 25\ \mu g/cm^2$), was placed on the central electrode common to both chambers. The foil completely absorbed the fragments and α particles from the natural radioactive decay of uranium which were emitted in the direction of the chamber detecting the long-range α-particles. The total energy threshold for recording the long-range α-particles (absorption in the layer of tin and the electronic circuit bias) was ~ 7 Mev.

The ionization pulses from the fragments, separated after amplification, were fed to a single-channel amplitude analyzer and then to one of the inputs of the coincidence circuit, the other input receiving the pulses from the long-range α-particles. Thus, with the help of the coincidence circuit it was possible to obtain the relation between the number of ternary fissions and the energy of one of the fragments. This relation for binary fission was obtained by recording the fragments directly from the amplitude analyzer.

The background of random coincidences corresponding to fragments of a given energy was determined from the counts of both channels and resolving time of the circuit. The resolving time was measured and checked during the experiment by recording cases of random coincidences between the fission fragments and the statistical time-distribution of pulses from an independent detector. The background of random

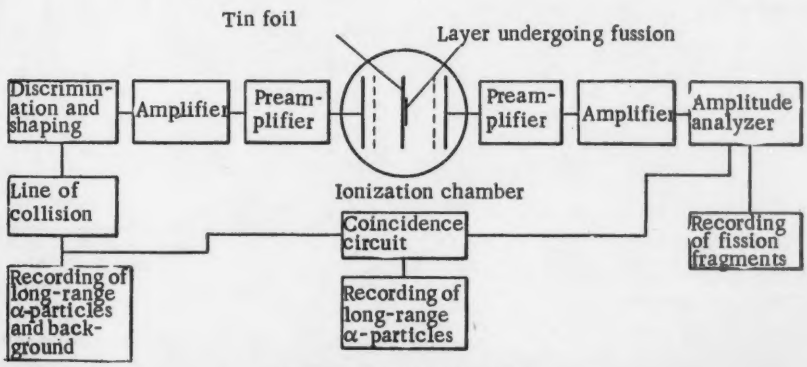

Fig. 1. Experimental Setup.

coincidences depended on the energy of the fragments and was 10-30% for the majority of points on the curve.

The measurements were made using a neutron beam from the VVR reactor. To decrease the counts in the long-range particle channel due to protons and α particles from the reactions (n, p), (n,α) in the gas and chamber materials, and from also γ rays, the neutron spectrum was specially shaped by the use of lead in the graphite column.

Figure 2 shows the kinetic-energy distribution of fragments in ternary fission (open circles and solid line). The total number of recorded cases of ternary fission was 17,644. For comparison, the distribution for ternary fission, measured under the same conditions, is also shown (black circles and broken line). The results of [2] were used to calibrate the energy scale.

It is seen from the figure that even with the use of a counting geometry of 2π, the areas obtained in the experiment for the two groups of fragments produced in ternary fission are appreciably different from each other. The ratio of the area of the light fragments to that of the heavy fragments is 0.82.

The simple counting geometry of the chamber allowed a reliable determination of the effect of the angular distribution of long-range α particles on the fragment counting efficiency. The ratio of the probability of recording a heavy fragment to that of a light fragment $P_H : P_L$, calculated by taking into account the distribution of the long-range α particles [3, 4], was 1.20, which fully explains the observed difference in areas.

Figure 3 shows the kinetic-energy distribution of the fragments for ternary fission, where the probability that the fragments are recorded is taken into account. The most probable energy of the heavy and light fragments is smaller by 5.7 ± 0.5 and 8.1 ± 0.3 Mev, respectively, than for binary fission, which is a somewhat smaller value than that obtained in [1]. It should be noted that the decrease in the kinetic energy by 13.8 Mev can be explained by the decrease in the charge of the fragments, owing to the emission of the α particles.

Apparently, the asymmetry of the fragments in ternary fission should be more marked than in binary fission.

The most probable value of the energy of the long-range α-particles emitted during the fission of U^{235} induced by thermal neutrons, as is known, is equal to 14.8 Mev [1, 3, 5]. Therefore the most probable value of the total kinetic energy released in ternary fission is 1 Mev greater than in binary fission.

Using this result and the data on the masses of the nuclei [6], we made an estimate of the excitation energy of the fragments in ternary and binary fission of U^{235} induced by thermal neutrons. In this estimate we assumed that in binary fission only fragments of masses 100 and 136 are produced. In ternary fission, the occurrence of pairs of fragments with masses 98-134, 96-136, and 100-132 were taken to be equally probable.

Under these assumptions, the mean excitation energy of the fragments in ternary fission should be 5.7 Mev smaller than in binary fission.

This estimate of the excitation energy of the fragments is in good agreement with the results of the measurements of the number of secondary neutrons $\nu_{\alpha f}$ in the ternary fission of U^{235} [7]. In this work, the value obtained for $\nu_{\alpha f}$ was 1.77 ± 0.09.

Actually, for the set of fragment masses which we chose for ternary fission, the mean binding energy of the neutron is 5.4 Mev [6]. It may be assumed that the mean kinetic energy of the neutrons (in the

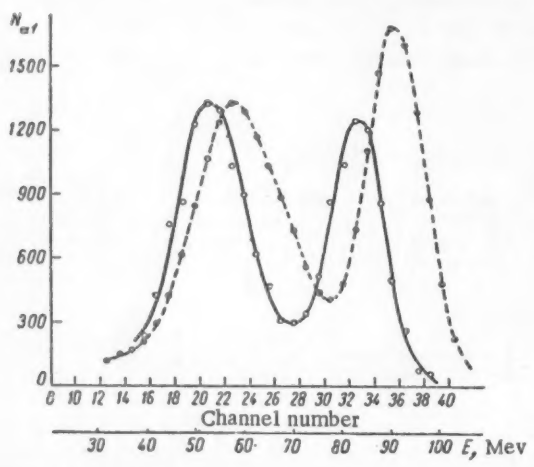

Fig. 2. Measured kinetic-energy distribution of the fragments.

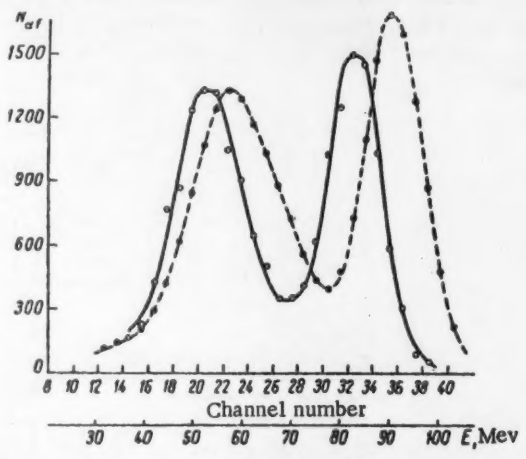

Fig. 3. Kinetic-energy distribution of fragments, taking into account the probability of their being recorded.

center-of-mass system) emitted by the fragments in ternary fission is the same as for binary fission (1.4 Mev) [8]. Thus, an average energy of 6.8 Mev is necessary for the emission of a neutron by a fragment. Therefore the decrease in the excitation energy by 5.87 Mev should lead to a decrease in the mean number of secondary neutrons by the value $\Delta\nu_{\alpha f} = 0.86$. This should correspond to a mean number of secondary neutrons in ternary fission of $\nu_{\alpha f} = 1.61$.

The half-widths of the kinetic-energy distribution of the light and heavy fragments in ternary fission are smaller than the corresponding half-widths in binary fission by 1.1 ± 0.5 and 4.3 ± 1.0 Mev. The decrease in the width of the distribution may partially be explained by the smaller mean number of secondary neutrons emitted. However, in the main, this decrease is apparently connected with the last stage of the division of the fragments in ternary fission. The difference in the dispersion of the kinetic energy should also indicate a dispersion in the number of neutrons emitted in ternary fission.

The distribution of kinetic energy of the fragments in ternary fission is not only shifted, but is also noticeably different in shape. This indicates that the mass distribution of the fragments in ternary fission should be different than the mass distribution in binary fission.

LITERATURE CITED

1. K. Allen and J. Dewan, Phys. Rev. 80, 181 (1950).
2. J. Wahl, Phys. Rev. 95, 126 (1954).
3. E. Titterton, Nature 168, 590 (1951).
4. Tsien San-tsiang, L. Chastel and Ho Zah-wei, J. Phys. et radium 8, 165 (1947).
5. B. Cohen and C. Fulmer, Proc. Intern. Conference on the Neutron Interactions with the Nucleus. New York, Columbia University, September, 1957 P III, B4.
6. A. Cameron, A Revised Semiempirical Atomic Mass Formula (Chalk River, Ontario, 1957).
7. V. F. Apalin, Yu. P. Dobrynin, V. P. Zakharova, I. E. Kutikov, and L. A. Mikaelyan, Atomnaya Énergiya, present issue, translation p. 853.
8. J. Terrell, Proc. Intern. Conference on the Neutron Interactions with the Nucleus. New York, Columbia University, September, 1957. P. III, B4.

* * *

MEAN NUMBER OF NEUTRONS EMITTED FROM U^{235} IN TERNARY FISSION

V. F. Apalin, Yu. P. Dobrynin, V. P. Zakharova, I. E. Kutikov and L. A. Mikaelyan

Translated from Atomnaya Énergiya, Vol. 7, No. 4, pp. 375-376
October, 1959
Original article submitted May 4, 1959

Ternary fission of heavy nuclei with the emission of α particles is a very uncommon and a comparatively little studied phenomenon. It is known that for approximately 400 binary fissions there is about one ternary fission [1]. The α-particle spectrum is continuous, having a broad maximum at an energy of about 15 Mev, and extends up to 28 Mev [2]. The α particles are emitted principally perpendicular to the line of flight of the fragments [3], and it may be assumed that their emission takes place at the instant of rupture of the last link of the splitting nucleus. This last factor makes ternary fission particularly interesting. In binary fission, during the formation and rupture of the final link, no radiation is observed, and therefore this stage escapes direct experimental investigation. The study of ternary fission can shed light on the mechanism of the first stages of the fission process. It is of interest to note that the limit of the α-particle energy spectrum (28 Mev) appreciably exceeds the value which could be obtained from the repulsive Coulomb forces of the uranium nucleus. In the low-energy region the α-particle spectrum has been studied from approximately 6 Mev, and its shape in this region permits the assumption that still softer α particles are present. As far as we know, this feature has not yet been qualitatively explained. Of greater interest, in our view, is the study of the characteristics of ternary fission and its dependence on the mass ratio of the fragments and the total energy balance.

Bearing in mind that the number of neutrons emitted during the fission of the nucleus is a measure of the excitation of the fragments, we measured the mean number of neutrons ν emitted during ternary fission of the U^{236} nucleus.

The work was carried out on a neutron beam from the VVR reactor. A layer of U^{235}, 0.7 mg/cm^2 thick, was deposited on the central electrode of a double ionization chamber. The fission fragments were recorded in one half of the chamber. The other half of the chamber was separated from the U^{235} layer by an aluminum filter 35 μ thick, in which the fission fragments and also the α particles from U^{235} were completely stopped, which permitted the recording in this half of the chamber of the long-range particles from ternary fission. Since in this half of the chamber there was always observed a background of pulses caused by the occurrence of recoil nuclei from fast neutrons and by reactions of the (n, p) type, the acts of ternary fission were separated by comparison of the pulses of both halves of the ionization chamber. A control experiment indicated that with an aluminum filter thickness of 340 μ, sufficient for stopping α particles from ternary fission, the coincidence counts decreased 300-fold and reached the level of the random coincidence background. Under the conditions of the experiment, 100 cases of ordinary fission were recorded per second, and the ternary coincidence counting rate was 160 coincidences per hour. The chamber was placed in the center of a high-efficiency fission-neutron detector [4]. The detector consisted of a tank 200 liters in volume, filled with a liquid scintillator. The fission neutrons, slowed down in the detector, were captured by cadmium introduced into the scintillator liquid and the pulses of light from the γ rays of the capture were registered by 32 photomultiplier tubes of type FÉU-24. The mean lifetime of the neutrons in the scintillator was 11 μsec. The operation of the electronic apparatus was controlled by coincidence pulses of the fragments and the α particles from ternary fission. The gate letting through the pulses from the neutron detector to the counting circuit was opened 0.6 μsec after the occurrence of this pulse for an interval of 25 μsec. The resolving power of the amplifier and counting circuit was 0.4 μsec. The background level under the conditions of the experiment amounted to about one count per fission. In the experiment ν was determined for ternary fission relative to ν for binary fission of U^{235}, which was taken as 2.45. Therefore, it was not necessary to determine the efficiency of the scintillation detector and the entire arrangement for recording the neutrons. During the measurement approximately 5,000 cases of ternary fission were recorded. The mean number of neutrons for one act of ternary fission was 1.77 ± 0.09. For an aluminum filter, thickness of 35 μ, the system recorded ternary fission accompanied by the emission of α particles of energy greater than 9 Mev. It seemed to us essential to explain the relation between the value ν and the energy of the α particle. This dependence was investigated by means of measurements with an aluminum filter 135 μ thick. The apparatus then recorded only cases of ternary fission accompanied by the emission of α particles with energies exceeding ~ 22 Mev, and the counting rate was 40 coincidences per hour.

The mean value of ν for $E \geq 22$ Mev turned out to be 1.79 ± 0.13, which, within the limits of experimental error, is in agreement with the results of the previous measurements. The data obtained shows that the excitation energy of the fragments does not depend on the energy of the long-range α-particles from ternary fission.

It is known that for the evaporation of a neutron from a fragment in binary fission an average of about 7 Mev is required [5, 6]. In ternary fission, this value, apparently, can only be decreased by overloading the fragments with neutrons. Therefore the decrease in the value of ν indicates that the excitation energy of the fragments, in the case of ternary fission, is smaller than for binary fission, in the extreme case, by 4-5 Mev. According to [7], before the final link ruptures, the fragments are deformed and the potential energy of the deformation is later changed into excitation energy. The observed decrease in the excitation energy of the fragments is probably connected with the decrease in their initial deformation.

The authors thank K. S. Mikhailov and his coworkers for help in preparing the scintillation preparations.

LITERATURE CITED

1. K. Allen and J. Dewan, Phys. Rev., 80, 181 (1950).
2. C. Fulmer, and B. Cohen, Phys. Rev. 108, 370 (1957).
3. E. Titterton, Nature 168, 590 (1951).
4. F. Reines, C. Cowan et al., Rev. Sci. Instr. 25, 1061 (1954).
5. V. I. Kalashnikova, V. I. Lebedev and P. E. Spivak, Atomnaya Énergiya 2, 18 (1957).*
6. W. Stein and S. Whetston, Phys. Rev. 110, 476 (1958).
7. N. Bohr and I. Wheeler, Phys. Rev. 56, 426 (1939).

* Original Russian pagination. See C. B. translation.

INTERACTION OF FAST NUCLEONS WITH NUCLEI OF NIKFI-R PHOTOEMULSION

V. S. Barashenkov, V. A. Belyakov, Wang Shu-fên, V. V. Glagolev, N. Dolkhazhav, L. F. Kirillova, R. M. Lebedev, V. M. Mal'tsev, P. K. Markov, K. D. Tolstov, E. N. Tsyganov, M. G. Shafranova, and Yao Ch'ing-hsieh

Translated from Atomnaya Énergiya, Vol. 7, No. 4, pp. 376-377
October, 1959
Original article submitted April 13, 1959

In this work we studied the interaction of 9-Bev protons accelerated in the beam of the synchrophasotron of the Joint Institute for Nuclear Studies with nuclei of NIKFI-R photoemulsion. The results of the measurements are shown in the table. In this table $\overline{n}_s$, $\overline{n}_g$, $\overline{n}_b$ are the mean number of charged particles (calculated for one star)*; $\overline{\theta}_{s1/2}$, $\overline{\theta}_{g1/2}$, $\overline{\theta}_{b1/2}$ are the angles within which half the particles are contained; $E_{s\pi}$, E_{sp}, $E_{g\pi}$, E_{gp}, and E_{bp} are the mean kinetic energies of pions and protons; $p_{s\perp\pi}$ and $p_{g\perp p}$ are the mean transverse moments of s-pions and g-protons.

On the basis of the data obtained, it is possible to draw some conclusions on the mechanism of interaction of fast protons with nuclei.

The assumption of an interaction of the primary nucleon with a "tunnel" leads to values of the angles $\overline{\theta}_{s1/2} \simeq 30°$ for the light nuclei and $\overline{\theta}_{s1/2} \simeq 40°$ for the silver and bromium nuclei. These values are appreciably higher than the experimental values of $\overline{\theta}_{s1/2}$. Any eventual secondary interaction of the particles produced in the nucleon – tunnel collision can only increase the calculated values of the angle.

Further, if the primary nucleon – nucleus collision is a nucleon – tunnel interaction, then the velocity of the center-of-mass in the case of a tunnel interaction in silver and bromium will be considerably less than in the case of an interaction with a light nucleus, and consequently, there should be a considerably greater number of s-particles. In the experiment, the number of s-particles for the heavy and light nuclei was almost the same. This can be understood on the basis of the cascade mechanism of interaction, whereby the s-particle energy in cascade collisions decreases rapidly, and along with this, the multiplicity in the production of particles also decreases.

Moreover, if the mechanism was one of a nucleon-tunnel interaction, then among the g-particles should be observed a mixture of π-mesons produced in the collision of the nucleon and the tunnel. In the experiment, most of the g-particles were nucleons, which can be explained by the cascade mechanism for the nucleon – nucleus interaction, where the majority of the g-particles are recoil nucleons. The characteristics, as shown in the table, for disintegrations of nuclei with the emission of more than 28 g- and b-particles, which are observed in about 2% of the cases, are still more difficult to explain by the tunnel interaction.

The same values of the transverse momenta $p_{g\perp p}$ for g-protons from interactions with light and heavy nuclei also speak in favor of the cascade mechanism of interaction.

A search for strange particles was also made by area scanning. The cross section for the production of K^+ particles of energy $E \leq 140$ Mev was found to be $(5 \pm 2)\ 10^{-27}$ cm^2 in the average emulsion nucleus.

The value of the cross section for the production of K-mesons, their broad angular distribution, and the greater number of prongs from the parent stars in comparison with the average also indicate that an appreciable number of slow strange particles is produced in the cascade process inside the nucleus.

The mean energy loss of a fast nucleon in a single act of collision was estimated. In the case of the average emulsion nucleus, a 9-Bev proton loses, on the average (5.1 ± 0.8) Bev (of which 4.05 Bev

*In what follows, the subscript s denotes data on fast particles (s-particles) with ionization $I \leq 1.4\ I_0$ (I_0 is the ionization loss corresponding to the ionization of 9-Bev protons); the subscript g denotes data on particles with $I > 1.4\ I_0$ and range $R > 3.74$ mm (g-particles); the subscript b denotes data on particles with $I > 1.4\ I_0$ and $R < 3.73$ mm (b-particles).

Characteristics of the Interaction of 9-Bev Protons with Photoemulsion Nuclei.

Characteristic	Light nuclei C, N, O	Heavy nuclei Ag, Br	Stars with $n_b + n_g \geq 28$	Mixture of emul. nuc.
$\bar{n}_s$	3,0±0,2	3,5±0,3	4,0±0,4	3,2±0,2
$\bar{n}_g$	1,4±0,1	4,1±0,5	32	3,1±0,4
$\bar{n}_b$	3,3±0,1	6,1±0,6	—	4,7±0,5
$\bar{\theta}^\circ_{s^1/_2}$	22,5±1	27,5±1,5	53	25,0±1,5
$\bar{\theta}^\circ_{s^1/_2}$	56,5±3	65±3	63	65±3
$\bar{\theta}^\circ_{s^1/_2}$	—	84±3	—	84,5±3
$E_{s\pi}$, Bev	—	—	—	1,0±0,2
E_{sp}, Bev	—	—	—	3,0±0,5
$E_{g\pi}$, Mev	—	—	—	40±3
E_{gp}, Mev	132±20	—	—	120±12
E_{bp}, Mev	—	—	—	11±1
$p_{s\perp\pi}$, Mev/c	—	—	—	370±70
$p_{g\perp p}$, Mev/c	344±20	354±20	—	350±20

is used in the production of π-mesons and 1.05 Bev is transferred to the nucleus), which represents (60 ± ± 10)% of the initial energy. Since the proton experiences approximately two collisions in the average nucleus, the proton loses ΔE = 35 ± 10% of its initial energy in a single act of nucleon – nucleon collision. From independent measurements of the energy spectrum of π-mesons in nucleon – nucleus collisions, it was found that ΔE = 40 ± 10%. According to the statistical theory of multiple production, ΔE = (40-50)% [1].

We thank G. Beznogikh, V. Vaksin, Z. Kuznetsov, and N. Metkin for help in the measurements, and L. Popov for help in the analysis of the results of the measurements.

LITERATURE CITED

1. V. Barashenkov, V. Belyakov, Wang Shou-feng, V. Maltzev, Ten-Gyn, and K. Tolstov, Nuclear Phys. 9, 74 (1958).

* * *

EXCITATION CURVES FOR THE REACTIONS B^{11} (d, 2n) C^{11}, Be^9 (α, 2n) C^{11}, B^{10} (d, n) C^{11}, and C^{12} (d, n)N^{13}

O. D. Brill' and L. V. Sumin

Translated from Atomnaya Énergiya, Vol. 7, No. 4, pp. 377-379
October, 1959
Original article submitted March 26, 1959

The excitation curves were measured by the activation method for an initial deuteron energy of 19.0 ± 0.2 Mev and an α-particle energy of 38.5 ± ± 0.4 Mev. The stack of foils was irradiated by an external beam from a cyclotron. In the irradiation of the foil the same target employed in [1] was used.

A stack of foils prepared from a mixture of boron and polystyrene, in which the polystyrene served as a bonding material, was irradiated by deuterons. Foils 5-10 mg/cm^2 thick with a boron concentration of 20-30% were used. Beryllium foils 2-3 mg/cm^2 thick were prepared by electrolysis of an alloy of BeF_2 and NaF layers. The energy of the bombarding particles in the individual foils was determined from the range-energy curves obtained by extrapolating the known curves for paraffin, air, and aluminum. The stream of charged particles on the stack was measured by a current integrator with an accuracy

not less than 5% and was maintained constant during the irradiation within the limits of ± 5%. The induced activity in the foils was measured by a Geiger counter under standard conditions. To obtain better statistics, the positrons were recorded directly. In order to calculate the absolute value of the cross sections, the activity of a number of foils was also measured with the annihilation γ rays. The sensitivity of the Geiger counter to the annihilation γ rays in the present measurements was taken as approximately equal to its sensitivity to the 0.412-Mev γ rays emitted by Au^{198}. The counter was calibrated with the help of thin samples of Au^{198}, whose absolute activity was determined from the β particles to an accuracy of 2-3% in a special β-counting arrangement in which the geometry was well known. The sources of error in determining the absolute value of the cross section were the nonuniformity of the foil composition, the error in the determination of the boron concentration in the foils, the value of the particle current through the stack, and the error in calibrating the Geiger counter. The total error in the absolute cross section scale in the figures is ± 20%.

After the irradiation of the boron-polystyrene foils by deuterons, two half-life periods were observed, 20.5 and 10 min, which are the decay periods for the nuclei C^{11} and N^{13}. These nuclei are formed in the following reactions on the boron and carbon which enter into the foil composition:

a) B^{11} $(d, 2n)$ C^{11}, $Q=-5{,}0$ Mev;
b) B^{10} (d, n) C^{11}, $Q=+6{,}5$ Mev;
c) C^{12} (d, t) C^{11}, $Q=-12{,}5$ Mev;
d) C^{12} (d, n) N^{13}, $Q=-0{,}28$ Mev.

The N^{13} nuclei are produced in the foils only in one reaction, C^{12} (d, n) N^{13}, and therefore the excitation curve for this reaction was obtained by separating the N^{13} and C^{11} activities by their half-life periods with the method of least squares. The relative shape of the excitation curve for the C^{12}(d, n)N^{13} reaction, shown in Fig. 1, is in agreement with the results of [2]. The absolute value of the cross section of the reaction C^{12} (d, n) N^{13} was determined by that author to an accuracy of 50%, and is an average of one and a half times the cross section measured in the present work. To separate the excitation curves for reactions a), b) and c), leading to the production of activity in C^{11} during the bombardment of the boron – polystyrene foils by deuterons, two stacks of foils enriched with the isotope B^{10} (88%) were irradiated and the excitation curves for the reaction C^{12} (d, t) C^{11} measured in [2] were used. The yield curve of the C^{11} activity in the stack of boron – polystyrene foils is shown in Fig. 2. At low deuteron energies, the curve has a maximum corresponding to the reaction C^{12} (d, t) C^{11}. Figures 3 and 4b show

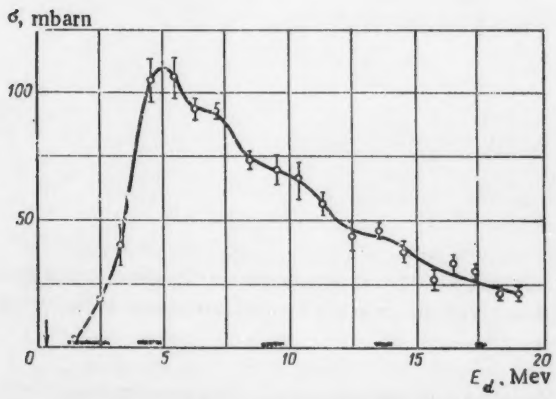

Fig. 1. Excitation curve for the reaction C^{12} (d, n) N^{13}.

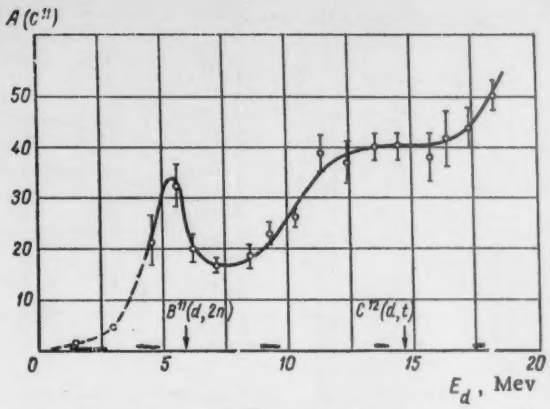

Fig. 2. Yield curve of C^{11} activity for the irradiation of the boron-polystyrene foils (22% of natural boron).

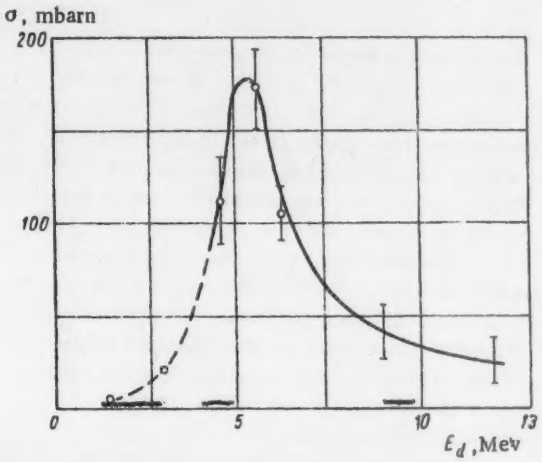

Fig. 3. Excitation curve for the reaction B^{10} (d, n) C^{11}.

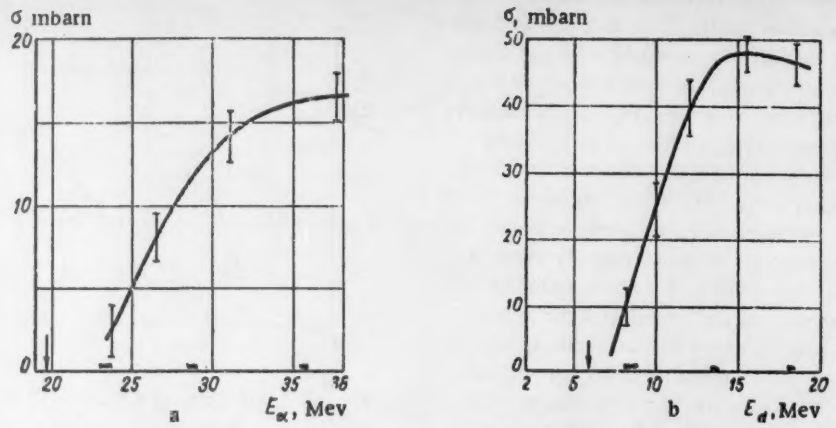

Fig. 4. Excitation curves for the reactions Be^9 (α, 2n) C^{11} (a) and B^{11} (d, 2n) C^{11} (b).

the excitation curves for the reactions B^{10} (d, n) C^{11} and B^{11} (d, 2n) C^{11} obtained after the separation. The vertical segments on the curves represent the mean square deviation of the results of the individual irradiations. The segments along the axis of abscissas indicate the mean thickness of the foils, in kev, for deuterons of the corresponding energy. The shape of the excitation curves at low deuteron energies ($E_d \leqslant 5$ Mev) may essentially differ from the true shape, because of the large thickness of the foils and the spreading of the energy of the deuterons in the beam at the end of their range, and therefore the value of the cross section in this energy region should be considered as approximate.

The excitation curve for the reaction Be^9 (α, 2n) C^{11} (Fig. 4a) was obtained from three irradiations of the beryllium foils stack. After the irradiation of the beryllium foils by the α particles there was observed, apart from C^{11} activity, a weak activity with a period of the order of 100 min, which could only be ascribed to F^{18} ($\tau_{1/2}$ = 110 min). This activity was excited in the reaction F^{19} (α, αn) F^{18} on fluorine, which could have entered the foil from the alloy.

The authors express their profound gratitude to N. A. Vlasov, S. P. Kalinin, and A. A. Ogloblin for their interest in this work.

LITERATURE CITED

1. N. A. Vlasov, S. P. Kalinin et al., Atomnaya Énergiya 2, 169 (1957).*
2. D. Wilkinson, Phys. Rev. 100, 32 (1955).

* Original Russian pagination. See C. B. translation.

* * *

THERMODYNAMICS OF URANIUM TETRAFLUORIDE REDUCTION BY MAGNESIUM

Translated from Atomnaya Energiya, Vol. 7, No. 4, pp. 379-382
October, 1959
Original article submitted April 9, 1959

At the temperature of magnesium-thermal reduction (~ 1400°C*), the system consisting of condensed phases (uranium, magnesium fluoride, and uranium tetrafluoride) and magnesium vapor may be considered as univariant if we neglect the slight mutual solubility of its components.

* According to our calculations and also data in [1], the theoretical temperature of UF_4 reduction by magnesium is 1263°C, i.e., equal to the melting point of MgF_2. Practically it is necessary to heat the charge to 1400°C to ensure complete fusion and superheating of the reaction products.

TABLE 1. Basic Thermodynamic Values

Thermodynamic function*	Dimensions	Reaction component	Value of thermodynamic function	Literature source	Heat capacity C_p, cal/mole · deg [2]	Temperature range of C_p, °K
Free energy of formation ΔF^0_{298}	kcal/mole	UF_4	-42.1	[3]	—	—
The same	The same	MgF_2	-250.8	[3]	—	—
Heat of formation ΔH^0_{298}	" "	UF_4	-443.	[3]	—	—
The same	" "	MgF_2	-263.5	[3]	—	—
Entropy under standard conditions ΔS^0_{298}	kcal/mole · deg	UF_4 (solid)	36.1	[4]	$25.6 + 8.67 \cdot 10^{-3} T$†	298-1309
The same	The same	MgF_2 (solid)	13.7	[2]	$16.88 + 2.7 \cdot 10^{-3} T - 2.66 \cdot 10^5 T$	298-1536
" "	" "	α-U	11.1	[2]	$3.25 + 8.15 \cdot 10^{-3} T + 0.8 \cdot 10^5 T^{-2}$	298-938
" "	" "	Mg_{TB}	7.77	[2]	$5.33 + 2.45 \cdot 10^{-3} T - 0.103 \cdot 10^5 T^{-2}$	298-923
Heat of conversion ΔH_{con}	kcal/mole	α-U→β-U	0.68	[2]	10.28	938-1045
The same	The same	β-U→γ-U	1.16	[2]	9.12	1045-1406
Heat of fusion ΔH_{fus}	" "	U	4.7	[6]	11.9‡	>1406
The same	" "	UF_4	5.7	[5]	36.25†	1309-1690
" "	" "	Mg	2.0	[2]	8.1	923-1376
" "	" "	MgF_2	13.9	[2]	22.57	>1536
Heat of evaporation ΔH_{ev}	" "	Mg	32	[2]	4.97‡	>1376

*The entropies of conversion were calculated from the formula $\Delta S_{con} = \Delta H_{con}/T_{con}$.

† The heat capacity equation may be found by calculation, starting from the known heat capacity of UF_4 at 300° K (C_p, = 117.81 joule/mole · deg = 28.16 cal/mole · deg [4]) and assuming that the increase in heat capacity with temperature is linear [2] and that the heat capacity of UF_4 at the melting point is 7.25 cal/deg · · g · at. or 36.25 cal/mole · deg.

‡ According to [7].

In this case, the equilibrium constants of the reaction at different temperatures may be determined from the equation of the reaction isotherm

$$\Delta F^0 = -4{,}576\, T \lg K,$$

or

$$\Delta F^0 = -4{,}576\, T \lg \frac{1}{P^2_{Mg}}, \qquad (1)$$

where P_{Mg} is the equilibrium pressure of magnesium vapor.

The change in free energy of the reaction ΔF^0_T for different temperature intervals is determined by the Gibbs-Helmholtz equation:

$$\Delta F^0_T = \left(\Delta H^0_{298} - \int_0^{298} \Delta C_p\, dT\right) + \int_0^T \Delta C_p\, dT -$$

$$- T\left(\Delta S^0_{298} - \int_0^{298} \frac{\Delta C_p}{T}\, dT\right) - T \int_0^T \frac{\Delta C_p}{T}\, dT,$$

or, assuming

$$\Delta H^0_{298} - \int_0^{298} \Delta C_p\, dT = \Delta H_{(0)}$$

TABLE 2. ΔF^0 of the Reaction $UF_4 + 2\,Mg = U + 2\,MgF_2$ for Various Temperature Ranges, According to (2)

Temp. range, °K	ΔF^0
298—923	$-85\,682+20,83T+0,01\cdot10^{-3}T^2-1,819T\lg T+2,157\cdot10^5T^{-1}$
923—938	$-86\,678-13,67T-2,44\cdot10^{-3}T^2+2,26\cdot10^5\cdot T^{-1}+10,931T\lg T$
938—1045	$-89\,098,6+33,16T+1,63\cdot10^{-3}T^2+2,66\cdot10^5\cdot T^{-1}-5,169T\lg T$
1045—1309	$-86\,728,6+22,83T+1,63\cdot10^{-3}T^2+2,66\cdot10^5\cdot T^{-1}-2,499T\lg T$
1309—1376	$-85\,871,6-48,76T-2,7\cdot10^{-3}T^2+2,66\cdot10^5\cdot T^{-1}+22,088T\lg T$
1376—1406	$-158\,485,6+49,2T-2,7\cdot10^{-3}T^2+2,66\cdot10^5\cdot T^{-1}+7,688T\lg T$
1406—1536	$-157\,694,3+68,77T-2,7\cdot10^{-3}T^2+2,66\cdot10^5\cdot T^{-1}+1,294T\lg T$
1536—1690 *	$-140\,658,3+137,05T-24,88T\lg T$

*Boiling point of UF_4 [4].

and

$$\Delta S^0_{298} - \int_0^{298} \frac{\Delta C_p}{T}\,dT = \Delta S_{(0)},$$

$$\Delta F^0_T = \Delta H_{(0)} + \int_0^T \Delta C_p\,dT - T\Delta S_{(0)} - T\int_0^T \frac{\Delta C_p}{T}\,dT. \qquad (2)$$

In determining the change in free energy of the reaction, the following phase transitions are considered [2]: 1) the fusion of magnesium at 923° K; 2) the transition of α-uranium into β-uranium at 938° K; 3) the transition of β-uranium into γ-uranium at 1045° K; 4) the fusion of UF_4 at 1309° K; 5) the boiling of magnesium at 1376° K; 6) the fusion of uranium at 1406° K; 7) the fusion of MgF_2 at 1536° K. The data in Table 1 were used for the calculations.

The results, calculated in the form of equations for the change in free energy of the reaction, are given in Table 2 and the corrected values of ΔF^0, on the figure.

Table 3 gives the numerical values of ΔF^0, lg K, and P_{Mg} for characteristic temperatures and data on other calculations of ΔF^0 [8] for comparison. As follows from this table and the figure, the reduction of UF_4 by magnesium at 1400°C will proceed practically completely toward the formation of metallic uranium and MgF_2, since the equilibrium pressure of magnesium vapor at this temperature is very low (0.8 mm Hg).

Naturally, the higher the magnesium vapor pressure in the closed reaction vessel (bomb) [9, 10], the faster and more complete will be the reduction over a reaction time, estimated in tens of seconds [10].

TABLE 3. Values of ΔF^0, lg K, and P_{Mg} for the Reduction of UF_4 by Magnesium.

Temp., °K	ΔF^0, kcal/mole	ΔF^0, according to data in [8], kcal/m.	lg K	P_{Mg} mm Hg
298	—80,1 *	—82,4	59,0	—
500	—77,8	—79,1	34,0	—
923	—71,2	—	16,9	—
938	—70,8	—	16,5	—
1000	—69,4	—69,0	15,1	—
1045	—68,7	—	14,4	—
1309	—64,0	—	10,7	—
1376	—62,5	—	9,93	$8,3\cdot10^{-3}$
1406	—60,0	—	9,32	$1,66\cdot10^{-2}$
1500	—54,0	—51,0	7,85	—
1536	—51,7	—	7,35	0,16
1673	—45,6	—	5,95	0,81
1690	—44,8	—	5,8	0,96

* The discrepancy between the given value of ΔF^0, calculated from the equation for $\Delta F^0_{298\text{-}393}$, and the value of ΔF^0_T, determined from the values of ΔF^0_{298} of the reaction components (see Table 1), lies within the limits of accuracy of the calculations (~0.65%).

With excess magnesium (0.5 – 10% [9, 10]) in the charge, its vapor pressure in the bomb is 8 atmos at 1400° C.† In vacuum remelting (refining) of the crude uranium (~ 1400° C) at a pressure lower than the equilibrium vapor pressure of magnesium for the reduction, the reaction between crude uranium and slag inclusions of MgF_2 proceeds in the reverse direction. In this case the freeing of the uranium from MgF_2 will proceed more completely due to volatilization of the magnesium and UF_4 obtained (the boiling point of UF_4 is 1417° C [4]).

† Calculated from the formula lg P = 9,52 -7840/ T- -1.22 lg T [11] (P is the pressure in atmos).

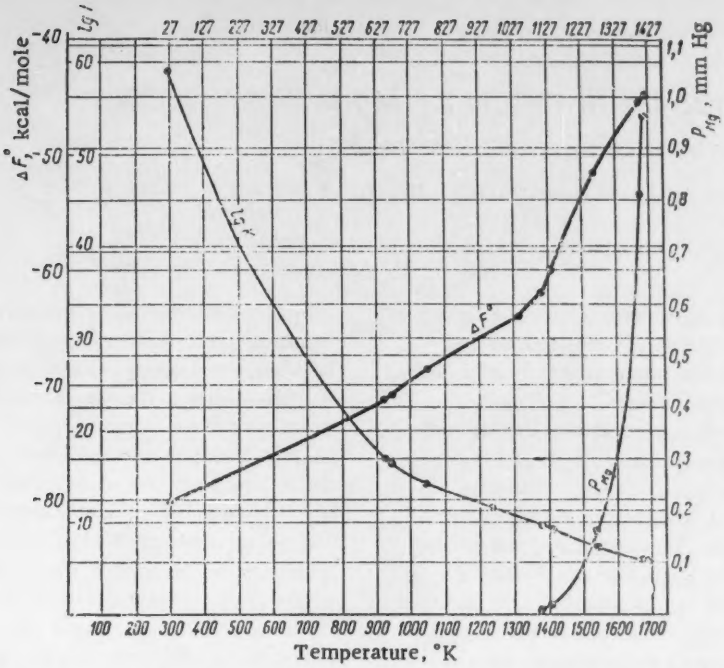

Temperature dependence of ΔF^0, lg K, and P_{Mg} for magnesium-thermal reduction of UF_4.

LITERATURE CITED

1. H. Finniston and J. Howe, Progress in Nuclear Energy. Series V. Metallurgy and Fuels, Vol. 1. (Pergamon Press, London, 1956).
2. O. Kubaschewski and E. Evans, Metallurgical Thermochemistry (Pergamon Press, London, 1958).
3. W. Latimer, Oxidation States of the Elements and Their Potentials in Aqueous Solutions [Russian translation] (Il, Moscow, 1954).
4. F. Rossini, D. Wagman, W. Evans, S. Levine and I. Ioffe, "Selected values of chemical theromdynamic properties," Circular of the Nat. Bur. Standards, US Gov. Printing Off. (1952) p. 359.
5. L. Brewer, L. Bromley et al., Thermodynamics of Uranium Compounds. Part I – Thermodynamic Tables, Table IV (US AEC, MDDC-1533, 1947).
6. F. G. Foot, Material of the International Conference on the Peaceful Use of Atomic Energy (Geneva, 1955)[in Russian] (Goskhinizdat, Leningrad, 1958) Vol. 9, p. 51.
7. A. Butts, Metallurgical Problems (McGraw-Hill, New York, 1943) 2nd ed.
8. A. Lemmon, J. Ward, S. Fisher, Theromdynamics the Reduction of Uranium Compounds to Uranium Metal (US AEC, BMI-550, 1952).
9. H. Thayer, Report No. 602, presented by the USA at the Second International Conference on the Peaceful Uses of Atomic Energy (Geneva, 1958).
10. H. A. Wilhelm, Material of the International Conference on the Peaceful Uses of Atomic Energy (Geneva, 1955) [in Russian] (Metallurgizdat, Moscow, 1958) Vol. 8, p. 199.
11. Kh. L. Strelets, A. Yu. Tairs, and B. S. Gulyanitskii, Metallurgy of Magnesium [in Russian] (Metallurgizdat, Moscow, 1950).

DISINTEGRATION OF HAFNIUM BY 660-MEV PROTONS

A. K. Labrukhin and A. A. Pozdnyakov

Translated from Atomnaya Énergiya, Vol. 7, No. 4, pp. 382-384
October, 1959
Original article submitted February 13, 1959

The aim of the present investigation was to determine the yield of the distintegration products and study some details of the interaction process of 660-Mev protons with hafnium nuclei.

The chromatographic separation of the disintegration products the calculation of the β^-, β^+ isotope yields and also the K-capture isotope yield were carried out by methods described in the literature ([1, 2, 3] respectively). The accuracy of the isotope yield determination for K-capture was 50-100%.

On the basis of the experimental and interpolated data for all identified elements, curves were constructed of the relation between the isotope yields and their mass numbers (Fig. 1). Also, as can be seen, a dome-shaped isotope distribution was observed for the disintegration of hafnium by 660-Mev protons, similar, for example, to the distribution of the disintegration products of copper [4]. In the case of copper, however, the dome is situated in the region of nuclear stability, while in the case of hafnium there is a strong shift of the dome toward the neutron-deficient nuclei. Owing to this difference, there is a change in the isotopic composition of the nuclei. In the disintegration of hafnium, nuclei deficient in neutrons are mainly produced: 67% of the total disintegration cross section; the share of stable nuclei and nuclei with a surplus of neutrons is 23 and 10%, respectively, while in the disintegration of copper, stable and neutron-deficient nuclei are produced in approximately equal amounts (~ 40%).

In the analysis of the isotope distribution vs mass number curves, it should also be noted that there is

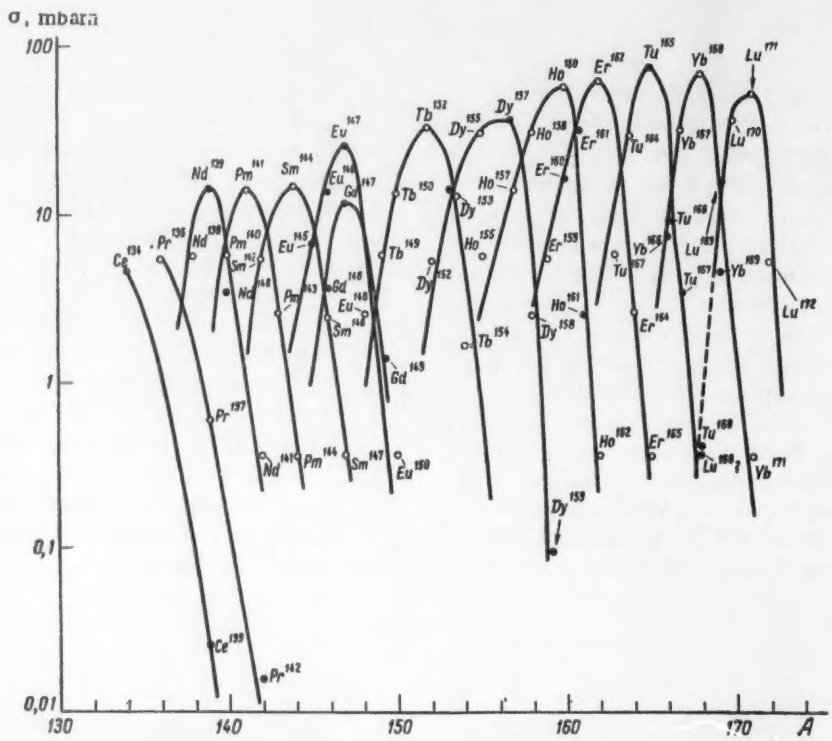

Fig. 1. Distribution curves for the isotope yields of the rare-earth elements as a function of the mass number. ●) experimental data; ○) interpolated data.

Mean Number of Emitted Particles

Element	Z	Mean no. of emitted particles		Mean no. of evap. particles		Ratio of mean no. of evap. neutr. to mean no. of evap. prot.
		n	p	n	p	
Cu	29	4.8	3.7	2.8	1.7	1.5
Hf	72	13.0	4.1	10.5	2.6	4.0

a shift in the dome-shaped curves from Z=64 in the direction of smaller mass numbers and smaller yields in comparison with the neighboring elements, which apparently may be explained, according to statistical theory, by the influence of closed subshells with Z=64.

The value of the total cross section for the production of isotopes was determined from the curve in Fig. 1. for each element. These values allowed us to establish that the total cross section for the disintegration process of hafnium nuclei is equal to $1.5 \cdot 10^{-24}$ cm^2 (taking into account the hafnium isotopes, whose total yield was taken as equal to the total yield of lutecium). The value found constituted 85% of the geometric cross section of hafnium nuclei. It is worth mentioning that in the fraction of lutecium there was found an activity with a period of 4 hr, which could belong to a new isotope Lu^{168}. Assuming that this isotope is β^+ active, we calculated its yield. The value obtained corresponds to the broken line extending from the left branch of the lutecium curve in Fig. 1.

Curve 1 in Fig. 2 represents the relation between the cumulative isobar yield and the number of emitted nucleons N. As may be seen, the cumulative isobar remains constant for $N \leq 20$, and for $N > 20$ it falls according to the exponential law

$$\ln \sigma_A = PA + \text{const},$$

where the value of the parameter P, determined from the angular coefficient of the curve of Fig. 2 is equal to 0.11. For isotopes with $N > 20$, the calculation of the production cross section for a given nucleus-product may be carried out by meams of the semi-empirical formula of Rudstam [6]:

$$\sigma(A_i, Z_i) = \exp[PA - Q - R(Z_i - SA_i)^2],$$

where the values of the parameters, according to our data, are P = 0.11, Q = 12.8, R = 1.2, S = 0.433.

To estimate the mean number of neutrons and protons emitted in the disintegration of hafnium, the weighted mean value of these particles was calculated (taking into account the isotopic composition of natural hafnium) with the formula

$$\frac{\Sigma \sigma_i x_i}{\Sigma \sigma_i}.$$

where σ_i is the production cross section for the ith isotope, x_i is the number of emitted neutrons or protons during the production of the ith isotope. The results of the calculations are compared in the table with the corresponding quantities for the copper disintegration process [4]. Moreover, with the help of the data of [7], we were able to estimate the mean number of evaporated neutrons and protons.

From the data of the table it follows that in the disintegration of hafnium by 660-Mev protons, the mean number of evaporated neutrons is 3.7 times the mean number of neutrons evaporated from copper, while the mean number of evaporated protons is only 1.6 times that for copper. The ratio of the mean

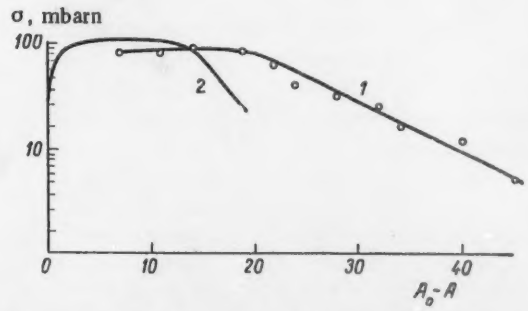

Fig. 2. Curve 1 is the relation between the cumulative isobar yield and the number of emitted nucleons, and Curve 2 is the theoretical relation calculated for A = 200 and E_p = 400 Mev [5].

number of evaporated neutrons to the mean number of evaporated protons for hafnium is almost three times as great as that for copper. These data are evidence of the sharp increase in the number of evaporated neutrons with the atomic number of the irradiated nuclei (from 29 to 72), while the number of cascade neutrons remains constant (2 for copper and 2.5 for hafnium). After the data were obtained, the mean excitation energy of the hafnium nucleus was determined. It turned out to be 150 Mev, which is in agreement with the calculated values in [7].

LITERATURE CITED

1. A. A. Pozdnyakov, Zhur. Anal. Khim. 2, 566 (1956).
2. A. P. Vinogradov, I. P. Alimarin, V. I. Baranov, A. K. Lavrukhina et al., Session of the Academy of Sciences, USSR on the Peaceful Uses of Atomic Energy (Meeting of the Division of Chemical Sciences) [in Russian] (Izd. AN SSSR, 1955) p.97.
3. T. V. Malysheva and I. P. Alimarin, Zhur. Éksp. i Teor. Fiz. 35, 1103 (1958).
4. A. K. Lavrukhina, L. D. Krasavina, F. I. Pavlotskaya, and I. M. Grechishcheva, Atomnaya Énergiya 2, 345 (1957). *
5. I. Jackson, Canad. J. Phys. 35, 21 (1957).
6. S. Rudstam, Phil. Mag. 44, 1131 (1953).
7. N. Metropolis, R. Bivis et al., Phys. Rev. 101, 204 (1958).

* Original Russian pagination. See C. B. translation.

* * *

AN AUTORADIOGRAPHIC METHOD OF INVESTIGATING INK AND PENCIL LINES ON DOCUMENTS

B. E. Gordon and V. K. Lisichenko

Translated from Atomnaya Energiya, Vol. 7, No. 4, pp. 384-385
October, 1959
Original article submitted April 23, 1959

The ascertainment of additions and corrections on documents, made at a later date after the original text was written, is of great importance in criminological practice. It has been proposed that the relative remoteness of the date on which alterations were made in texts written with a ferric gallate ink, which contains large amounts of ferrous chloride or ferrous sulfate, be determined with respect to the migration of chlorine or sulfate ions from the written lines into the paper.

However, the usual chemical analysis of chloride line traces yields satisfactory results only for a considerable concentration of chlorine ions in the ink, and, therefore, we replaced this method by autoradiographic detection.

The part under investigation of the document in question was soaked in a 0.1 N solution of $AgNO_3$, which was labeled with Ag^{110} with an activity of mC ml, or in a 0.1 N solution of HNO_3 or a solution of monovalent thallium sulfate, which were labeled with Tl^{204}. After 5 min, the document was rinsed five times in a 0.01% solution of HNO_3 in order to remove the excess reagent. After drying, the document was placed in contact with photographic paper in darkness. After one day, the obtained radiogram was developed and fixed in the usual manner.

In investigating lines made with aniline ink, which contans a negligible amount of chlorides, it appeared that the migration of chlorine ions could not be detected. However, it was established that, due to the adsorption of the radioactive reagent by the ink dye, the radiographic image of the ink line was obtained. Such an image is obtained also if an ink made of a chemically pure methyl violet dye, where extraneous chlorine ions are almost completely absent, is used. The image does not become blurred after the document

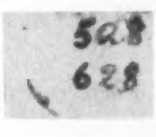

Fig. 1. Autoradiogram of a text consisting of figures, which was written with a methyl violet ink, after treatment with an $AgNO_3$ solution which was labeled with Ag^{110} The original text was written a year and a half ago; a month before the investigation, the numbers 5 and 6 were added with the same ink.

is kept in air saturated with water vapor, and its size almost exactly corresponds to that of the ink lines. It appeared that the adsorbability of silver by ink lines depends on whether the text was written a long time ago. As can be seen from the photograph (Fig. 1), the lines made recently on the paper yield more intensive radiographic prints than the lines which were made a long time ago.

In contrast to acid dyes, the basic ink dyes adsorb also radioactive isotopes which enter the composition of certain anions. However, in this, the remoteness of the date on which the text was written is not manifested. Thus, even in treating faded texts with solutions of Na_2S, NaI, or $K_4Fe(CN)_6$, which are labeled with S^{35}, I^{131}, and C^{14}, respectively, clear radiographic prints are obtained.

Especially good prints of texts written with violet and blue inks were obtained by adsorption of complex $Fe(CN)_6^{4-}$, $Zn(CNS)_4^{2-}$, $TlBr_4^-$, and CdI_4^{2-} anions. The last three anions are readily formed when $ZnSO_4$, $Tl_2(SO_4)_3^-$, and $CdSO_4^-$ are dissolved in excess amounts of KCNS, KBr, and NaI, respectively. Any atom of a complex anion can be labeled with a suitable radioactive isotope.

According to the Fajans – Panet rule, anions which form least soluble compounds with the dye are adsorbed best, and consequently, they provide more contrasting radiographic prints. This provides the possibility of differentiating inks and of detecting additions in the text. For instance, lines written with a blue ink, based on the "Ts" methylene blue dye, adsorb ferro-cyanide ions more intensively than lines containing the ordinary methylene blue dye. This can be clearly seen on the autoradiograph (Fig. 2).

The paper of documents also adsorbs radioactive isotopes, especially if they enter the composition of cations. Third-class writing paper adsorbs radioactive isotopes to a lesser extent than the first- and second-class writing papers. Coated paper with large amounts of fillers adsorbs silver ions so strongly that ink lines can be hardly distinguished from the general radiogram background.

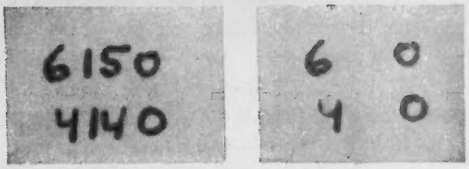

A B

Fig. 2. A) Photograph of a text consisting of figures. The two middle figures in both lines are written with methylene blue ink, and the end figures are written with the "Ts" methylene blue . B) Autoradiograph of the same text after treatment with a solution of $K_4Fe(CN)_6$ which is labeled with C^{14}.

Lines made with graphite, graphite tracing, and colored pencils also adsorb radioactive isotopes. The adsorption by pencil lines containing basic dyes is determined by the latter. However, the dependence on time is not observed in all cases. Acid dyes which enter the composition of pencil lines (for instance, eosin) actually adsorb only cations. Soft-graphite pencils, which contain more graphite and carbon black than hard pencils, adsorb cations better than the latter. Printing dyes adsorb also silver and thallium cations.

Thus, in a number of cases, by means of the described method and by using radioactive isotopes, more contrasting photostats of faded originals can be prepared, and additions written with different writing materials or written at different times can be detected.

* * *

REFLECTION OF NEUTRONS WITH DIFFERENT ENERGIES FROM PARAFFIN AND WATER

A. M. Kogan, G. G. Petrov, L. A. Chudov, and P. A. Yampol'skii

Translated from Atomnaya Énergiya, Vol. 7, No. 4, pp. 385-386
October, 1959
Original article submitted April 2, 1959

In solving problems in connection with the biological action of neutrons, it is very important to know the quantity characterizing the reflection of neutrons with different energies from tissue and the dependence of the reflection coefficient on the beam geometry. In connection with this, we measured the

magnitude and the angular dependence of neutron reflection from tissue-equivalent substances in a wide-energy interval.

In experiments, we determined the ratio of the reflux of neutrons of all energies from a medium to the incident flux of the neutrons under investigation. Our aim was to find the portion of the over-all number of incident neutrons which was absorbed in the substances.

Two methods of reflection measurement were used. The first method was used in those cases where the neutron source had small dimensions so that it could be considered almost as a point-source. The second method was used in measuring the albedo of slow neutrons in neutron beams extracted from the channel of a nuclear reactor.

The first method consisted in the following. By means of manganese foils, the radial distribution of the absorption density was measured in a large water tank, at the center of which the source was placed. The integration of the activity of foils throughout the entire tank volume made it possible to determine the source strength in relative units which were related to the activity of a standard foil. If, after this, the source was placed at a sufficiently great distance from the boundary of the material under investigation, the incident flux at the boundary could be considered as a plane flux. Then, for reasons of symmetry, it was considered that the activity integral of standard foils throughout the depth of the material reflected the number of neutrons which were absorbed, i.e., the number of neutrons which did not leave the surface. At the same time, the number of incident neutrons was determined with respect to the source strength and the distance between the source and the surface. If the source strength in water was determined and the reflection from paraffin was measured, a correction, connected with different macroscopic absorption cross sections of paraffin and water, was introduced in the result. A water tank 110 cm in diameter and 130 cm high and a rectangular paraffin block in the shape of a parallelpiped with dimensions equal to 40 × 40 × 60 cm were used in the experiments. The distance from the source to the surface was 50-150 cm.

By this method, we measured the paraffin reflection of neutrons from a polonium-beryllium source (average energy: 5 Mev) and the reflection of photoneutrons from sodium-beryllium (0.83 Mev), sodium-deuterium (0.22 Mev), and antimony-beryllium (25 kev) sources.

In measurements in a reactor, the second method was used. For a relative determination of the incident flux, the collimated neutron beam from the nuclear reactor reflector was introduced into a device which, for the neutrons, acted as an absolute black body. This device was made in the shape of a thin-walled tube, which ended with a hollow sphere that was surrounded with a thick layer of a weak water solution of manganous chloride. The sphere diameter was 24 cm and the tube diameter was 3.5 cm. Thus, the neutron beam was not reflected back after it reached the inside of the sphere, but was entirely absorbed. The total solution activity characterized the magnitude of the incident neutron flux. The following filters were used for separating neutrons of different energies: a cadmium filter with a thickness of 1 mm (which absorbed thermal neutrons) and a boron 0.4 g/cm^2 thick filter (which absorbed, beside thermal neutrons, also neutrons with an energy of several electron volts). For a combination of a boron filter with a cobalt layer, also neutrons with an energy of ~ 130 ev were knocked out of the beam; this was due to resonance scattering. In a similar manner, the sodium filter extracted neutrons with an energy of ~ 2.7 kev from the beam. The sodium and the cobalt filters were placed in such a manner that the neutrons scattered by these filters did not fall into the sphere. After the incident flux was measured, the reflection of neutrons from the water surface was determined. For this, a calibrated neutron beam was directed toward a thin-walled aluminum tank, which was filled with a solution of manganous chloride. The number of non-reflected neutrons was determined with respect to the activity of the solution in the tank. The effect of neutrons with different energies was determined by fractionating the beam by means of filters.

The activity of solutions was determined with respect to standard metallic manganese specimens,

TABLE 1. Neutron Reflection Coefficient for Normal Incidence

Neutron energy	Paraffin reflection coefficient	Neutron energy	Water reflection coefficient
5 Mev	0.06	2.7 kev	0.47
0.83 Mev	0.12	130 ev	0.56
0.22 Mev	0.19	5 ev	0.71
25 kev	0.38	Thermal	0.58

TABLE 2. Dependence of the Reflection Coefficient on the Angle of Neutron Incidence

Neutron energy	Angle of incidence					
	0°	15°	30°	45°	60°	75°
5 Mev	0,06	0,110	0,21	0,32	0,50	0,74
0,22 Mev	0,19	—	—	0,44	0,61	—
5 ev	0,71	—	0,74	—	0,80	—
Thermal	0,58	—	0,63	—	0,76	—

which were deposited electrolytically. The irradiation of the rectangular tank at different fixed angles θ between the beam and the normal to the surface provided data on the angular dependence of the neutron reflection coefficient.

The results of all measurements are shown in Tables 1 and 2. In considering these data, it should be first noted that the coefficient of neutron reflection from a hydrogenous substance decreases with an increase in energy, and that an increase in albedo is observed only in passing from thermal energies to energies of several electron volts. Such a character of the relation between the albedo and the energy of neutrons is in agreement with data from [1].

The dependence of the albedo on the incidence angle θ for all investigated energy values can be expressed by the relation $(1-\alpha)_\theta = (1-\alpha)_{\theta=0} \cos\theta$.

The reflection coefficient equal to 0.58, which was obtained for the normal incidence of thermal neutrons, is considerably smaller than the albedo of neutrons for paraffin, whose magnitude, equal to 0.83, is ordinarily used in literature. This albedo value for an isotropic distribution of incident neutrons was obtained earlier in [2]. If the albedo for an isotropic distribution is calculated by using the obtained angular dependence of the albedo and the albedo magnitude for the normal neutron incidence, it will be equal to 0.73, which is considerably closer to the value of 0.83.

The authors extend their thanks to the graduate of the Leningrad Polytechnical Institute, G. P. Gordeev, who collaborated in measuring the albedo of slow neutrons.

LITERATURE CITED

1. L. Cave, Brit. J. Radiol. 27, 273 (1954).
2. E. Amaldi and E. Fermi, Phys. Rev. 50, 899 (1936).

* * *

DISTRIBUTION OF THE ABSORPTION DENSITY OF NEUTRONS IN PARAFFIN

A. M. Kogan, G. G. Petrov, L. A. Chudov, and P. A. Yampol'skii

Translated from Atomnaya Énergiya, Vol. 7, No. 4, pp. 386-388
October, 1959
Original article submitted April 2, 1959

The neutron tissue dose is partially determined by the energy which is liberated inside the tissue in the capture of neutrons. In dependence on the initial neutron energy, this portion of the tissue dose will constitute different contributions to the over all dose. For instance, for neutrons with an initial energy of several kiloelectron volts, the tissue dose will almost entirely be determined by energy which is released in capture. For neutrons with an initial energy of 1 Mev, a substantial part of the dose will be determined by energy which is dissipated by neutrons in the slowdown process. In order to determine the capture component of a neutron dose, we investigated the spatial distribution of neutron absorption in paraffin, which simulated the biological tissue. These measurements were performed for a normal incidence of an extensive neutron beam on a flat paraffin surface. The paraffin block was in the shape of a rectangular parallelpiped with dimensions equal to 40 × 40 × 60 cm. The neutrons were aimed at the 40 × 40 cm face. The length of 60 cm was chosen for the purpose of making the neutron density approach zero at a sufficiently great distance from the back face of the paraffin block, so that the neutrons were completely absorbed in the block for any initial neutron energies used in experiments.

In order to obtain data for determining the transverse block dimensions, we performed measurements of neutron density in paraffin (along the block axis) for different transverse dimensions of the block. For small block dimensions, the neutron density at the axis depended on its transverse dimensions; however, when certain critical dimensions were attained, a further increase in the block size did not influence the magnitude of neutron density. The critical block dimensions, depending on the initial neutron energy for an energy of 5 Mev, were less than 40 cm. Thus, the absorption of neutrons in a block of the indicated size coincided with the absorption in semiinfinite space filled with paraffin.

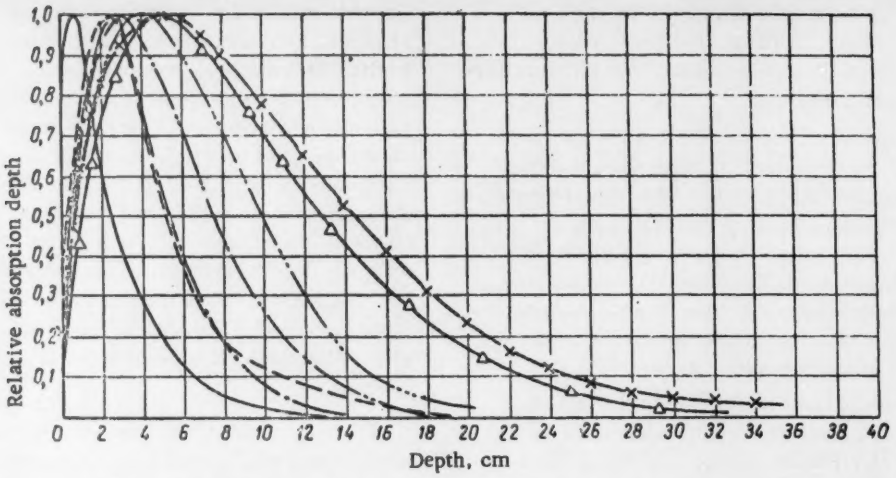

Density distribution of the absorption of neutrons with different energies in paraffin. Neutron energies: ——) thermal neutrons; — — —) 5 ev; —·—·— 25 kev; —··—··— 220 kev; —···— 0.83 Mev; —Δ—) 2.9 Mev; —x—) 5 Mev.

The measurement of neutron density was performed by means of thin manganese foils.

In experiments, the depth distribution of the absorption density of incident neutrons with the following energies was determined:

1. thermal neutrons which were obtained by filtering a beam extracted from the channel of a nuclear reactor through cadmium (thickness: 1mm);
2. neutrons with an energy of ~ 5 ev, which were separated from a beam of resonance neutrons from a nuclear reactor by combining a boron (0.6 g/ cm^2) and a cadmium (1 mm) filter;
3. photoneutrons from an antimony-beryllium source with an energy of 25 kev;
4. photoneutrons from a sodium-deuterium source with an energy of 220 kev;
5. photoneutrons from a sodium-beryllium source with an energy of 0.83 Mev;
6. neutrons produced by the $H_1^2(d, n)He_2^3$ reaction with an energy of 2.9 Mev (the deuteron energy was 1.8 Mev, and the emergence angle of neutrons in the laboratory coordinate system was 90°);
7. neutrons from a polonium-beryllium source with an average energy of 5 Mev.*

The maximum statistical error in measuring the activity of foils was ~ 3%.

The measurement results are shown in the figure. All the curves are characterized by the presence of a maximum, which is shifted toward the depth of paraffin as the energy increases. In passing from thermal neutrons to neutrons with an energy of several electron volts, a drastic shift of the maximum from 0.5 to 2.5 cm is observed. This is perhaps connected with the fact that the maximum absorption probably takes place at a depth which is of the order of the transport path length of an incident neutron, and since the scattering cross section of neutrons in paraffin decreases approximately fourfold for a neutron energy exceeding the energy of the proton bond in a paraffin molecule, the free neutron path correspondingly increases. The comparatively slow shift of the maximum toward the depth as the energy increases to 5 Mev can also be explained by a weak dependence of the scattering cross section in this energy interval.

It is obvious from the figure that the ratio of absorption at the maximum to absorption at the surface tends to increase, which can to a certain extent characterize the relative amount of slow neutrons leaving the front paraffin surface, i.e., it can characterize the reflection coefficient.

The rate of the drop in absorption density beyond the maximum decreases as the energy of incident neutrons increases; this is to be expected, as the length of the free neutron path increases. The departure from this regularity at greater depths in the case of neutrons with an energy of ~ 5 ev was obviously connected with the fact that, in the boron filter which separated these neutrons, a small amount of faster neutrons was separated from the beam; this was also due to the inaccuracy in measuring the activity by means of cadmium and cadmium-boron filters. The difference between these measurements determined the values given in the figure.

* J. Elitot, W. McGarry, W. Faust. Phys. Rev. 93, 1348 (1954).

INTERNATIONAL CONFERENCE ON COSMIC RAYS

V. Parkhit'ko

The International Conference on Cosmic Rays, convened under the auspices of the International Union of Pure and Applied Physics, met June 6-11, 1959, in the auditorium of the M. V. Lomonosov Moscow State University. The Conference was attended by representatives of scientific organizations from 25 nations.

The widespread interest in this Conference is to be explained by the particular significance attached to problems of cosmic rays in physics today. Cosmic-ray particles of exceptional high energy are a powerful tool in the study of the atomic nucleus, and also provide information to science on the spectacular events taking place in the Universe which give birth to these remarkable rays. A new landmark in this field of research, as emphasized in the introductory remarks by Academician D. V. Skobel'tsyn, has been established by the launching of the first artificial satellites of the earth and sun, an achievement of historical import. A completely novel approach to research on the Cosmos has been inaugurated, and new phenomena of exceptional interest have been reported. The exchange of views on the essence of those scientific achievements constitutes a significant contribution to cosmic-ray research.

The most prominent problem in the field of cosmic-ray studies is the unraveling of the nature of nuclear interactions at critically high energies beyond the reach of present-day accelerators. A session of the Conference, chaired by Britain's leading scientist, C. F. Powell, an honorary member of the Academy of Sciences of the USSR, was devoted to the achievements of world science in this area.

The first report was delivered by Prof. M. Schein (USA). He gave an account of research on nuclear interactions at energies in excess of 10^{12} ev.

Photoemulsion tracking techniques showed great promise in studies of high-energy particles. Prof. D. H. Perkins reported on research using this technique, carried out at an altitude of 10,000 meters on board a jet plane. Experiments employing photoemulsion techniques resulted in the discovery of new cosmic-ray processes, and involved thousands of flying hours. The data reported stimulated a lively discussion at the Conference.

The Soviet scientist N. L. Grigorov reported a novel technique facilitating research for cosmic-particle energies. Interest was also heightened by announcements of work conducted at Pamir under the supervision of Prof. N. A. Dobrotin. The pattern of interaction between nucleons and nuclei was studied at heights in the mountains. The particle energy was successfully measured by Grigorov's method.

Valuable data on high-energy interactions were also reported in papers by physicists of the Kazakh SSR and in experiments of Hungarian and Japanese scientists.

The second session of the Conference discussed one of the fundamental problems in modern physics, that of the interaction of elementary particles with atomic nuclei at energies thousands and millions of times in excess of anything achieved in the largest accelerators now in existence.

A review report delivered by Prof. E. L. Feinberg (USSR) was followed by reports on new research efforts in that field of study.

Soviet and foreign scientists expounded their views on the essentials of the process of multiple production of particles. The basic fact is that each collision between particles at exceptionally high energies results in the production of a large number of new fragment particles. Seven experiments on this topic performed in Japan were described at the Conference by Japanese scientists S. Hayakawa and J. Nishimura. The Soviet physicist D. S. Chernavskii told of research carried out at the P. N. Lebedev Institute of Physics in Moscow.

The following days at the Conference were used for discussion of the results of investigations of broad atmospheric showers. A special session dealt with studies of primary cosmic radiation. The outstanding feature of this primary radiation is that during its travel it gives rise to a host of "descendants," the secondary particles. Some of these "descendants" possess great penetrating power. Mu-mesons, for example, are known to penetrate a thousand meters deep into the earth.

The session of July 10 was extremely interesting. Results of research on primary cosmic radiation by means of airborne balloons, rockets, and satellites were discussed. Special attention was focused on the problem of the origin of the cloud of charged particles enveloping the earth. Prior to the launching of earth satellites, no one had suspected the existence of such a cloud. The phenomenon was subjected to painstaking investigation with instruments carried on board the third Soviet earth satellite. The first Soviet cosmic rocket later passed right through that cloud and beyond it, measuring the composition of the radiation in detail.

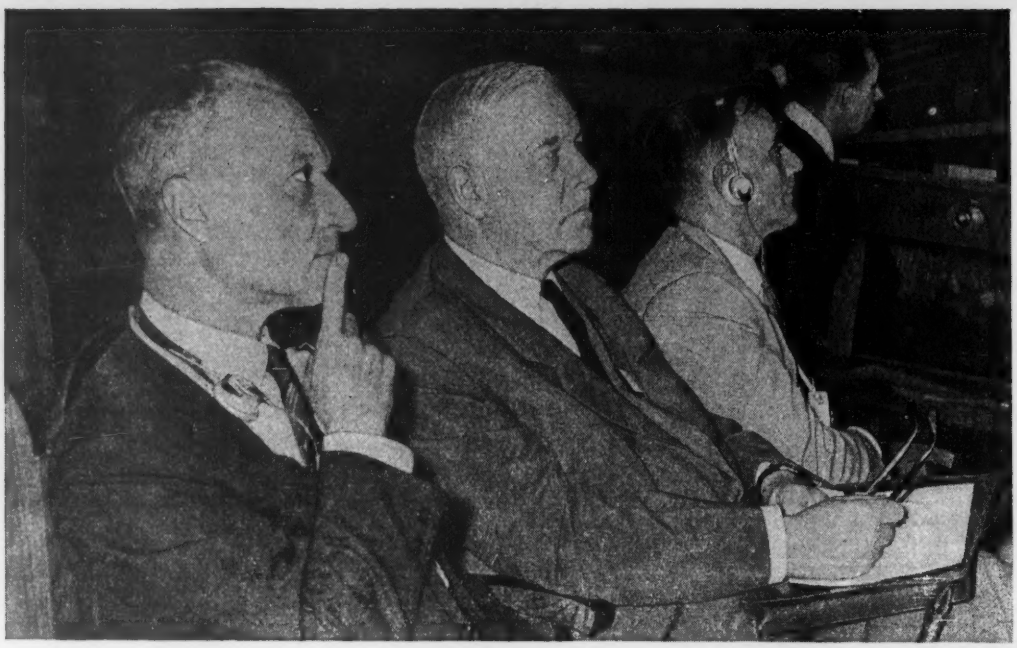

Photo taken in the Conference auditorium. Seated, from left to right: Prof. B. Rossi (USA), Academician D. V. Skobel'tsyn (USSR), and Prof. C. F. Powell (Britain) (photo by the author).

At the present conjuncture, ample experimental material has been accumulated on the origin of the two cloud belts (inner and outer belts), a report on which was made at the Conference. The inner belt passes above the equator at a height of several thousand kilometers, and is made up of high-energy protons. The outer belt extends to a distance of the order of about 50,000 km from the earth, and is made up of relatively low-energy electrons. Prof. J. Van Allen, who was the first to discover the radiation belts, delivered a report on American research in that area. Soviet research on the same topic was summed up in a report by Corresponding Member of the Academy of Sciences of the USSR S. M. Vernov, and Candidate in Physical and Mathematical Sciences A. E. Chudakov.

Soviet and American researchers have reached the conclusion that the charged particles found in the inner cloud belt are formed as a result of decay of neutrons emitted by the earth's atmosphere as cosmic rays impinge on the atmosphere. Particles in the outer cloud belt may possibly be of solar origin, in the view of some scientists.

A report delivered by Soviet scientists N. V. Pushkov and S. F. Dolginov stating that electric currents which appreciably alter the geomagnetic field flow in the charged-particle clouds made a deep impression. This phenomenon was detected by means of a magnetograph mounted on board the first Soviet space rocket (Lunik).

Interest was stimulated by a paper delivered by Australian scientists, telling of observations of Soviet artificial earth satellites by Australian observation teams.

The closing day of the Conference, devoted to the problem of the origin of cosmic rays, had as its most interesting papers reports by Soviet scientist V. L. Ginzberg, "Some problems concerning the theory of the origin of cosmic rays," L. Davis (USA), "On diffusion of cosmic rays throughout the Galaxy," and S. Hayakawa, M. Koshiba, and N. Hiroshima (Japan), "The acceleration mechanism of cosmic-ray particles."

Speaking in the name of foreign guests at the close of the Conference, Prof. B. Rossi, chairman of the Cosmic-Rays Commission of the International Union of Pure and Applied Physics, addressed the gathering. He thanked the Soviet scientists for their hospitality, and remarked on the favorable conditions provided to expedite the work of the Conference.

* * *

NINTH INTERNATIONAL CONFERENCE ON HIGH-ENERGY PHYSICS

B. Govorkov

The Ninth International Conference on High-Energy Physics met in Kiev, July 15-25, 1959. Over 300 scientists of prominence from 32 nations were in attendance at the Conference, with delegates from the largest international research institutions, e.g., the Joint Institute for Nuclear Studies (Dubna), the Center of European Nuclear Research (CERN), and including Prof. A. I. Alikhanov, D. I. Blokhintsev, N. N. Bogolyubov, V. I. Veksler, L. D. Landau, B. M. Pontecorvo, I. E. Tamm (all from the USSR), L. Alvarez, V. Weisskopf, E. McMillan, W. Panofsky, E. Segre, G. F. Chew, L. Schiff, J. Steinberger (USA), R. Peierls, A. Salam (Britain), Wang Hang-chang (China), H. Yukawa (Japan), E. Amaldi (Italy), and G. Bernadini, R. Hofstadter (CERN).

A system of review papers was adopted at the Conference. Leading specialists in the fundamental branches of high-energy particle physics appeared with participants in the panel sessions, and discussed the review reports to be delivered in the plenary sessions.

The first plenary session, held on July 20, was opened by the chairman of the organizing committee for the conference, D. I. Blokhintsev. The participants remained standing in silence to honor the memory of the distinguished physicists Frederic Joliot-Curie, Ernest Lawrence, and Wolfgang Pauli, all of whom passed away during the interim between the Eigth and Ninth conferences.

Prof. G. Bernadini delivered a review report on photoproduction of pions and the Compton effect on a proton. He analyzed in detail some new data reported during the previous year in several American laboratories, relating to the nature of the maxima 2 and 3 detected in the photoproduction cross sections of the mesons.

Despite the fact that with the commissioning of the ~ 1 Bev synchrotrons (in USA, Italy), the interests of physicists have shifted to the higher-energy region (~ 600 Mev to 1 Bev), there are still a host of classical effects in meson physics observable in the region close to the photoproduction threshold for mesons which require measurement and refinement, these being: measuring the threshold photoproduction cross sections of pions, interaction constants, applicability of theoretical descriptions of threshold phenomena based primarily on the Chew-Low model or on dispersion relations. The most complete experimental results relating to this energy region are those reported by Soviet physicists working with the synchrotron of the Institute of Physics of the Academy of Sciences of the USSR.

Questions pertaining to nucleon scattering of nucleons and single production of pions in π^-n^- and n^-n^- interactions, intimately associated with the photoproduction of pions, were dealt with in a report by Prof. B. M. Pontecorvo. An analysis of the experi-

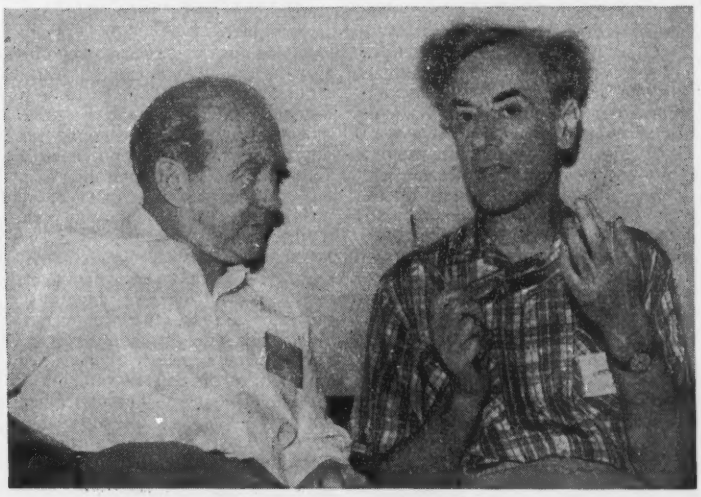

During a break in the proceedings.

ments carried out on the accelerators available at the Dubna, and Chicago laboratories, and other institutions, for the purpose of verifying the principle of charge invariance in processes involving participation of pions and nucleons, failed to show a single reliable case of violation of that principle; the promising method pursued to verify the principle was the study of an interaction, forbidden with respect to isotopic spin, between two deuterons, resulting in the formation of a neutral π-meson and a helium nucleus. It was noted in the report that, as a result of completion of experiments on π^- p-scattering at 400 Mev (USSR, USA), much knowledge has been gained on the phase shifts of π^-p-scattering. More accurate measurements of the total cross sections for π^-p-interactions at 1 Bev energy have fully confirmed R. Wilson's hypothesis, which held that two maxima must exist (corresponding to photoproduction of mesons) in the energy dependence of total π^-p-scattering. These maxima have been found, and there are now three resonance peaks in the total cross section of the π^-p-interactions: the first at ~ 190 Mev, due to a strong interaction between the state T = 3/2 and I = 3/2 (positive parity); the second at ~ 650 Mev, a strong interaction between states T = 1/2 and I = 3/2 (negative parity); the nature of the third maximum, at 950 Mev energy, is more obscure, but apparently marks a state having I = 5/2.

It is to be noted that many new "discoveries" were reported at the Conference. Experiments performed in the USSR (at Dubna) and in Great Britain invalidated the hypothesis of the existence of an isotopic scalar π_0^0-meson having a mass close to that of the conventional π^0-meson. This hypothesis had been advanced to account for several contradictions in the field of low-energy meson physics. New data on π^-p-scattering showed that no serious discrepancies exist between experimental π-p -scattering data and dispersion relations (known as the Puppi-Stähelin problem).

A lively discussion and considerable interest centered around data on the pair production of pions from meson-nucleon collisions studied in the USSR (Dubna), Italy, and USA (Berkeley), opening up new avenues of research into the nature of the π-π-interaction. B. M. Pontecorvo reported, in a number of significant successes achieved in experimental technique, the development of a gaseous Cerenkov counter with an index of refraction continuously variable from 1.00 to 1.23 (MIT, United States), and a hodoscopic system with pulsed power supplies for polarization experiments (Joint Institute, Dubna).

The most interesting data obtained on the world's two largest proton synchrotrons, at Dubna and Berkeley, were reviewed in reports delivered by Prof. E. Segrè and Academician V. I. Veksler.

Segrè reported something rather new in experimental technique: the production of enriched beams of antiprotons (as much as one antiproton per accelerator pulse), by means of absorbers and magnets, and especially by means of electrostatic separators. Experiments using photoemulsions (in Italy and the USA) have resulted in corrected values for the mass ratio of the antiproton to the proton. This mass ratio is equal to unity to an accuracy of ± 1%. The report reviewed new data on measurements of interaction cross sections (elastic scattering and annihilation cross sections) of antiprotons with hydrogen, deuterium, and carbon. Segrè greeted the physicists of the Joint Institute, where a team has produced an antiproton beam with a 2.8 Bev/c pulse, and has begun research work in this intriguing realm of physics.

The Chinese scientist Prof. Wang Hang-chang (working currently at the Dubna Joint Institute) took the floor in the discussion of Segrè's presentation, to demonstrate two interesting plates obtained in work with a propane bubble chamber. These plates, showed, for the first time, strikingly clear cases of antiproton generation.

One of the most interesting reports was made by Academician V. I. Veksler, and provided, for the first time, a systematic analysis of nucleon-nucleon and pion-nucleon interactions at energies ranging from 1.5-2 to Bev.

Examination of the results of highly precise measurements of elastic p-p-scattering at 8.5 Bev (Dubna) and 3 Bev (Berkeley) demonstrated the existence of what is termed potential scattering, i.e., leads to the conclusion that the scattering amplitude at high energies is not a purely imaginary quantity, as would follow from the optical theorem. These results were made possible by a new research technique, in which photographic plates are placed at right angles to the accelerator beam (a practice initiated at Dubna), allowing a shift of as much as 0.2° in the laboratory system or coordinates.

An analysis of experiments on inelastic π-π- and π-n-interactions carried out at energies of 2.6 and 9 Bev by the Berkeley and Dubna groups shows an important discrepancy between the empirical data and predicted statistical theory, and leads to an understanding of the existence and prominent role of peripheral encounters. With the aid of an idea advanced by Academician I. E. Tamm, these encounters are associated to concepts of single-meson exchange where one or two isobars appear as a result. The essentially new approach contained in Tamm's suggestion is that by making the assumption of single-meson exchange, it becomes possible to obtain completely specified quantitative relationships between the probabilities of different isotopic channels of the reactions. Experimental results from peripheral

collisions studied by the Dubna team show excellent agreement with Tamm's predictions. An examination of empirical data on π-p-interactions reported by the Dubna and Berkeley teams shows the totality of the available experimental results to be at variance with predictions of statistical theory for both low (~ 1.5 Bev) and high energies. The only model which is evidently not at odds with the totality of all facts reported on π-p-interactions in that energy range is the model according to which a high-energy pion interacting with a proton results in a δ-meson knocked out of the mesonic shell of the nucleon.

As demonstrated by a phase analysis of elastic π-p-scattering, the mechanism underlying scattering of this type at high energies (> 2 Bev) is essentially different from the elastic p-p-scattering mechanism. For π-p-scattering as an example, spin interactions are negligible, while the scattering amplitude is a purely imaginary quantity. A typical feature of π-p- and p-p-scattering at high energies (2-10 Bev) is the fact that the effective collision parameter determining the magnitude of the interaction cross section is energy-independent over a broad range of energies. In Veksler's view, it would be important to tie up this quantity with meson theory.

Questions related to investigations of the structure of nucleons and checking the validity of quantum electrodynamics at small distances were taken up in reports by Profs. F. Hofstadter, W. Panofsky, and L. Schiff. Hofstadter's report dealt with the results of experiments on studies of proton and neutron structures, performed by the reporter and his associates on the linear accelerator at Stanford (USA). The basic problem encountered in studies of proton structure is the determination of the phenomenological form-factors $F_{1p}(q^2)$ and $F_{2p}(q^2)$, the first of which takes the charge distribution of the Dirac magnetic moment into account, while the second accounts for the distribution of the anomalous magnetic moment. Both form factors are independent functions of the pulse $\underline{q}$ transmitted in the event of a collision between an electron and a proton. An analysis of the experimental data, adduced in the report, shows that $F_{1p} = F_{2p}$ within the limits of accuracy attainable (~ 15%), and that they are actually dependent on $\underline{q}$ alone. New data from neutron studies at Stanford, based on the method of direct determination of the difference between the cross sections of quasielastic scattering of electrons on deuterons and elastic scattering of electrons on protons, were discussd in detail in this paper. The results showed agreement with the fact that $F_{1n} = 0$, $F_{2n} = F_{1p} = F_{2p}$, where if we use some model for the exponential distribution of charge density and magnetic dipole moment in interpreting the results, we get $\sqrt{r_n^2} = 0.8 \cdot 10^{-14}$cm.

V. Panofsky's report was most interesting for the experiments proposed for verifying the validity of quantum electrodynamics at short range. The necessity for such verification arises from the fact that in interpreting experimental data on nucleon scattering of electrons, we must presently assume that quantum electrodynamics remains valid for all values of the momentum transferred in the collision.

One of the proposed experiments is in the preparatory stage at Stanford University, and involves scattering of electrons on electrons, based on the use of the method of head-on collisions of electron beams emergent from two separate annular storage paths. A precision of ~ 3% which is fully attainable in this experiment makes it possible to approximate to the elemental length $3 \cdot 10^{-15}$ cm. R. Wilson (USA) took the floor in the discussion to tell of an experiment now in preparation aimed at probing the structure of the neutron, and based on a technique of recording coincidences of recoil electrons and neutrons scattered on deuterons.

Some theoretical problems underlying strong interactions of common particles were discussed in papers presented by Prof. G. F. Chew (USA) and Prof. Ya. A. Smorodinskii (USSR). Smorodinskii's paper gave a phenomological analysis of experiments on nucleon scattering of nucleons (N – N) carried out on synchrocyclotrons at Berkeley, Rochester, Cambridge (USA), Dubna (USSR), Liverpool, and Harwell (Great Britain).

These experiments are geared to a program with the pace set predominantly by Soviet physicists. Pointing out the fact that presently available data are inadequate for a complete analysis of N – N –scattering, the reporter sketched a program of further experimental research work in clear outline. The report emphasized the fact that the total available data on N – N – scattering could not be described by a potential dependent solely on the coordinates and spins, so that the potential must include the relation between spin and orbital motion. It is therefore natural that the results presented by Soviet theoreticians A. F. Grashin and I. Yu. Kobzarev, who computed the spin-orbital interaction potential from approximate dispersion relations, stimulated much discussion.

Chew's report dealt with a new approach to the problem of strong interactions between ordinary particles, based on the binary dispersion concepts advanced by Mandel'shtam. According to that concept, all three reactions, N – N –, π–N, π-π-interactions, may be described by means of a single analytic function, while the behavior of the analytic function over a small region of the complex plane is determined principally by the closest singularities, according to the assumption of Mandel'shtam and Chew. The problem reduces to finding the functions having

the required singularities, which in turn calls for a solution of complex nonlinear integral equations. The solution of this problem must be reduced to the fact that the amplitudes of the processes will be expressed in such parameters as interaction constants and masses. The hope remains that the mathematical tools developed will make possible a description of nuclear forces as far as to the core of the nucleus, and right up to an energy of 1 Bev for π-N- and π-π scattering reactions. The discussion on Chew's paper was devoted in the main to questions concerning the possibility of measuring π-π-interactions, with Prof. D. I. Blokhintsev, V. N. Gribov (USSR), Prof. E. L. Lomon (Canada), and others taking the floor on that point.

Questions related to the production of strange particles and their interactions were discussed in the plenary session chaired by Prof. Wang Hang-chang, and in reports presented by Professors J. Steinberger, L. Alvarez, and A. Salam.

Steinberger's report, devoted to the formation of strange particles, had as its high point of interest the data accumulated by a team under Prof. Alvarez, from hydrogen bubble chamber observations of events involving the formation of a neutral cascade hyperon in an interaction between a K^--meson and a proton, of the type $K^- + p \longrightarrow \Xi^\circ + K^\circ$.

Measurements demonstrated that the neutral cascade hyperon decayed according to the decay scheme $\Xi^\circ \to \Lambda^\circ + \pi^\circ$, and had a mass, 1326 ± 20 Mev, which fits well with the mass found for the negative cascade hyperon, 1321 ± 35 Mev.

The report delivered by Prof. Alvarez was based to a considerable extent on papers treating K-meson interaction experiments performed by his group with the aid of liquid-hydrogen and deuterium bubble chambers. In addition, the results of interactions between K^+-mesons and nucleons, as well as data on hyperon-nucleon interactions were dealt with. The report furnished information on an increase in the number of decay events involving Λ°-particles formed in the $K^- + D \to \Lambda^\circ + \pi^- + p$ reaction. This increase showed that the apparent asymmetry observed about a year ago in Λ°-decay is in reality a statistical fluctuation, and that there are consequently no reasons for assuming that parity is not conserved in strong interactions in which strange particles take part. In the discussion ensuing after presentation of the papers on strange particles, the greatest interest was evoked by statements made by Ting Ta-tsao, Prof. Wang Hang-chang (Joint Institute), and M. Stevenson (USA). Ting Ta-tsao took the floor to report some results obtained by a team of research scientists at the Joint Institute for Nuclear Studies bearing on the production of strange particles in interactions between 8.6 Bev π^--mesons and protons. Wang Hang-chang demonstrated an interesting slide of a plate taken in a bubble chamber; analysis of the plate shows that we are dealing here with what seems to be a new particle of mass 742 ± 218 Mev, which disintegrates into a π^+-meson and a K°-meson. Stevenson demonstrated a plate obtained by the Alvarez group where we see for the first time the production of the $\bar{\Lambda} + \Lambda$ pair in an antiproton-proton collision event.

Since the method of dispersion relations is the principal theoretical research method used in studies of interactions between elementary particles, a separate plenary session of the Conference was devoted to an analysis of that method, with D. V. Shirkov (Dubna) and Prof. G. Lehmann (West Germany) reporting.

Shirkov's report discussed the theoretical aspects of dispersion relation studies of the usual type (based on the energy variable). Summing up the results of work carried on during the past year, the reporter noted that the year is characterized, on the one hand, by the extension of the general methods of proofs of dispersion relations to a large number of elementary-particle interaction processes and on the other hand, by the fact that the possibilities have been apparently exhausted for discrete dispersion relation processes, at least in their present form. It is therefore quite natural that much attention should be given, precisely this year, to a method for investigating the range of applicability of dispersion relations by means of an analysis of diagrams of the theory of perturbations.

The basic point driven home in Lehmann's presentation involved problems in investigating the analytic properties of scattering amplitudes with respect to transfer of momentum and questions relating to binary dispersion concepts. These concepts apparently constitute a very promising and bold hypothesis, but for now it isstill only a hypothesis. It is therefore to be expected that many discussions taking place at the Conference would be devoted to various justifications for these concepts. We refer here in particular to the discussion between the reporter and Academician L. D. Landau.

One of the sessions of the Conference, under the chairmanship of Academician I. E. Tamm, was devoted to new theoretical ideas advanced in the field of elementary-particle physics. Interesting reports were presented at this session by Academician L. D. Landau, Prof. M. A. Markov (USSR), Prof. W. Heisenberg (West Germany), Prof. I. Nambu (USA), Prof. W. Thirring (Switzerland), and others.

Problems in strong interactions were dealt with in review reports presented by Academician A. I. Alikhanov (USSR), Prof. D. Glaser (USA), and Prof. R. Marshak (USA).

Alikhanov's presentation was devoted to a consideration of decay of nuclei, μ-mesons, and π-mesons. The most substantial event registered since the last conference was, as noted in the report, the elimination of the last explicit contradiction marring the universal

theory of V − A-interaction (Gell-Mann, Feynmann, Marshak, Saunderson), by discovering π-e-decay in the approximately correct relationship to conventional π-μ-e-decay.

The report provided a painstaking analysis of the accuracy of the experimental proof of the two-component neutrino theory of Salam, Landau, Lee and Yang, invariance under time reversal in weak interactions, and the universality of the Fermi interaction constant, which is uniform to an accuracy of $\sim$ 2-3% both in the process of β-decay of nucleons, i.e., strongly interacting particles, and in the decay process of the muon.

It is a well-known fact that decay of strange particles proceeds very slowly, and represents a typical weak interaction. Glaser's report was devoted to this question. A theoretical treatment of the problems of weak interactions was furnished in Marshak's report. After these presentations, a lively discussion ensued. Of particular interest were the remarks made by Prof. V. Telegdi and J. Steinberger. Telegdi gave an account of experiments investigating K-capture of a μ-meson by a nucleus of nonzero spin, and stressed the point that the spin of the μ-meson could be computed directly from the experiment performed by the Dubna team (A. E. Ignatenko et al.). Steinberger, in his report, told of an experiment in which the parity of the π°-meson is determined directly. Experiments carried out with the aid of a liquid hydrogen chamber have confirmed the pseudoscalar nature of the π°-meson.

The concluding session of the Conference was devoted to nuclear processes at exceptionally high energies. Experimental results obtained by means of cosmic-ray research were the theme of a report delivered by Prof. C. F. Powell (Great Britain). These results had been discussed extensively at the International Conference on Cosmic Rays convened in Moscow in July, 1959. Theoretical questions concerning multiple production of mesons at extremely high energies were discussed in a report by Prof. E. L. Feinberg (USSR).

Concluding remarks at the Conference were delivered by Academician I. E. Tamm. In the name of the International Union of Pure and Applied Physics, the chairman of the Committee on High-Energy Physics of that body, Prof. C. J. Bakker, expressed his thanks to the organizing committee for their splendid job in preparing and expediting the work of the Conference.

A number of seminars were held during the Conference for the benefit of persons working in of the various fields of high-energy physics: a theoretical seminar, a seminar on bubble-chamber techniques, a seminar on electron accelerator experiments. In the course of these seminars, and personal encounters, those in attendance at the Conference had the opportunity to discuss in detail the problems of greatest interest to them, and to share information on future research projects.

The Conference was a great aid to the cause of strengthening international collaboration between scientists.

The proceedings of the Conference will be published by the USSR Academy of Sciences Press, in the form of a special collection of papers.

* * *

THE SECTION ON ATOMIC SCIENCE AND ENGINEERING AT THE AMERICAN EXPOSITION IN MOSCOW

The United States Exposition was open to the public from July to September, 1959, in Moscow. The atomic science section took up a very insignificant amount of floor space in the exhibition, and reflected superficially, and in general outline, the work of American scientists in the field of atomic energy.

The sponsors of the exhibit were apparently of the opinion that a detailed account of problems touching on the use of atomic energy in the USA would be of no interest to the man-in-the-street visitor to the exhibit. This was not the case, however, as borne out by the large number of inquiries on the subject voiced by visitors. It is most unfortunate that visitors to the exhibition, including Soviet specialists on atomic energy, could not find on display any material in any way fully reflecting the achievements of American scientists in the field of atomic energy.

There was only one model on display in the entire atomic section of the American exhibit, that being a model of the atomic-powered cargo and passenger vessel "Savannah." At the present time, superstructure work and finishing touches are underway with the hull of the vessel already launched, and the ship will be ready for its maiden run in the summer of 1960. This section of the exhibit reflected only three types of work in the field of atomic energy: experimental reactors, power reactors, and radioactive isotopes. Photographs showed the reactor of the Shippingport power station, the portable boiling-water reactor of the ALPR project, the organic-moderated and organic-

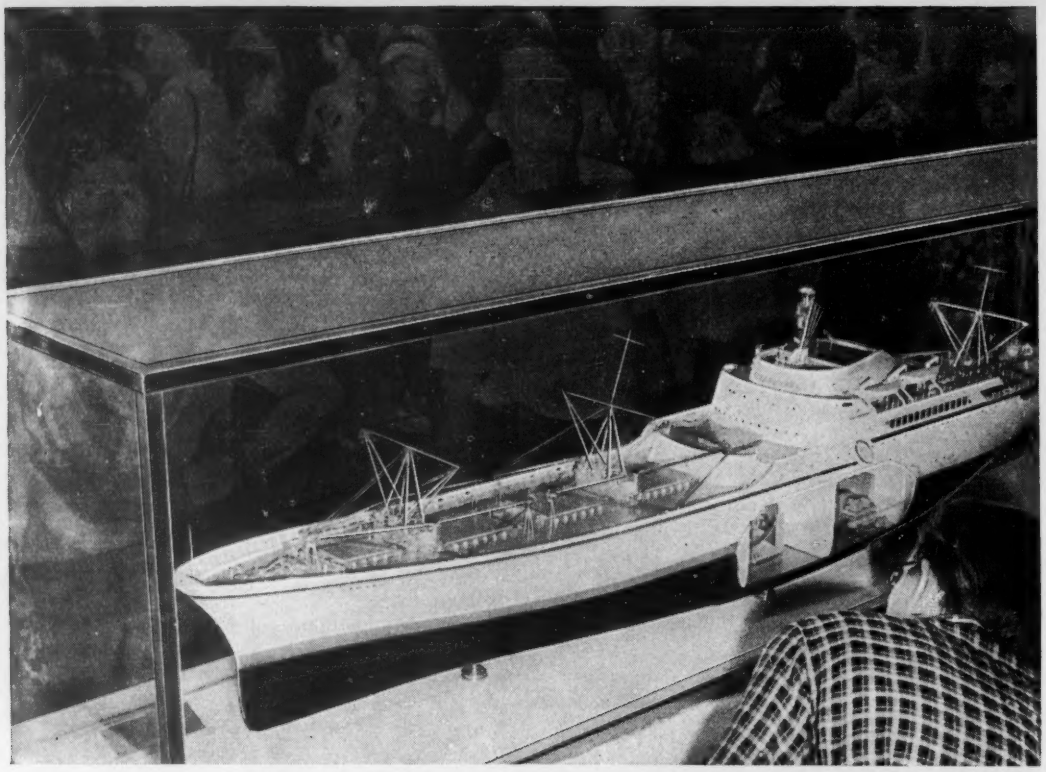

Crowd viewing a model of the atomic-powered cargo and passenger vessel "Savannah."

cooled OMRE power reactor, the materials testing reactor MTR, the Brookhaven research reactor and the reactor of the Dresden power station. One could learn from the stands and diagrams that 15 atomic-fueled power stations, delivering a total power output of 1000 Mw, are presently being planned in the USA, and that the number of reactors of all types has reached 200.

A relatively large area in this section was occupied by the radioactive isotopes and isotope applications exhibit, primarily in medicine, biology and agriculture. However, even this topic was dealt with in a very cursory and schematic fashion.

Several photographs showed examples of American assistance to the Federated German Republic (West Germany) in building the research reactors at the Frankfurt and Munich Universities.

* * *

ANNULAR FIXED-FIELD STRONG-FOCUSING ACCELERATORS

The need for increased output current in cyclic accelerators has put a premium on the most rational exploitation of the advantages of time-invariant magnetic fields in such machines.

Existing cyclic accelerators of the cyclotron and synchrocyclotron types, while providing very high beam intensities, are beset by the sizable drawback that the size, weight, and cost of the facilities limit the peak proton energies attainable in the machines to < 1 Bev. The use of annular magnets of the synchrotron type has proved unfeasible because of the instability of the motions executed by the particles. Actually, in order to keep particle orbits within a narrow annular region upon acceleration, the magnetic field in that region must be increased 10^3-10^4 times. Recourse to an axisymmetric field is no solution, since this runs counter to the well known stability condition $0 < n < 1$, where $n = -r/H \cdot \partial H/\partial r$.

A solution, in the form of the accelerator known as the annular phasotron (a synchrocyclotron) in which

axial symmetry is discarded, was proposed as far back as 1953 [1]. In 1955, scientists in the USA also proposed two types of annular fixed-field accelerators: one similar to the annular phasotron, the other of a spiral type, a modification of the Thomas cyclotron with azimuthal variation of the field.

The major advantage derived in facilities of this type, as against other variants of annular accelerators, is the possibility of effecting an abrupt increase in both acceleration cycle frequency and in intensity at the same time. Some small machines may, in addition, be operated in the betatron mode of operation, at greater intensity than ordinary betatrons.

The magnetic field of an annular phasotron (ring-shaped FM cyclotron) is a sensitive function of the radius with roughly the same field index $\underline{n}$ as in strong-focusing synchrotrons of the same size. In contrast to the latter type, $\underline{n}$ is independent of azimuth and is of constant magnitude. The stability of particle motion is brought about by introducing sectors with field direction reversed into the magnetic field, the result being that some portions of the orbit have inverse curvature, while the orbit as a whole comprises a closed undulating curve. Since the angular dimensions of the sectors having direct and inverse field directions must have one order of magnitude in order to ensure stability, the minimum radius of curvature of the orbit is found to be several times smaller than the mean radius. The radial dimensions of a ring-shaped synchrocyclotron therefore turn out to be 6-7 times larger than in a synchrotron built to achieve the same energy. However, the increased intensity attainable in annular synchrocyclotrons may well compensate for that drawback.

Moreover, the presence of reversed-field sectors in the magnetic train of the machine lends a new and remarkable feature to the annular synchrocyclotron. It has been noted in the literature [2, 3] that when sectors with positive and negative fields are equal, i.e., in what we call the symmetrical annular phasotron, there is no specified direction of rotation of the particles, so that acceleration of two beams of particles moving in opposite senses may take place simultaneously in the same magnetic field. This conclusion, at first glance paradoxical, is illustrated in Fig. 1, where the orbits of two opposing beams are diagrammed schematically. Since the field increases as sharply as the radius, it is obvious that the mean field along the orbit of both beams has different signs, which in turn makes it possible for the particles to rotate in opposing senses. This peculiarity of the ring phasotron is of course used to advantage to build up opposing beams and cause interactions between them.

Despite the specific engineering difficulties associated with the establishment of sharply reversed magnetic fields, the design of the ring phasotron, as well as any other strong-focusing accelerator, imposes very tight tolerances on the parameters of the magnetic system. The specifications are not insuperably difficult to meet, however, and accelerators based on this principle are now being developed in a vigorous program being pursued in various nations.

An electron model of a ring synchrocyclotron had been put into operation at Michigan State University (USA), in 1956. The magnet used in this accelerator consists of 16 sectors, the reversed-field sectors accounting for less than half. The maximum radius of the operating region is 50 cm, at a magnetic field rise index $n = -3.36$, makes is possible to obtain electrons with 400 kev energy. The model was built for researching particle dynamics in the strongly nonlinear field of the annular synchrocyclotron, on the effect of resonances, and other similar effects. Acceleration is achieved by means of an auxiliary betatron core operated at a frequency of 500 cps. About 10^8 accelerated electrons were obtained in each cycle.

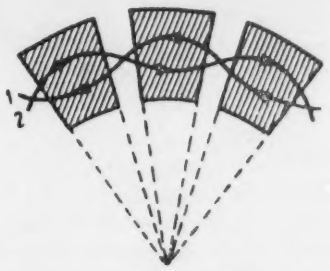

Fig. 1. Diagram of orbits in a symmetrical-ring phasotron: 1, 2) orbits of beams traveling in opposing directions.

Data on a symmetric annular electron synchrocyclotron accelerating electrons to 40-50 Mev (designed by scientists of the above University) are available [5]. The accelerator, at present in the assembling stage (Fig. 2), is apparently designed for accelerating two opposing beams.

According to available data, a similar installation accelerating to an energy of about 100 Mev is being designed at CERN (Switzerland). It is expected that the intensity will be adequate to bring about an interaction between the two beams. The fixed magnetic field also increases as the radius, on an average, in a spiral type accelerator, but goes through maxima and minima forming a spiral with a constant angle of inclination. The orbits in a field of this type form geometrically similar closed curves which rotate as the radius increases in conformity with the periodicity of the spiral.

The focusing in a spiral accelerator may be explained in qualitative terms by the fact that the

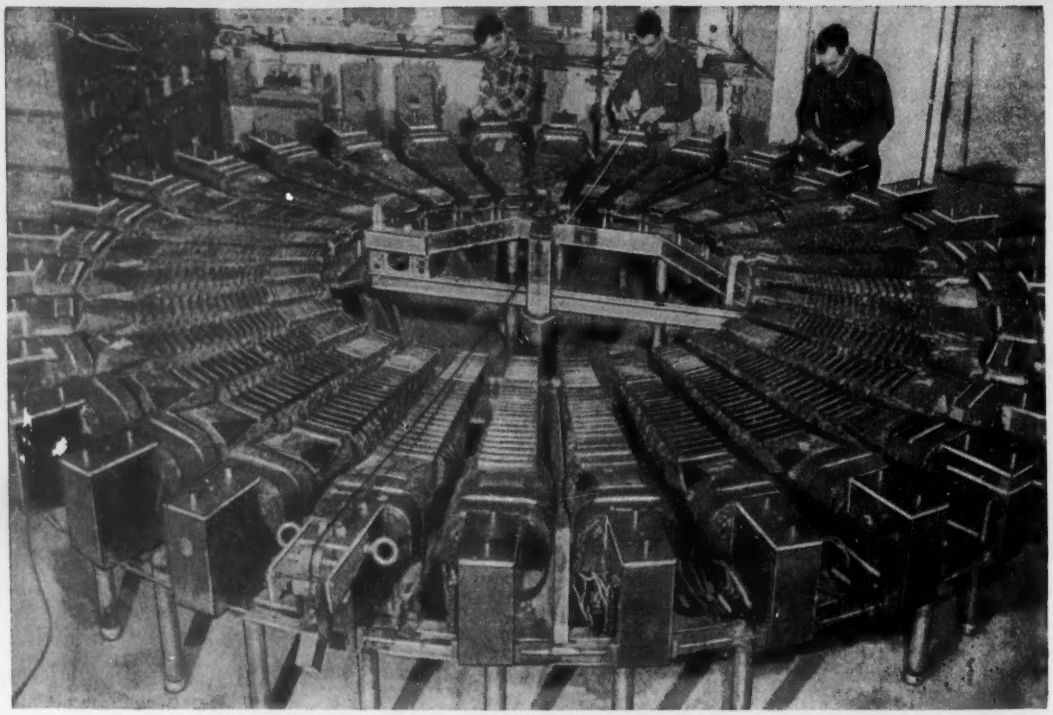

Fig. 2. Assembly of annular synchrocyclotron.

particles, in intersecting the periodic crests and troughs of the field at a small angle, move from a field of one gradient into a field of opposite gradient. What then results is alternating-gradient strong-focusing acting primarily in the vertical direction. The absence of fields of reversed polarity and consequent smaller size than the annular synchrocyclotron is an attractive feature of this type of accelerator. On the other hand, strong nonlinear effects and the elaborateness of the field configuration introduce serious difficulties into the design and installation of such facilities. At the present time, there is only one electron model machine, 120 kev, in operation [6], with focusing effected by six spiral sectors (USA).

There are other methods available for achieving focusing in a fixed inhomogeneous magnetic field. A team of scientists working at the Physics and Engineering Institute (Leningrad) has developed a focusing method which makes use of cylindrical magnetic lenses situated along the orbit [7].

Some new and highly interesting possibilities have opened up recently in conjunction with the use of a vertically increasing magnetic field [8]. In this type of accelerator, orbits corresponding to different energies no longer lie in the same plane. Alternating gradient focusing comes about through spiral ridges placed at the magnet poles. These accelerators have, combined with the advantages of the spiral type (e.g. smaller size), the limitations attendant on that type, namely the complexity of the associated magnetic system. However, a system employing a vertically increasing field enjoys the further advantage that the frequency of revolution is made independent of energy, at the same time that the cyclotron mode of acceleration is sustained.

LITERATURE CITED

1. A. A. Kolomenskii, V. A. Petukhov and M. S. Tabinovich, Symposium: Some Problems in the Theory of Cyclic Accelerators [in Russian] (Izd. AN SSSR, 1950).
2. A. A. Kolomenskii, Zhur. Éksp. i Teor. Fiz. 33, 298 (1957).
3. T. Ohkawa, Rev. Sci. Instr. 29, 108 (1958).
4. F. Cole et al., Rev. Sci. Instr. 28, 403 (1957).
5. Sci. News Letter 75, 179 (1959).
6. D. Kerst et al., Rev. Sci. Instr. 27, 970 (1956).
7. Yu. V. Vandakurov, Zhur. Tekh. Fiz. 28, 1065 (1958).
8. J. Teichman. Czechoslov. J. Phys. 9, 262 (1959).

* * *

NEW RULES FOR TRANSPORTING HOT MATERIALS

A. Shpan' and N. Leshchinskii

The Main Control Board on the Uses of Atomic Energy, under the aegis of the Council of Ministers of the USSR and the State Health Inspection Service of the USSR, has ratified new rules governing the transportation of radioactive substances.* The rules cover haulage of radioactive substances by rail, air, waterway, and road. In conformity with these new regulations, radioactive substances are broken down into three groupings according to the physical characteristics of their radiations. The first group includes radioactive materials which emit gamma rays in addition to α and β particles (Co^{60}, I^{131}, Ir^{192}, Cs^{137}, etc.). The second group has assigned to it any radioactive substances which act as sources of neutron, or of neutron and gamma emissions. Alpha and beta emitters are assigned to the third grouping (Po^{210}, Sr^{90}, P^{32}, S^{35}, C^{14}, etc.).

The last grouping is subdivided further into four transportation categories, depending on the gamma-ray dose rate at the surface of the container in which the hot materials are being transported, or the dose rate at a distance of 1 meter from the surface of the container.

The first category includes containers in which the gamma-ray dose rate at the surface is not in excess of 0.1 μr/sec. Such packages, being completely free of hazard, are allowed free passage by any means of transportation and may be stored in conventional facilities without expressly setting them apart from other cargo. However, the activity in a single package must not exceed 2000 mc.

Containers showing a gamma-ray dose rate exceeding 3 μr/sec at the surface, or 0.1 μr/sec at a distance of 1 meter from the container, are assigned to the second category. These containers may be shipped by any means of transportation and stored in conventional facilities, but the number of second-category containers which may be shipped as part of a single shipment or stored in a single warehouse section is restricted to 10 units (or 20 units on board freight-carrying airplanes), and they may not be shipped in baggage or mail cars. To avoid spoilage, undeveloped photosensitized materials must not be placed within a radius of 1 meter of such containers.

The third category includes containers showing a gamma-ray dose rate not exceeding 55 μr/sec at the surface, or 2.5 μr/sec at a distance of 1 meter. These containers must not be placed closer than 1-10 meters to any area frequented by human beings (depending on the means of transportation concerned), and not closer than 5 meters to photosensitive materials.

A fourth transportation category is set aside to cover rules of transportation for radioactive materials which for reasons of any nature whatever (e.g., excessive weight of the container) could not feasibly be transported in containers meeting the previous specifications. Containers of this last type may be shipped in separate railroad cars, trucks, or airplanes, or in remote bays of ships' holds, keeping them at the proper safe distance from photosensitive materials or from areas frequented by people.

Further requirements must be met to ensure safe conditions for haulage, applying to the containers themselves.

Fluids and gases must be placed, primarily, in leakproof containers (welded-in-glass or metal vials, etc.), while powders and solids must be shipped in tightly closed containers. Vials containing hot liquid materials must be surrounded by in absorbent material filling the interior of the container not occupied by the vial. The amount of absorbent material must be such as to be capable of absorbing all of the radioactive material, should the hermetic sealing of the primary package be impaired.

The main container is packaged inside an auxiliary outer container (of cardboard, plastic, wooden, etc., material) and the outer container must be free from radioactive contamination.

Fulfilling these enumerated conditions guarantees elimination of any hazard of radioactive contamination under the usually encountered transportation conditions.

Rules are being put into effect regarding requirements for monitoring the gamma-ray dose rate outside of the containers, and monitoring the degree of contamination of the container surface, also as to the shipping of used containers following removal of the hot materials, and regarding proper marking and labeling of the containers, shipping, transporting and receiving of all shipments containing radioactive materials.

Observation of the rules is binding upon all organizations engaged in the production, transportation, and use of radioactive materials.

To ensure observance of the rules, the shipping organizations concerned must devise and obtain approval of specific instructions on the order of application of rules bearing on specific points in the various means of transportation.

Observance of these new rules will contribute to improved servicing of the growing needs of the national economy with respect to radioactive isotopes.

* Provisional Sanitary Rules Governing the Transportation of Radioactive Materials [in Russian] (Medgiz, Moscow, 1959).

A NEW CONTAINER FOR HIGH-ACTIVITY RADIATION SOURCES

V. Sinitsyn, N. Leshchinskii and A. Gusev

In connection with the widespread use of powerful isotope devices, it became necessary to transport large amounts of high-activity radiation sources and also to charge irradiators directly from transport containers.

The containers which were used earlier were designed for transporting radiation sources with an activity of up to 400 g-eq Ra. The unloading of sources from such containers was possible only in special water tanks, which prevented their use for directly charging devices which had a dry shielding system.

A new container type, which is specially designed for transporting high-activity radiation sources and for directly charging various devices by radiation sources, has been developed recently (see figure). Up to four standard cobalt radiation sources, each having a nominal activity of 700 g-eq Ra, can be simultaneously transported in this container.

The container consists of a cast iron frame 1, inside of which the main lead shield 2 and the mechanism for filling the container with sources, for holding them in transport, and for discharging them into devices are mounted.

The mechanism controls are located at the container top. A lug and a channel are provided on the container frame for fixing its position in charging devices with a dry shielding system.

The container is loaded with sources in a tank under a protective water layer. For this, lid 7 is removed and plug 6 is taken out, and then a guiding funnel is inserted. The locating handle 5 is placed in the first loading position. The radiation source is lowered through the funnel into drum 3. A calibrated bushing, which prevents the placement of sources with a larger diameter in the container, is provided at the top of the loading opening. After the source is placed in the container, the drum is brought into the next loading position by means of the locating handle. After the loading is completed, the locator is placed in the zero position, the funnel is taken out, the plug is replaced, and the container is taken out of the tank. The container is held above the tank for a certain time to allow the water to run off; a channel from the footstep bearing of the drum and a groove on pin 4 are provided for draining.

In order to reduce the possibility of chance contamination, the container surface is made with a minimum amount of projections, and the openings around the screw heads and the clearances between

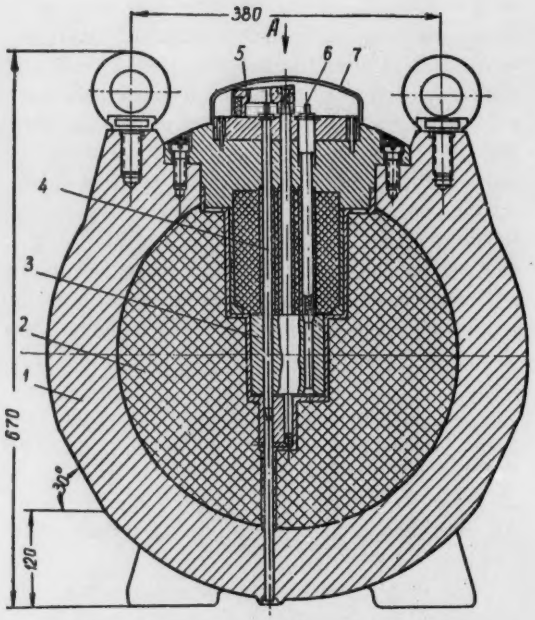

View of the dial from A
(Lid removed)
Scale 1:1

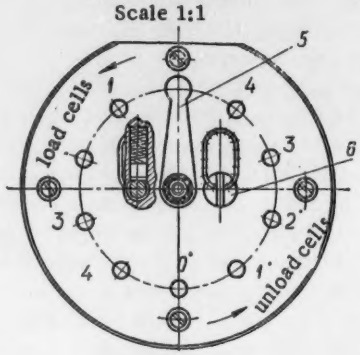

Source container.

the dial plate and the lid are sealed with lead. The container lid is sealed.

The sources can be unloaded from the container under a protective water layer or directly into the charge channels of devices with a dry shielding system. For unloading, the lid is opened, and the pin which opens the discharge opening is pulled out. By successively placing the locator handle into the unloading positions, the drum is rotated, and the sources are

moved to the discharge opening, through which they freely fall out. If, for any reason, a source does not fall through the discharge opening, it is pushed through by means of the pin.

The container can be transported by ordinary transport means, for which its frame and the lead shield are designed in such a manner that the radiation dose rate at a distance of 0.5 m from the container surface does not exceed 2.5 μr/sec. The container weighs approximately 1 ton.

* * *

BRIEF COMMUNICATIONS

USSR. A gamma-ray detector for checking moisture determination in local lightweight concrete (foam-kuckersite* and foam-silicalcite) has been developed, at the Institute of Construction and Construction Materials of the Academy of Sciences of the Estonian SSR, for improving the thermal insulation properties of those structural materials. A beam of gamma rays emitted by a Co^{60} irradiator is passed through a test sample and, after suffering gradual attenuation in its passage, is allowed to impinge on a gamma counter. The percentage of moisture in the material is determined by the attenuation of the gamma beam intensity. The same method is being used to study the dynamics of migration of moisture in different materials and construction models, which will have great bearing in design, to offset possible heat losses in finished installations.

This method is faster and more reliable than any form of gravimetric moisture analysis employed higherto.

IAEA. The regularly scheduled session of the governing Council of the International Atomic Energy Agency met in Vienna during June, 1959.

The agenda included 26 points, the main items being the general principles underlying the control and inspection system of the Agency, the Agency's 1960 program and budget, problems concerning technical assistance to underdeveloped nations, appointment of members of the Board of Governors for the following term of office, confirmation of reports submitted to the UN General Assembly and the General Conference of the Agency on the activities undertaken by the body.

* Kuckersite is an oil shale mined in Estonia.

NEW LITERATURE

Books, Symposia, Periodicals

V. V. Malyarov, Fundamentals of the Theory of the Atomic Nucleus, Moscow. Physics and Mathematics Press, 1959, 471 pp, 9 rubles, 75 kopeks.

The book comprises a series of organized lectures read by the author to students in the physics and mathematics department of the Odessa State University. The material comprising the lectures is presented under the headings: "Basic properties of atomic nuclei," "Elementary theory of the deuteron," "Theory of elastic collisions," "Nuclear forces," "Alpha decay," "Beta decay," "Gamma radiation," and "Inelastic collisions, nuclear reactions." The book thus embraces all of the fundamental aspects of the theory of the nucleus. It may be recommended as a textbook for physics and engineering institutions and departments.

Articles from the Japanese periodical Genshiryoku Kogyo Nuclear Power Engineering, Vol. 5 (1959).

No. 1

Hattori Manbu and Anahari Reji: Design and Construction of a Nuclear Reactor for Practical Research Use (pp. 22-23)*; Kakimato Hiroshi and Takeoka Kinichi: Determination of Zinc Content in Aluminum Castings, Using Radioisotopes (41-45); Ozawa Naoshi: Studies of Fiber Wear Mechanisms, Using Radioisotopes (46-50); Kimura Kazuji: Organizations of Research on Nuclear Processes, at Tohoku University (51-58); Miwa Hirohide: Measuring Devices Employing Radioactive Radiations (62-67).

No. 2

Kamogawa Hiroshi: Nuclear Research and the Manufacture of Equipment for Pursuing Nuclear Research (15-21); Yamakake Noboru: Studies of Radioactive Substances Contained in Sea Salts (26-31); Tomita Kenji. Flotation Using Ca^{45} (41-46); Kobayashi Jutaro: Studies of Atmospheric Electricity, Using Po^{210} (47-51).

No. 3

State of the Art in Nuclear Power Engineering (4-14); Use of Atomic Engines in Shipbuilding (15-19); Melting of Metallic Uranium (20-23); Otani Kanji: Detection of Gas Leaks in Underground Piping, Using Rn^{222} (24-32); Wakatsuki Tetsuo: Nuclear Studies at Osaka University (41-48); Suzuki Masaji: Health Safety Measures Pertaining to the Development of Atomic Industry (55-60); The 4-Mev Linear Accelerator at Toshiba (68).

No. 4

Okano Shinji: Selection and Handling of Radioisotopes (11-14); Owaki Ken-ichi, Miwa Hirohide: Measuring Instruments for Radioisotopes and Their Use (15-24); Kawakami Tatsuya: Use of Radioisotopes in the Textile Industry (25-28); Makino Naobumi and Oyama Ichize: Use of Radioisotopes in the Electrical Machine Industry (29-32); Fuji Takashi: Use of Radioisotopes in Metallurgy and Machine Manufacture (33-36); Tomita Kenji: Use of Radioisotopes in the Mining Industry (37-40, 45); Shigemitsu Tomomichi et al: Use of Radioisotopes in the High-Polymer Industry (41-45); Fujisaki Tatsuo et al: Use of Radioisotopes in the Chemical Processing Industry (46-49); Tsudano Satoshi and Umehara Akira: Use of Radioisotopes in the Petroleum Industry (50-54); Noda Michihiro: Use of Radioisotopes in the Coal Industry (55-57); Nichigaki Susumu et al: Use of Radioisotopes in Agriculture, Forestry, Animal and Fish Husbandry (58-66, 32); Watanabe Wataru: Use of Radioisotopes in the Food Industry (67-69); Yamaata Hisao: Use of Radioisotopes in Medicine (70-78).

Articles from the Periodical Literature

I. I. Abramovich, "Uranium and thorium in intrusive rocks of the Central and Western Tuva," Geokhimiya No. 4, 358-363 (1959).

Z. N. Bak, "Chemical shielding against ionizing radiations," Priroda No. 7, 33-38 (1959).

V. I. Baranovskii et al., "A note on the natural neutron activity in arsenic and antimony," Vestnik Leningr. Univ. No. 10. Seriya fiziki i khimii No. 2, 25-26 (1959).

A. Ya. Berlovskii, "Protective devices for storage of covered radioactive sources," Vestnik rentgen. i radiologii No. 3, 61-65 (1959).

E. K. Gerling and Yu. A. Shukolyukov, "Isotope composition and xenon content of uraniferous minerals," Radiokhimiya 1, 212-222 (1959).

A. A. Gusev, "Use of radioactive radiations for detection of air accumulations and obstructions in central heating piping," Izvest. vyssh. ucheb. zaved. Stroitel'stvo i arkhitektura No. 1, 109-114 (1959).

G. S. Davtyan et al., "Study of some aspects of the assimilation of phosphorus by plants, using the labeled atom technique," Soobshch. laboratorii agrokhimii (AN Arm. SSR) No. 2, 5-18 (1959).

V. I. Danilov and O. V. Savchenko, "Method of focusing charged particles emerging from an accelerator," Pribory i Tekh. Éksp. No. 3, 17-20 (1959).

*Figures in parenthesis are page numbers of articles.

I. L. Dvorkin et al., "Experience in the use of radioactive logging for determining the position of the water-oil contact," Neft. Khozyaistvo No. 6, 50-55 (1959).

Yu. N. Denisov, "Magnetic field stabilizer based on nuclear induction," Pribory i Tekh. Éksp. No. 1, 96-100 (1959).

Ya. B. Zel'dovich, "Storing of cold neutrons," Zhur. Éksp. i Teor. Fiz. 36, 1952-1953 (1959).

S. A. Kaplan, "On the 'Larmor' theory of plasma," Zhur. Éksp. i Teor. Fiz. 36, 1927-1929 (1959).

F. M. Karavayev, "An ionization chamber for the absolute measurement of the activity of radioactive preparations," Izmerit. Tekh. No. 5, 60-62 (1959).

V. A. Karnaukhov, "Interaction of accelerated nitrogen and bismuth nuclei," Zhur. Éksp. i. Teor. Fiz. 36, 1933-1935 (1959).

L. M. Kovrizhnykh, "On the motion of a plasma coil in axisymmetric magnetic fields," Zhur. Éksp. i Teor. Fiz. 36, 1834-38 (1959).

Yu. Ya. Konakhovich and I. S. Panasyuk, "A flat-crystal neutron spectrometer," Pribory i Tekh. Éksp. No. 3, 26-31 (1959).

N. P. Korableva, "Effect of gamma rays on the sulfhydryl compounds content of potato tubers," Doklady Akad. Nauk SSSR 126, 880-883 (1959).

M. I. Korsunskii and V. V. Zashkvara, "On the possibility of reducing aberration factors in analyzers with inhomogeneous fields," Pribory i Tekh. Éksp. No. 3, 21-25 (1959).

S. A. Losev and N. A. Generalov, "On measurements of gas temperatures downstream of a shock wave," Pribory i Tekh. Éksp. No. 3, 108-110 (1959).

S. Yu. Luk'yanov and V. I. Sinitsyn, "Spectroscopic investigations of a power pulse discharge in hydrogen. III. Determination of parameters of a high-temperatures plasma," Zhur. Éksp. i Teor. Fiz. 36, 1621-24 (1959).

L. S. Lur'e and L. G. Ter-Simonyan, "On the possibility of utilizing gammas for decontaminating soil and coping with clubroot in mustard plants," Doklady VASKhNIL No. 6, 28-29 (1959).

V. S. Merkulov, "Radioactive sources in measuring instrumentation," Izmerit. Tekh. No. 5, 62-63 (1959).

M. A. Miller, "Acceleration of plasma bunches by high-frequency electromagnetic fields," Zhur. Éksp. i Teor. Fiz. 36, 1909-17 (1959).

D. A. Panov and N. N. Semashko, "Thermonuclear magnetic mirrors," Nature No. 7, 13-18 (1959).

L. K. Ponomareva and V. L. Zolotavin, "Determination of radioactive strontium in the waters of open reservoirs," Radiokhimiya 1, 208-211 (1959).

A. N. Protopopov et al., "Effect of Nuclear shells on the kinetic-energy distribution of fast-neutron fission fragments," Zhur. Éksp. i. Teor. Fiz. 36, 1932-33 (1959).

Yu. V. Sivintsev, "Radiometry of internal irradiation (review article)," Med. radiologiya 4, 81-86 (1959).

I. M. Tetenbaum, "Use of radiometric measurements in prospecting and exploitation of uranium deposits," Trudy Moskv. geolog. inst. 36, 125-136 (1959).

A. S. Freidin et al., "Effect of ionizing radiation on the chemical stability of wood," Gidrolizn. i lesokhim. prom. No. 4, 4-7 (1959).

I. F. Kharchenko et al., "Computer for studying the motion of particles in a linear electron accelerator," Pribory i Tekh. Éksp. No. 3, 71-76 (1959).

I. S. Shapiro, "Strange particles," Nauka i Zhizn' No. 7, 9-12 (1959).

D. Armstrong and J. Spinks, Canad. J. Chem. 37, 1002-1003 (1959).

A. Bain and J. Robertson, J. Nuclear Materials 1, 109-110 (1959).

M. Barmat et al., Nucleonics 17, 166-168, 171-173 (1959).

D. Beard et al., Nucleonics 17, 90-91, 93, 94, 96 (1959).

N. Beecher and M. Benedict, Nucleonics 17, 64-67, 100 (1959).

R. Boucher, J. Nuclear Materials 1, 13-27 (1959).

H. Bowen, Research 12, 226-231 (1959).

D. Bowersox and J. Leary, J. Inorg. and Nucl. Chem. 9, 108-112 (1959).

W. Bradley, Ind. Chemist 35, 230-236 (1959).

W. Buzzard, Chem. Eng. 66, 147-150 (1959).

M. Cabell, Canad. J. Chem. 37, 1094-1103 (1959).

I. Cambell, et al., J. Inorg. and Nucl. Chem. 10, 225-237 (1959).

V. Campanile and C. Wagner, Nucleonics 17, 74 (1959).

G. Cannon, Nuclear Sci. and Eng. 5, 219-224 (1959).

A. Casey and A. Maddock, J. Inorg. and Nucl. Chem. 10, 289-305 (1959).

Chem. Eng. 66, 98, 100 (1959).

Chem. Eng. 66, 140-143 (1959).

C. Cohn, Nuclear Sci. and Eng. 5, 331-335 (1959).

R. Constant, "Production of radioactive isotopes in Belgium," Industries Atomiques 3, 63-65 (1959).

R. Coppens, "Radioactivity and the age of the earth," Industries Atomiques 3, 37-52 (1959).

G. Coulon and P. Zweifel, Nuclear Sci, and Eng. 5, 203-204 (1959).

J. Davidson et al., Nuclear Sci. and Eng. 5, 227-236 (1959).

J. Dawson, Phys. Rev. 113, 383-387 (1959).

W. DeMarcus, Nuclear Sci. and Eng. 5, 336-337 (1959).

V. Duggal et al., Nuclear Sci. and Eng. 5, 199-200 (1959).

B. Dyson et al., J. Inst. Metals 87, 340-342 (1959).

C. Ells and E. Perryman, J. Nuclear Materials 1, 73-84 (1959).

J. Ferraro, J. Inorg. and Nuclear Chem. 10, 319-322 (1959).

J. Ferrel, Phys. Rev. 113, 527-541 (1959).

W. Foland and R. Present, Phys. Rev. 113, 613-621 (1959).

H. Frisby et al., J. Nuclear Materials 1, 106-108 (1959).

S. Fujii, Progr. Theoret. Phys. 21, 511-532 (1959).

W. Gambill, Chem. Eng. 66, 151-152 (1959).

H. Glubrecht et al., "Use of γ radiation for determining the thickness of biological objects," Atompraxis 5, 237-239 (1959).

J. Goldberg and M. Sankovich, Nuclear Sci. and Eng. 5, 215-218 (1959).

M. Goldsmith and T. Ryan, Nuclear Sci. and Eng. 5, 299-305 (1959).

G. Grover, Nucleonics 17, 54-55 (1959).

H. Henry et al., Nuclear Sci. and Eng. 5, 285-290 (1959).

K. Hernquist, Nucleonics 17, 49-53 (1959).

E. Inonu, Nuclear Sci. and Eng. 5, 248-253 (1959).

H. Irving and D. Edgington, Inorg. and Nucl. Chem. 10, 306-318 (1959).

F. Jablonskii and R. Carter, Nuclear Sci. and Eng. 5, 257-263 (1959).

J. Juillard-Feyler, "Development of atomic energy in Switzerland," Industries Atomiques 3, 69-74 (1959).

Yu. Kato, Progr. Theoret. Phys. 21, 409-420 (1959).

Yu. Kato and T. Taniuti, Progr. Theoret. Phys. 21, 606-612 (1959).

W. Kato and D. Butler, Nuclear Sci. and Eng. 5, 320-330 (1959).

E. Kindermand et al., Nuclear Sci. and Eng. 5, 264-268 (1959).

R. Kladnik, Nucleonics 17, 85-87 (1959).

J. Klumpar et al., "Dosimetry of radioactive isotopes using a windowless counter, and comparison with results of measurements obtained with an end-window G-M counter," Jaderna Energie 5, 190-193 (1959).

G. Knight, Chem. Eng. 66, 171-174 (1959).

M. Krongerg, J. Nuclear Materials 1, 85-95 (1959).

P. Lafore and J. Millot, "Monte Carlo determination of the moments of flux in the slowing down of neutrons emitted by a plane source in an infinite medium," Industries Atomiques 3, 50-53 (1959).

P. Lafore and J. Millot, "Study of isotropic neutron diffusion," Industries Atomiques 3, 66-68 (1959).

P. Lelong and J. Herenguel, J. Nuclear Materials, 1, 58-72 (1959).

D. Longsdail, Ind. Chemist 35, 213-220 (1959).

W. Loosemore, Nuclear Power 4, 112-116 (1959).

B. Lowe et al., Nucleonics 17, 70-72 (1959).

A. Macdonald, Ind. Chemist 35, 243-245 (1959).

J. Macku, "Equipment for counter parameter measurements," Jaderna Energie 5, 194-198 (1959).

J. MacPhee, Nuclear Sci. and Eng. 5, 273-284 (1959).

J. Merritt et al., Canad. J. Chem. 37, 1109-1114 (1959).

D. Morris and C. Bell, J. Inorg. and Nucl. Chem. 10, 337-339 (1959).

C. Muehlhause, Nuclear Sci. and Eng. 5, 225-226 (1959).

J. Murray, J. Inst. Metals 87, 349-352 (1959).

M. Nevitt and S. Zegler, J. Nuclear Materials 1, 6-12 (1959).

C. Nordling and S. Hagstrom, Arkiv fysik 15, 431-443 (1959).

Nucleonics 17, 56-59 (1959).

Nucleonics 17, 88 (1959).

S. Pearlstein, Nuclear Sci. and Eng. 5, 269-270 (1959).

R. Platford and J. Spinks, Canad J. Chem. 37, 1022-1028 (1959).

J. Puig, "Perspectives in the industrial use of radiation chemistry," Industries Atomiques 3, 53-62 (1959).

J. Ransohoff, Nucleonics 17, 80-82 (1959).

J. Rich et al., J. Nuclear Materials 1, 96-105 (1959).

D. Rose, Physics Today 12, 18-21 (1959).

K. Sagel, "Nomogram for design of gamma-ray shielding for a point-source," Atompraxis 5, 229-232 (1959).

T. Sato, J. Inorg. and Nucl. Chem. 9, 188-190 (1959).

R. Scott et al., J. Nuclear Materials 1, 39-48 (1959).

B. Simons, Nuclear Sci. and Eng. 5, 254-256 (1959).

N. Sjostrand et al., Arkiv fysik 15, 471-482 (1959).

R. Skinner and E. Cohen, Nuclear Sci. and Eng. 5, 291-298 (1959).

G. Sonnemann, Nuclear Sci. and Eng. 5, 242-247 (1959).

A. Suss, "Effect of ionizing radiations on the growth and harvesting of plants," Atompraxis 5, 219-223 (1959).

R. Swindeman and D. Douglas, J. Nuclear Materials 1, 49-57 (1959).

T. Taganami, Progr. Theoret. Phys. 21, 533-561 (1959).

H. Takahashi, Nuclear Sci. and Eng. 5, 237-241 (1959).

H. Takahashi, Nuclear Sci. and Eng. 5, 338-346 (1959).

G. Wachter, "Detection and dosimetry of neutrons using a BF_3 counter, part II," Atompraxis 5, 232-236 (1959).

C. Wagner and V. Campanile, Nucleonics 17, 99 (1959).

R. Walker, Nucleonics 17, 68 (1959).

W. Wendland, J. Inorg, and Nucl. Chem. 9, 136-139 (1959).

H. Wilf, Nuclear Sci. and Eng. 5, 306-319 (1959).

J. Wilkins, Nuclear Sci. and Eng. 5, 207-214 (1959).

J. Williams et al., J. Nuclear Materials 1, 28-38 (1959).

SOVIET

research in

ANALYTICAL CHEMISTRY

OF URANIUM

A collection of ten papers from the Consultants Bureau translations of the Soviet Journal of Analytical Chemistry and the famous "Doklady" of the Academy of Sciences (1949-58)... This collection will acquaint the analytical chemist working in this field with Soviet techniques for the determination of uranium in solutions, in ores and the products of their treatments, and in accessory minerals, plus methods for the determination of impurities in uranium.

heavy paper covers illustrated $10.00

CONTENTS

- Extraction of Uranyl α-Nitroso-β-naphtholate and Separation of Uranium from Vanadium and Iron.
- The Composition of Uranyl Selenite. A Volumetric Method of Determining Uranium.
- The Composition of the Luminescence Center of Sodium Fluoride Beads Activated by Uranium.
- Rapid Luminescent Determination of Uranium in Solutions.
- Preparation of Slightly Soluble Compounds of Quadrivalent Uranium Using Rongalite.
- Investigation of Complex Compounds of the Uranyl Ion Which are of Importance in Analytical Chemistry.
- Uranyl and Thorium Selenites.
- The Evaporation Method and Its Use for the Determination of Boron and Other Impurities in Uranium.
- Spectrographic Determination of Uranium in Ores and the Products Obtained by Treatment of These Ores.
- Determination of Uranium in Accessory Minerals.

c/b CONSULTANTS BUREAU
227 WEST 17TH STREET NEW YORK 11, N. Y.